TiO_2-SUPPORTED DEALUMINATED CLINOPTILOLITE: SYNTHESIS, CHARACTERISATION AND KINETIC STUDIES FOR ENHANCED PHOTOCATALYTIC DEGRADATION OF VOLATILE ORGANIC COMPOUNDS

SAHEED OLALEKAN SANNI

(211127817)

This dissertation is submitted to Vaal University of Technology in fulfillment of the requirements for the degree of Magister Technologiae in Chemistry

Supervisor: Prof. S.J. Modise

Co-supervisor: Prof. A.M. Sipamla

June 2014

DECLARATION BY CANDIDATE

I hereby declare that the master dissertation titled "TiO_2-supported dealuminated Clinoptilolite: Synthesis, characterization and kinetic studies for enhanced photocatalytic degradation of volatile organic compounds" submitted for M-Tech: Chemistry, at Vaal University of Technology has never been submitted to any other institution of higher learning. I further declare that all cited sources are acknowledged by list of referencing.

……

SO Sanni

Vaal University of Technology (June 2014)

ACKNOWLEDGEMENTS

All praise is due to Almighty “Allah”, the most beneficent, the most merciful for the guidance and good health throughout the course of this research work.
Sincere appreciation goes to my Supervisor Prof. S.J. Modise and Co-supervisor Prof A.M. Sipamla for their patience and support. May God bless them for their kindness.

I am also grateful to all other Senior lecturers of Chemistry Department, Vaal University of Technology (VUT) for their positive criticism, guidance shown to me during the course of this work. I am also grateful to all laboratory technicians of the department Mike, Neo, Puleng for their understanding and technical related issues. My enumerable thanks goes to my fellow master student colleagues from Chemistry, Chemical Engineering, Mechanical and Electrical Engineering department for their immense support towards this work.

My deepest appreciation goes to Dr Uyi Idemundia of Chemistry Department, University of Fort Hare (UFH) for his enumerable assistance during analysis of my samples, guidance and positive information shared with me during the course of this work. Great respect to Mr Thabo Brooms, my predecessor in this membrane office for setting the pace to achieve higher goals and never to stop believing in myself.

My appreciation goes to my Mentor “Dr Adewale Adeloye” for his constant positive critique of me and guidance throughout this work. I am also grateful to my sunshine Miss Khanyiswa Mbuqe and her family for their support, prayers and understanding during those tedious days.

Final appreciation goes to all academic staff of “Sanitary Engineering Department” under Faculty of Civil Engineering and Geosciences, Tue Delft University of Technology for knowledge and time well spent with them during my exchange programme. I appreciate South Africa - VU University Amsterdam-Strategic Alliances (SAVUSA), Tue Delft African Students Association (TUDASA) and also Association of Students of African Heritage (ASAH NL) for making my stay in Netherlands memorable and positive insights about life.

DEDICATION

This master work is dedicated to my Family for their unconditional love, support, motivational talks and prayer.

PRESENTATION/PAPER PUBLICATION

This master work presented in this dissertation was presented in some conferences and also future event as shown below:

- Sanni S.O., Modise S.J., Sipamla A. Enhancement of methyl orange removal from wastewater using TiO_2/HCP: Optimization of operational parameters. Oral Presentation, Renewable energy and water postgraduate conference, Vaal University of Technology Science Park, Gauteng South Africa. March 28, 2013.

- Sanni S.O., Modise S.J., Sipamla A. (2013) TiO_2 Supported Clinoptilolite: Characterization and Optimization of Operational Parameters for Methyl Orange Removal. Advanced Material Research, Volume 781-784, Pages 2249-2252.

- Sanni S.O., Modise S.J., Sipamla A. Synthesis of TiO_2/HCP as reusable catalyst for enhanced hydrogen generation. Poster Presentation, Energy Post Graduate Conference, iThemba Labs, Cape Town, August 11-14th 2013.

- Sanni S.O., Modise S.J., Sipamla A. Enhancement of methyl orange removal from wastewater using TiO_2/HCP. Poster Presentation. 41st SACI Convention, River Park Conference Center, East London, South Africa. December 1st-6th 2013.

- Sanni S.O., Modise S.J., Sipamla A. Batch adsorption studies and regeneration of TiO_2/HCP from methyl orange solution. “Poster Presentation” WISA Biennial Conference, South Africa. May 25th 2014.

ABSTRACT

Advanced oxidation processes (AOPs) are supposedly effective means for removal of low concentration of organic pollutants from wastewater as compared to conventional treatment methods. However, TiO_2 metal semiconductor is the most promising photocatalyst for degradation of organic pollutant under heterogeneous photocatalysis as compared to other metal semiconductors. Challenges such as aggregation in solution, low adsorptive ability for non-polar organic contaminants and recycling are limitations in application of TiO_2 for commercial purposes. The other limitations of TiO_2, is it only utilizes 4-6% of the solar energy reaching the earth's surface which is in the UV region and also rapid electron-hole recombination due its wide band gap.

In this work, the limitations are overcome by synthesis of a new photocatalyst material and further applied on degradation of model organic contaminants. The first part of this work focused on preparation and characterization of photocatalyst material. The photocatalyst synthesized were characterized using X-ray diffraction (XRD), scanning electron microscopy (SEM), energy-dispersive X-ray analysis (EDAX), Fourier transform infrared spectroscopy (FTIR), thermal gravimetric analysis (TGA) and UV-VIS diffuse reflectance spectrophotometer (DRUV-VIS).

Supporting characterization techniques revealed partly dispersion of TiO_2 within the cavities of dealuminated Clinoptilolite (HCP). TiO_2 exist as nanoparticles or clusters on the HCP surface ascribed to lower loading of TiO_2. XRD analysis showed that the support material employed was mainly Clinoptilolite and absorption band of prepared photocatalyst was red-shifted into the visible region, with slight reduction in band gap of photocatalyst.

The second part focused on adsorption and photocatalytic degradation of methyl orange solution (MO) conducted under UV-irradiation in the presence of TiO_2/HCP. The influence of operational parameters on degradation efficiency of photocatalyst material on MO was carried out in this study. Parameters such as initial dye concentration, pH, calcination temperature, inorganic anions and peroxide concentration were varied during degradation activities of MO. Comparative degradation efficiency of TiO_2/HCP, TiO_2 and HCP were conducted on dye mixture (Methyl orange and Methylene Blue) under UV irradiation. Kinetic analysis employing Langmuir-Hinshelwood model on dependencies of organic contaminants degradation was also conducted at different operational parameters.

The adsorption capacity of MO was highest in the presence of TiO_2/HCP at lower loading, which is ascribed to good dispersion of TiO_2 on HCP and increased surface area of dealuminated Clinoptilolite. The photocatalytic degradation of methyl orange in the presence of TiO_2/HCP was optimized at low dye concentration (30 ppm), acidic condition (pH 4), and calcination temperature of 873 K. Nitrate ion of Sodium salt accelerates degradation activities on methyl orange as compared to other inorganic anions. Photocatalytic degradation of methyl orange was greatly enhanced upon addition of oxidant (H_2O_2) and the photocatalyst possessed good repeatability after 3 cycles. TiO_2/HCP exhibit highest degradation activities, followed by HCP as compared to TiO_2 during the degradation of dye mixture. The degradation of MO by the photocatalyst fits into pseudo-first order kinetic model, while for comparative analysis of photocatalyst on dye mixtures follows second order kinetic model.

TABLE OF CONTENTS

ACKNOWLEDGEMENTS iii
DEDICATION iv
PRESENTATION/PAPER PUBLICATION v
ABSTRACT vi
LIST OF ABBREVIATIONS xii
LIST OF SYMBOLS xiv
LIST OF FIGURES xv
LIST OF TABLES xvii
LIST OF APPENDICES xviii

CHAPTER ONE 1
OVERVIEW OF PRESENT STUDY 1
Introduction 2
1.1 Waste water treatment 2
1.2 Advanced oxidation processes (AOPs) 3
1.3 Metal semiconductor photocatalyst 4
1.4 TiO_2 Photocatalyst 5
1.5 Aims and Objectives of current study 7
1.6 Dissertation Outline 8
References 10

CHAPTER TWO 13
LITERATURE REVIEW 13
Introduction 14
2.1 Advanced oxidation processes 14
2.1.1 Homogenous photocatalysis 16
2.1.2 Heterogeneous photocatalysis 16
2.1.3 Principle of Heterogeneous photocatalysis 16
2.2 Metal semiconductor for photocatalytic process 18
2.2.1 Titanium dioxide (TiO_2) Semiconductor 19

2.2.2 Titanium dioxide preparation 21
2.2.3 Sol-Gel Method 21
2.3 Organic micro pollutant 22
2.4 Factors affecting Photocatalysis 23
2.4.1 TiO_2 structural properties 25
2.4.1.1 Crystal structure 25
2.4.1.2 Surface area 25
2.4.1.3 Particle dimensions 25
2.5 Kinetics and Photocatalytic reactor 26
2.6 Photocatalysis coupled with other operations 27
2.7 Surface modifications of TiO_2 27
2.7.1 TiO_2 Doping 28
2.7.2 Metal deposition 29
2.7.3 Composite Semiconductors 29
2.7.4 Surface sensitization 30
2.7.5 TiO_2 composite catalysts 30
2.8 Zeolites 31
2.9 Organic compounds employed in this present study. 35
References 36

CHAPTER THREE 43
EXPERIMENTAL AND METHODOLOGY 43
Introduction 44
3.1 Materials 44
3.2 Detailed preparation of photocatalyst 45
3.2.1 Preparation of dealuminated Clinoptilolite (HCP) 45
3.2.2 Preparation of supported photocatalyst (TiO_2/HCP) and pure TiO_2 45
3.3 Characterization of synthesized photocatalyst 46
3.3.1 XRD Analysis 47
3.3.2 Fourier-transform infrared spectroscopy (FT-IR) 47
3.3.3 SEM/EDAX analysis 47
3.3.4 Thermal gravimetric analysis (TGA) 47
3.3.5 DRUV-VIS 48

3.4 Experimental Details of Photocatalytic degradation of model pollutants 48
3.4.1 Experimental setup 48
3.4.2 Experimental procedure 49
References 50

CHAPTER FOUR 51
RESULTS AND DISCUSSIONS 51
4.1 Characterization of prepared photocatalyst 52
4.1.1 XRD Analysis 52
4.1.2 SEM and EDAX Analysis 53
4.1.3 FTIR analysis 56
4.1.4 TGA analysis 57
4.1.5 Diffuse Reflectance Spectroscopy 59
4.2 Batch Adsorption and Photocatalytic degradation of MO 59
4.2.1 Adsorption of Methyl Orange (MO) 59
4.2.2 Adsorption kinetic analysis 62
4.2.3 Photocatalytic degradation of Methyl Orange (MO) 64
4.2.4 Effect of TiO_2 loading rate on MO degradation 64
4.2.5 Effect of Initial Methyl orange (MO) concentration 66
4.2.6 Effect of pH on MO degradation 67
4.2.7 Effect of calcination temperature on MO degradation 68
4.2.8 Effect of inorganic anions on MO degradation 69
4.2.9 Effect of oxidant on MO degradation 71
4.2.10 Recycling of photocatalyst on MO degradation 72
4.3 Comparison activities of the photocatalyst on dye mixtures 73
4.4 Kinetics of photocatalytic degradation of Methyl orange and Dye mixture 76
4.4.1 Loading rate kinetics 77
4.4.2 Kinetics of other operational parameters and on dye mixture 79
References 88

CHAPTER FIVE 91
CONCLUSIONS AND RECOMMENDATIONS 91
5.1 Conclusions 92

5.2 Recommendation 93

APPENDICES.....94

PUBLISHED JOURNAL 109

LIST OF ABBREVIATIONS

Abbreviations

AOP	Advanced oxidation processes
H_2O_2	Hydrogen Peroxide
UV	Ultraviolet
O_3	Ozone
TiO_2	Titanium dioxide
$OH^{\bullet}$	Hydroxyl
$O_2^{\bullet-}$	Superoxide
H_2O	Water
CO_2	Carbon dioxide
ZnO	Zinc oxide
ZrO_2	Zirconium oxide
Fe_2O_3	Iron (III) oxide
CeO_2	Cerium (IV) oxide
WO_3	Tungsten trioxide
CdS	Cadmium sulphide
CdSe	Cadmium selenide
ZnS	Zinc sulphide
SnO_2	Tin (II) oxide
CVD	Chemical vapour deposition
SSD	Solid state dispersion
PVD	Physical vapor deposition
SPD	Spray pyrolysis deposition
VOCs	Volatile organic compounds
MO	Methyl orange
MB	Methylene blue
CP	Clinoptilolite
HCP	Dealuminated Clinoptilolite
SC	Metal semiconductor
VB	Valence band

CB	Conduction band
NHE	Normal hydrogen electrode
L-H	Langmuir-Hinshelwood
FT-IR	Fourier transform infrared spectroscopy
XRD	X-ray diffraction
SEM	Scanning electron microscopy
EDAX	Energy dispersive X-ray spectroscopy
TGA	Thermal gravimetric analysis
DSC	Differential scanning calorimetry
DRUV	Diffuse reflectance spectrophotometer

LIST OF SYMBOLS

Symbols

h^+	Hole
wt	Weight
eV	Electron volt
E_{bg}	Band gap energy
rpm	Revolutions per minute
µm	Micrometres
ppm	Parts per million
ml	Millilitres
nm	Nanometres
e^-	Electron
hυ	Light energy
λ	Wavelength
<	Less than
>	Greater than
^oC	Degree celcius
%	Percentage
min	Minute
hr	Hour
cm	Centimetre
kV	Kilovolt
W	Watt

LIST OF FIGURES

Chapter 2

Figure 2. 1 Heterogenous photocatalysis on a semiconductor 18
Figure 2. 2 Crystal structure of anatase (a) rutile (b) and brookite (c).....20
Figure 2. 3 An $[SiO_4]^{4-}$ or $[AlO_4]^{5-}$ tetrahedra (primary building unit).....32
Figure 2. 4 Model framework structure of Clinoptilotile.....34
Figure 2. 5 Chemical structure of (a) Methyl orange and (b) Methylene blue.....35

Chapter 3

Figure 3. 1 Flow chart of detailed preparation of HCP.....45
Figure 3. 2 Flow chart of detailed preparation of TiO_2/HCP.....46
Figure 3. 3 Pictorial diagram of Photoreactor.....48

Chapter 4

Figure 4. 1 X-Ray diffraction patterns of CP, HCP and TiO_2/HCP at 550 ^oC.....53
Figure 4. 2 SEM images of (a) HCP and (b) 5 wt% TiO_2/HCP.....54
Figure 4. 3 EDAX of (a) HCP and (b) 5 wt% TiO_2/HCP.....55
Figure 4. 4 FTIR of Raw CP, HCP and TiO_2/HCP.....56
Figure 4. 5 TGA of (a) Raw CP, (b) HCP and (b) 5 wt% TiO_2/HCP.....58
Figure 4. 6 DRUV-VIS of (a) Raw CP, (b) HCP and (b) TiO_2/HCP.....59
Figure 4. 7 Dark adsorption studies of photocatalyst on MO degradation.....60
Figure 4. 8 Influence of loading rate on the adsorption of MO by TiO_2/HCP.....61
Figure 4. 9 Linear plot of pseudo first order kinetic model for MO adsorption.....63
Figure 4. 10 Linear plot of pseudo second order kinetic model for MO adsorption.....63
Figure 4. 11 Effect of loading wt% TiO_2 on HCP.....65
Figure 4. 12 Effect of initial MO concentration in the presence of TiO_2/HCP.....67
Figure 4. 13 Effect of pH on degradation rate of Methyl orange.....68
Figure 4. 14 Effect of calcination temperature on degradation rate of MO.....69
Figure 4. 15 Effect of inorganic ions on degradation rate of MO.....70

Figure 4. 16 Effect of peroxide on degradation rate of MO 72
Figure 4. 17 Effect of recycling rate on degradation of MO....73
Figure 4. 18 Characteristic wavelengths of MO and MB....74
Figure 4. 19 Photodegradation of dye mixture in the presence photocatalyst....75
Figure 4. 20 UV-absorption spectra of dye mixture 76
Figure 4. 21 Pseudo first order kinetics of MO degradation at loading of TiO_2....78
Figure 4. 22 Plot of $1/K_{app}$ versus C_o at different initial concentration of MO degradation....79
Figure 4. 23 Pseudo first order kinetics of MO degradation at various initial concentration 80
Figure 4. 24 Pseudo first order kinetics for degradation of MO at different pH....81
Figure 4. 25 Pseudo first order kinetics of MO degradation at different calcination temperature 82
Figure 4. 26 Pseudo first order kinetics of MO degradation using different anions 83
Figure 4. 27 Pseudo first order kinetics of MO degradation at different recycling rate 84
Figure 4. 28 Second order kinetics of MO degradation in presence of oxidant 85
Figure 4. 29 Second order kinetics of dye mixture degradation using different catalyst 86

LIST OF TABLES

Chapter 2

Table 2. 1 Hydroxyl radical generation in different Homogenous catalysis 15
Table 2. 2 Band gap and wavelength of Semiconductors.....19
Table 2. 3 Volatile organic compounds degraded by TiO_2.....23

Chapter 3

Table 3. 1 Physical properties of Methyl Orange (MO) and Methylene Blue (MB) 44

Chapter 4

Table 4. 1 Vibrational bands of prepared photocatalyst.....57
Table 4. 2 Percentage weight loss of prepared photocatalyst.....58
Table 4. 3 Adsorption kinetic model constants for MO adsorption at various loading 64
Table 4. 4 Kinetic model parameters of degradation of MO at different loading of TiO_2.....78
Table 4. 5 Parameters of degradation of MO at different initial concentration of MO 80
Table 4. 6 Kinetic model parameters of degradation of MO at different initial concentration.....81
Table 4. 7 Kinetic model parameters of MO degradation at different pH.....82
Table 4. 8 Kinetic model parameters of MO degradation under different calcination temperature 83
Table 4. 9 Kinetic model parameters of MO degradation in presence of different anions 84
Table 4. 10 Kinetic model parameters of MO degradation at different recycling rate 85
Table 4. 11 Kinetic model parameters of MO degradation in presence of oxidant 86
Table 4. 12 Kinetic model parameters of dye mixture degradation 87

LIST OF APPENDICES

Appendix 1 Sem image of (a) 7.5 wt% TiO_2/HCP and (b) 10 wt% TiO_2/HCP 95
Appendix 2 EDAX of (a) 7.5 wt% TiO_2/HCP and (b) 10 wt% TiO_2/HCP 96
Appendix 3 FTIR of 7.5 wt% and 10 wt% TiO_2/HCP 97
Appendix 4 TGA of 7.5 wt% and 10 wt% TiO_2/HCP 98
Appendix 5 DRUV-VIS Spectra of calcined photocatalyst at different temperature.....99
Appendix 6 Comparison of kinetic models for q_e for MO adsorption 100
Appendix 7 Zeroth and Second order kinetics at different loading of TiO_2 101
Appendix 8 Zeroth and second order kinetics at different initial concentration rate.....102
Appendix 9 Zeroth and second order kinetics at different pH 103
Appendix 10 Zeroth and second order kinetics at different calcination temperature 104
Appendix 11 Zeroth and second order kinetics in presence of different anions 105
Appendix 12 Zeroth and second order kinetics at different recycling rate 106
Appendix 13 Zeroth and pseudo first order kinetics in presence of oxidant 107
Appendix 14 Zeroth and pseudo first order kinetics for degradation of dye mixture 108

CHAPTER ONE

OVERVIEW OF PRESENT STUDY

Introduction

In this chapter, a general overview of the present study is highlighted especially the challenges facing scarcity of clean water worldwide. Summary of conventional methods in treating waste water will be highlighted and their challenges are discussed. The aims and objectives of the present study will also be reviewed.

1.1 Waste water treatment

Water is the source of life for human beings, animals and plants. It forms 70% of the earth's surface. Population and industrial growth are major challenges to access to clean water worldwide. Industrial and agricultural activities consume the majority of available water for their operational activities and subsequently contaminate the environment with toxic contaminants worldwide (Wintgens *et al*., 2008). Population worldwide demand for pure water for drinking and household purposes is however increasing at an alarming rate. Increased awareness about water pollution worldwide is forcing stringent alternative means to generate clean water and conserve the available for present and future purposes.

South Africa, a semi-arid country (DWAF Report, 1998) has challenges of water shortage. There is a need to manage and use water efficiently for present and future purposes. Overcoming the issue of water pollution specifically to meet environmental legislations has been the focal activities of researchers for the development of cost effective and improved water treatment processes. Ideally, it is imperative for industries to eliminate and reduce organic contaminants in wastewater before discharge into the environment.

Conventional methods (physical, chemical and biological) in their form or combinations have been applied for treatment of waste water with their shortcomings (Gaya and Abdullah, 2008). Physical process via “Adsorption” employs adsorbent (i.e. Granular activated carbon) to remove toxic organics from the water. The materials are left behind after regeneration and convert the adsorbed pollutant to innocuous side products (Padmanadhan *et al*., 2006). In case of membrane technologies, high investment costs and potential membrane fouling are the challenges affecting this process (Gaya and Abdullah, 2008).

In chemical treatment, chlorination and ozonization are majorly employed for disinfection and oxidation of organic contaminants in waste waters. Chlorination possesses the tendency of forming toxic disinfection by-products such as trihalomethanes, which are mutagenic and carcinogenic to human health (Yang and Cheng, 2007). Ozonisation possesses intrinsic properties over Chlorination by non-production of disinfection by-products. It can generate cancer causing agent and involves the high cost of wastewater treatment.

Biological treatments in their natural form and ease of use also possess their challenges. It converts the pollutants into sludge which is equivalent to a volume of treated water. Transfer to other secondary pollutant present major challenge for long term purposes of treating these toxic organic contaminants. In limelight of these setbacks, attention turns to "*Advanced oxidation processes*" which employs radical species to degrade this toxic organic contaminant in waste water into mineralized products without any selectivity (Hoffmann *et al*., 1995).

1.2 Advanced oxidation processes (AOPs)

Advanced oxidation processes (*AOPs*) are effective treatment methods for complete degradation of toxic organic compounds. They are cost effective to operate in mild conditions, specifically in areas where conventional treatment has failed. *AOPs* are homogeneous or heterogeneous in nature. Homogenous *AOPs* (H_2O_2/UV, O_3/UV and H_2O_2/O_3/UV) employs chemicals/oxidants. Heterogeneous *AOPs* (TiO_2/UV) employs catalyst for degradation activities (Lergini *et al*., 1993). These activities occur in the presence of solar or UV light, which in turns generates radical species like hydroxyl ($OH^{\bullet}$) and superoxide ($O_2^{\bullet-}$) for degradation of waste water into mineralized products. Heterogeneous photocatalysis is at the focal point of attention in recent years for treating waste water with toxic organic contaminants as compared to homogenous process (Guillard *et al*., 1999).

Heterogeneous photocatalysis makes use of low UV-A light or solar light, reusable catalyst and no additional chemical oxidants except oxygen. This process operates at ambient conditions and employs low cost material that are non-toxic, stable catalyst for degradation activities. The reaction occurs via irradiation of a semiconductor (photocatalyst) by UV source light, with energy more than the band gap energy of the photocatalyst. This represents the energy gap between the valence and conduction band of the photocatalyst. Holes and electron generated

via irradiation of the photocatalyst in turn oxidized toxic organic contaminants into mineralized products.(Carp *et al*., 2004)

The real understanding of heterogeneous photocatalysis began in 1972 through the pioneer work of Fujishima and Honda on splitting of water into hydrogen and oxygen using UV irradiated TiO_2 photoanode and Pt counter electrode (Fujishima and Honda, 1972). This paved way for application of metal semiconductor for other applications. Carey *et a*l., investigated TiO_2 as a metal semiconductor for photocatalytic degradation of organic contaminants (Carey *et al*., 1976). With increased concern for environmental preservation and clean-up, attention now focuses on metal semiconductor catalysed photochemistry for air, water and soil clean-up. Complete mineralization of the toxic organic contaminants in industrial waste water and drinking water to H_2O, CO_2 and inorganic substituents was achievable with metal semiconductor catalysed photochemistry (Konstantinou and Albanis, 2004).

1.3 Metal semiconductor photocatalyst

Generally, metal semiconductor catalyst and light source determine reaction activities for waste water treatment. Metal semiconductor catalysts applied in photochemistry possess intrinsic properties such as light absorption properties, charge transport characteristics and lift time of excited state (Herrmann, 2005). Metal semiconductor with a specific electronic structure of a filled valence band and the empty conduction band makes it applicable as a photocatalyst. The conduction band comprises of occupied molecular orbital high in energy, required for free movement of electrons from atom to atom under influence of applied energy. The valence band is made up of occupied molecular orbital low in energy. The difference in energy between the two is referred to as band gap energy (E_{bg}), an applied energy required for electron promotion from the valence band to the conduction band. Band gap energy and the required energy differs in various metal semiconductors as well as required energy (Litter, 1999).

When photons of light strike the semiconductor, electron jumps from filled lower energy valence band to higher energy empty conduction band, now with conduction band partially filled which in turn allows electron free movement in the semiconductor lattice. Also, a vacant electron in the partially filled valence band can move, this vacant electron is known as hole (h_{vb}^+) (Li Puma *et al*., 2008). Lower band gap energy is preferable for semiconductors photocatalyst required for activation by higher wavelength visible light with low energy. Band gap energy of a

semiconductor material and required threshold wavelength of light source can be determined from scheme 1.1 and wavelength of light source is equal or less than the threshold wavelength of semiconductor for easy activation (Pucher *et al*., 2007).

$$\lambda_{bg} = \frac{1240}{E_{bg}} (eV) \qquad 1.1$$

Heterogeneous photocatalysts, mainly in solid forms promotes reactions in degradation of organic contaminants in the presence of UV-light and do not get consumed in the overall reaction (Neppolian *et al*., 2002). A wide range of chalcogenide metal semiconductors which produce excited high energy state of e^-/h^+ were applied as photocatalyst for the degradation of toxic organic contaminants. These semiconductors includes TiO_2, ZnO, ZrO_2, Fe_2O_3, CeO_2, WO_3, CdS, CdSe and ZnS (Herrmann, 2005). Ideal photocatalyst should be photoactive, biologically and chemical inert, photostable, inexpensive, non-toxic and excited in visible and near UV light (Bhatkhande *et al*., 2002).

Some of these metal semiconductors possess short term stability in aqueous media (CdS and CdSe) and undergo photoanodic corrosion, which can be partly suppressed by addition of sulphide and sulphite to contacting solution (Beydoun *et al*., 1999). These materials are also toxic in nature. Haematite (Fe_2O_3) adsorptive power in the visible region is very low for photocatalytic activities as compared to TiO_2 or ZnO, which results from corrosion. WO_3 is also less photocatalytic active as compared to TiO_2 (Beydoun *et al*., 1999). ZnO displays instability in illuminated aqueous solutions with $Zn(OH)_2$ forming on the particle surface resulting in deactivation of the photocatalyst (Neppolian *et al*., 2002). TiO_2 possesses chemical stability, resistance to chemical corrosion, non-toxicity and cost effective materials, which found wide application as white pigment in paints (51%), plastic (19%) and paper (17%) (Music *et al*., 1997 and Schneider and Baiker, 1997). With these properties, degradation of toxic organic contaminants in waste water using irradiated TiO_2 suspension offer promising prospects for water treatment.

1.4 TiO_2 Photocatalyst

TiO_2 has intrinsic properties for degradation of organic contaminants to mineralized products, when operated at ambient temperature and resistance to corrosion. However, the challenges of

using bare TiO_2 in solution such as (i) rapid aggregation due to its small size, which results in decrease of surface area as well as catalytic efficiency (Qiang et al., 2001), (ii) TiO_2 is a non-porous material with low adsorptive ability (Torimoto *et al*., 1996) and (iii) also poor adsorbent for non-polar organic compounds due to its polar surface (Xu and Langford, 1995). Generally, adsorption and pre-concentration of organic contaminants in waste water on the catalyst surface is vital for surface reaction. Judging from TiO_2 limitations and economic point of view, immobilization on porous adsorbent material and doping of TiO_2 with metals or non-metal offers a promising solution for degradation of organic contaminants (Gao *et al*., 2008 and Tasbihi *et al*., 2010).

Immobilization of TiO_2 on porous materials such as ceramic, fibreglass (Shifu, 1996), glass matrix, quartz and stainless steel plate (Fennandez *et al*., 1995) eliminates agglomeration. However, the photocatalytic efficiency of the above mentioned materials are less when compared to suspended TiO_2 (Xu and Langford, 1995). Specific surface area decrease when fixing TiO_2 on these non-porous supports and reduces their adsorption capacity. Attention now focus on the immobilisation of TiO_2 on porous materials such as silica (Lepore *et al*., 1996), alumina (Anderson *et al*., 1988), activated carbon (Yoneyama and Torimoto, 2000), clay (Shimizu *et al*., 2002) and zeolites (Xu and Langford, 1997).

These porous adsorbents material provides higher specific surface area and effective adsorption sites more than bare TiO_2, which in turn degrade organic contaminants effectively into mineralize products (Torimoto *et al*., 1997). In photodegradation process, intermediates formed are adsorbed on the supported catalyst and further oxidized to mineralization products. Among these porous adsorbents, Zeolites have attracted considerable attention in recent years for the degradation of toxic organic contaminants (Durgakumari *et al*., 2002). Zeolites are more attractive catalyst supports than activated carbon and clay, due to their low polar surface, large surface area, chemical inertness and activity in electron-transfer process during degradation activities (Huang *et al*., 2008).

The other limitation of TiO_2 is that it only utilizes 4-6% of the solar energy reaching the earth's surface which is in the UV region and also rapid electron-hole recombination due its wide band gap. These limitations can be overcome by modifying with doping of metal or non-metal ions, other metal semiconductors and photosensitization by coloured organic materials. These

modifications extend photo-response of large band gap semiconductors in the visible region for enhanced degradation of organic contaminants (Yu *et al*., 2010)

Several preparation techniques have been employed for TiO_2-supported photocatalyst such as wet chemical impregnation, chemical vapour deposition, solid state dispersion (SSD), ion exchange mechanical mixture, sol-gel method and spray pyrolysis (Konstantinou and Albanis, 2004). A detailed study on TiO_2-supported zeolite and doped photocatalyst for photodegradation of selected toxic organic contaminants will be presented in this work.

1.5 Problem statement

The application of bare TiO_2 for degradation of organic contaminants in waste water is not desired due to it impedeing challenges. Due to its small size and rapid aggregation in solution, TiO_2 results in decrease of photocatalytic efficiency. Judging from TiO_2 limitations and economic point of view, immobilization on porous adsorbent material offers a promising solution for enhanced degradation of organic contaminants and also efficient recovery from solution after degradation activities.

TiO_2 utilizes 4-6% of the solar energy reaching the earth's surface which is in the UV region and also rapid electron-hole recombination due its wide band gap is another challenge. Doping of TiO_2 with metals or non-metal ions, other metal semiconductors and photosensitization by coloured organic materials. These modifications extend photo-response of large band gap semiconductors in the visible region for enhanced degradation of organic contaminants.

1.6 Aims and Objectives of current study

The aim of the study is to develop a composite material consisting of TiO_2 and dealuminated clinoptilolite. This composite material should possess enhanced absorption in the visible region, efficient photocatalytic activities and also good recovery from the solution after degradation of organic contaminants.

The main objective of this study is focused on treatment of recalcitrant organic compounds present in wastewater which cannot be treated by conventional methods. In the realm of increasing the photodegradation efficiency and improving the economics of the process, this work will be carried out on degradation of Methyl orange (MO). Comparative degradation efficiency of prepared photocatalyst will be conducted on dye mixture of methyl orange and methylene blue. Clinoptilolite of chemical formula $(MgCaNa_2K_2)_{2.5}(AlO_2)_7(SiO_2)_{30}\cdot 21H_2O$ will be

applied as support material for TiO_2 during the course of this study. The objectives of this work are:

- Preparation and characterization of TiO_2 catalyst supported on dealuminated Clinoptilotile (HCP);
- Comprehensive evaluation of operational parameters such as irradiation time, TiO_2 (wt%) loading on Clinoptilotile, initial dye concentrations, pH, effects of anions, peroxide;
- Comparative evaluation of photocatalytic efficiency of supported photocatalyst TiO_2/HCP, unsupported TiO_2 and HCP conducted on mixtures of MO and MB;
- Kinetics of degradation of model contaminants using various models.

1.7 Dissertation Outline

This dissertation comprises of five chapters:

Chapter 1 focuses on the general introduction on challenges of clean water in the environment. The aims and objectives of this study are presented and the outline of the dissertation is also included.

In Chapter 2, a literature review on “Advanced oxidation processes” (AOPs) down to application of TiO_2 as a semiconductor photocatalyst under heterogeneous photocatalysis is described. The challenges of application of TiO_2, factors affecting its performance and solution to impending large scale application for commercial purposes are highlighted.

Chapter 3 highlights summary of the materials used, general methodology and a description of the techniques used in the characterization of the prepared photo-catalytic materials.

In Chapter 4, results of the preparation of titania dispersed on dealuminated Clinoptilotile (TiO_2/HCP) and characterized using analytical means are given and discussed. The photocatalytic degradation of methyl orange solution conducted under UV-irradiation in the presence of photocatalyst. Influences of operational parameters were varied during degradation activities. The comparative activities between the photocatalysts performed on a dye mixture of dye solution (Methyl orange and Methylene blue) are discussed.

Chapter 5 outlines general conclusion of the research results and recommendations for future work.

References

ANDERSON, M. A., GIESELMAN, M. J. & XU, Q. (1988) Titania and Aluminia Ceramics Membranes. *J. Membr. Sci.,* **39,** 243-248.

BEYDOUN, D., AMAL, R., LOW, G. & M_CEVOY, S. (1999) Role of nanoparticles in photocatalysis. *J. Nano. res.,* **1,** 439-458.

BHATKHANDE, D. S., PANGARKAR, V. G. & BEENACKERS, A. (2002) Photocatalytic degradation for environmental applications-a review. *J. Chem. Technol. Biotechnol., 80,* **77,** 102-116.

CAREY, J. J., LAWRENCE, J. & TOSINE, H. M. (1976) Photodechlorination of PCB's in the presence of titanium dioxide in aqueous suspensions. *Bull. Environ. Contam. Toxicol.,* **16,** 697-701.

CARP, O., HUISMAN, C. L. & RELLER, A. (2004) Photoinduced reactivity of titanium dioxide. *Prog. Solid State Chem.,* **32,** 33.

DURGAKUMARI, V. S., SUBRAHMANYAM, M., SUBBA RAO, K. V., RATNAMALA, A., NOORJAHAN, M. & TANAKA, K. (2002) An easy and efficient use of TiO_2 supported HZSM-5 and TiO_2 + HZSM-5 zeolite combinate in the photodegradation of aqueous phenol and p-chlorophenol. *Appl. Catal. A: Gen.,* **234,** 155-165.

FENNANDEZ, A., LASSALETTA, G., JIMENEZ, V. M., JUSTO, A., GONZÁLEZ-ELIPE, A. R., HERRMANN, J.-M., TAHIRIB, H. & AIT-ICHOU, Y. (1995) Preparation and characterization of TiO_2 photocatalysts supported on various rigid supports (Glass, Quartz and Stainless Steel). Comparative studies of photocatalytic activity in water purification. *Appl. Catal. B: Environ.,* **7,** 49-63.

FUJISHIMA, A. & HONDA, K. (1972) Electrochemical photolysis of water at a semiconductor electrode. *Nature,* **238,** 37-38.

GAO, B., PENG, C., CHEN, G. Z. & LI PUMA, G. (2008) Photo–electro–catalysis enhancement on carbon nanotubes/titanium dioxide (CNTs/TiO_2) composite prepared by a novel surfactant wrapping sol–gel method. *Appl. Catal. B. Environ., 42,* **85,** 17-23.

GAYA, U. I. & ABDULLAH, A. H. (2008) Heterogeneous photocatalytic degradation of organic contaminants over titanium dioxide: A review of fundamentals, progress and problems. *J. Photochem. Photobiol. C: Photochem. Rev.,* **9,** 1-12.

GUILLARD, C., DISDIER, J., HERRMANN, J.-M., LEHAUT, C., CHOPIN, T., MALATO, S. & BLANCO, J. (1999) Comparison of various titania samples of industrial origin in the solar photocatalytic detoxification of water containing 4-chlorophenol. *Catal. Today,* **54,** 217.

HERRMANN, J. M. (2005) Heterogeneous photocatalysis: State of the art and present applications. *Top. Catal.,* **34,** 49-65.

HOFFMANN, M. R., BAHNEMANN, D. W., MARTIN, S. T. & CHOI, W. (1995) Environmental applications of semiconductor photocatalysis. *Chem. Rev.,* **95,** 69-96.

HUANG, M., XU, C., WU, Z., HUANG, Y., LIN, J. & WU, J. (2008) Photocatalytic discolorization of methyl orange solution by Pt modified TiO_2 loaded on natural zeolite. *Dyes and Pigments,* **77,** 327-34.

KONSTANTINOU, I. A. & ALBANIS, T. A. (2004) TiO_2-assisted photocatalytic degradation of azo dyes in aqueous solution: kinetic and mechanistic investigations: A review. *Applied Catalysis B: Environ.,* **49,** 1-14.

LEPORE, G. P., PERSAUD, L. & LANGFORD, C. H. (1996) Supporting Titanium Dioxide Photocatalysts on Silica Gel and Hydrophobically Modified Silica Gel. *J. Photochem. Photobio. A: Chem.,* **98,** 103-111.

LERGINI, O., OLIVEROS, E. & BARUN, A. M. (1993) Photochemical processes for water treatment. *Chem. Rev., 95,* **93,** 671-710.

LI PUMA, G., BONO, A., KRISHNAIAH, D. & COLLIN, J. G. (2008) Preparation of titanium dioxide photocatalyst loaded onto activated carbon support using chemical vapor deposition: A review paper. *J. Hazard. Mater. 137,* **157,** 209-219.

LITTER, M. I. (1999) Heterogeneous photocatalysis, transition metal ions in photocatalytic systems. *Appl. Catal. B. Environ.,* **23,** 89-114.

MUSIC, S., GOTIC, M., IVANDA, M., POPOVIC, S., TURKOVIC, A., TROJKO, R., SEKULIC, A. & FURI, K. (1997) Chemical and microstructural properties of TiO_2 synthesized by sol–gel procedure. *Mater. Sci. Eng. C,* **347**, 33-40.

NEPPOLIAN, B., CHOI, H., SACKTHIVEL, S., ARABINDOO, B. & MURUGESAN, V. (2002) Solar light induced and TiO_2 assisted degradation of textile dye reactive blue 4. *Chemosphere,* **46,** 971.

PADMANADHAN, P. V. A., SREEKUMAR, K. P., THIYAGARAJAN, T. K., SATPUTE, R. U., BHANUMURTHY, K., SENGUPTA, P., DEY, G. K. & WARRIER, K. G. K. (2006) Nano-crystalline titanium dioxide formed by reactive plasma synthesis. *Vacuum,* **80,** 11-12.

PUCHER, P., BENMAMI, M., AZOUANI, R., KRAMMER, G., CHHOR, K., BOCQUET, J. F. & KANAEV, A. V. (2007) Nano-TiO_2 sols immobilized on porous silica as new efficient photocatalyst. *Appl. Catal. A: Gen.,* **332,** 297-303.

QIANG, W., XIJUN, H., YUE, P. L., XIU, S. Z. & GAO, Q. L. (2001) Copper/MCM-41 as catalyst for the Wet Oxidation of Phenol. *Appl. Catal. B: Environ.,* **32,** 151-156.

SCHNEIDER, M. & BAIKER, A. (1997) Titania–based aerogel. *Catal. Today,* **35,** 339-365.

SHIFU, C. (1996) Photocatalytic degradation of organic pesticide containing phosphorous by TiO_2 supported on fiber glass. *Environ. Sci. Technol.,* **17,** 33-35.

SHIMIZU, K., KANEKO, T., FUJISHIMA, T., KODAMA, T., YOSHIDA, H. & KITAYAMA, Y. (2002) Selective oxidation of liquid hydrocarbons over photoirradiated TiO_2 pillared clays. *Appl. Catal. A: General,* **225,** 185-191.

TASBIHI, M., LAVRENČIČ ŠTANGAR, U., SEVER ŠKAPIN, A., RISTIĆ, N. & NOVAK TUŠAR, N. (2010) Titania–containing mesoporous silica powders: structural properties and photocatalytic activity towards isopropanol degradation. *J. Photochem. Photobiol. A***,** 167-168.

TORIMOTO, T., ITO, S., KUWABATA, S. & YONEYAMA, H. (1996) Effects of adsorbents used as supports for Titanium dioxide leading on photocatalytic degradation of Propyzamide. *Environ. Sci. Technol.,* **30,** 1275-1281.

TORIMOTO, T., OKAWA, Y., TAKEDA, N. & YONEYAMA, H. (1997) Effect of activated carbon content in TiO_2-loaded activated carbon on photodegradation behaviors of Dichloromethane. *J. Photochem. Photobio. A: Chem,* **103,** 153-157.

WINTGENS, T., SALEHI, F., HOCHSTRAT, R. & MELIN, T. (2008) Emerging contaminants and treatment options in water recycling for indirect potable use. *Water Sci Technol,* **57,** 99-107.

XU, Y. & LANGFORD, C. H. (1995) Enhanced photoactivity of a Titanium (IV) Oxide supported on ZSM 5 and Zeolite A at low coverage. *J. Phys. Chem. B.,***99,** 11501-11507.

XU, Y. & LANGFORD, C. H. (1997) Photoactivity of Titanium dioxide supported on MCM-41, Zeolite X, and Zeolite Y. *J. Phys. Chem. B,* **101,** 3115-3121.

YANG, H. & CHENG, H. (2007) Controlling nitrite level in drinking water by chlorination and chloramination. *Sep. Purif. Technol.,* **56,** 392-396.

YONEYAMA, H. & TORIMOTO, T. (2000) Titanium Dioxide adsorbent hybrid photocatalysts for photodestruction of organic substances of dilute concentrations. *Catal. Today,* **58,** 133-140.

YU, T., TAN, X., ZHAO, L., YIN, Y., CHEN, P. & WEI, J. (2010) Characterization, activity and kinetics of a visible light driven photocatalyst: cerium and nitrogen co-doped TiO_2 nanoparticles. *Chem. Eng. J.* ***157***, 86-92.

CHAPTER TWO

LITERATURE REVIEW

Introduction

In this chapter, literature review about advanced oxidation processes (AOPs), operations and also discussion about the value of using TiO_2 as photocatalyst for degradation of waste water will be emphasized. This chapter focus on ways to enhance the limitations of TiO_2 application for commercial purposes.

2.1 Advanced oxidation processes

Environmental protection and eradication of environmental pollutants (such as volatile organic compounds) represent major challenges for improved quality of life and sustainable development. Water a important source of life, has diverse applications in domestic, agriculture, industry and energy production. The exponential growth in human population, agriculture and industrial development has led to increased demand for fresh water worldwide. Moreover, a large amount of organic compounds from industrial and agricultural activities further escalates the scarcity of fresh water. Many water borne diseases are associated with inadequate fresh and clean water. Studies revealed estimated 1.2 billion people lack access to drinking water (Blue Planet Network, 2006) and death as a result. This makes production of clean water and storage for future purpose vital worldwide.

Conventional water treatment technologies have been employed for removing these organic compounds from water; however these add more challenges to treating contaminated water. In order to suppress the water pollutants, development of advanced technologies with low operation costs and high efficiency for complete destruction of recalcitrant organic contaminants are desired. Attention shifts to advanced oxidation processes (AOPs) for removal of recalcitrant organic contaminants from waste waters even at low concentration (Mahamuni and Pandit, 2006).

AOPs possess the ability to mineralize organic compounds into simpler forms, which are biodegradable and enable their treatments in conventional processes and are cheaper than other processes. AOPs employ radical species such as $OH^{\bullet}$ in oxidising the pollutants to simpler forms, due to its high oxidation potential (2.8 eV). The $OH^{\bullet}$ radicals can be generated via: (i) photochemical irradiation with ultraviolet light with assistance of oxidising agents like O_3,

H_2O_2 and semiconductor), (ii) Fenton and photo-Fenton catalysis (iii) Electron beam irradiation technique and (iv) Sonolysis.

AOPs can be classified into 2 broad categories namely; homogenous and heterogeneous photocatalysis, which are based on different phases of catalyst and reacting species. These operations employ the ultra-violent spectrum range for degradation activities of volatile organic compounds. The ultra-violent spectrum is mainly divided into three bands: UV-A (315-400 nm), UV-B (280-315 nm) and UV-C (100-280 nm). Basically, UV-A and UV-C are used in environmental applications (disinfection of water and wastewater), while UV-A are known as long-wave radiation, long wavelength radiations or black light and UV-C is known as short wave radiations. UV-B is destructive in nature and possesses high energy to destroy biological tissues.

Table 2. 1 Hydroxyl radical generation in different Homogenous catalysis

Method	Key reaction	Drawbacks
UV/H_2O_2	$H_2O_2 + h\upsilon \rightarrow 2HO^{\bullet}$	(i) Low molar extinction co-efficient. (ii) Absorbs λ < 300nm, lesser component in solar radiation.
UV/O_3	$O_3 + h\upsilon \rightarrow O_2 + O(^1D)$ $O(^1D) + H_2O \rightarrow HO^{\bullet} + HO^{\bullet}$	Absorbs λ < 300nm, a lesser component in solar radiation.
$UV/O_3/H_2O_2$	$O_3 + H_2O + h\upsilon \rightarrow O_2 + H_2O_2$	Absorbs λ < 300nm, a lesser component in solar radiation.
Fe^{3+}/H_2O_2	$H_2O_2 + Fe^{3+} \rightarrow Fe^{2+} + {}^{\bullet}OH + OH^-$ $Fe^{2+} + H_2O + h\upsilon \rightarrow Fe^{3+} + {}^{\bullet}OH + H^+$	(i) The process is expensive. (ii) Sludge disposal problem during the operation. (iii) Continuous supply of feed chemicals needed.

2.1.1 Homogenous photocatalysis

Homogenous photocatalysis operates in a single phase for treatment of contaminated water and through application of oxidants such as: UV/H_2O_2, UV/O_3, $UV/O_3/H_2O_2$ and Photo-Fenton system (Fe^{3+}/H_2O_2) to generate radicals ($HO^{\bullet}$) in destroying the organic contaminants to simpler forms. However the oxidising power of H_2O_2 alone is weak, but the presence of UV light increases the oxidation strength via additional amounts of hydroxyl radicals involved in the degradation processes. Hydrogen peroxide can also enhance other AOPs (at low concentrations) as the molecule splits into 2 hydroxyl radicals. In Table 2.1 are key reactions and drawbacks of homogenous photocatalysis on degradation of volatile organic compounds.

2.1.2 Heterogeneous photocatalysis

Heterogeneous photocatalysis occur via more than one reaction process with the generation of oxidising species or free holes by appropriate UV light radiation on the photocatalyst semiconductor material. Organic pollutants can be mineralized via reaction with oxidizers to form carbon dioxide (CO_2), water (H_2O) and mineralized inorganic acids. This process employs near UV light radiation (λ < 380 nm) for destruction of organic compounds (Malato *et al*., 2002). Heterogeneous photocatalysis also employs both solid (semiconductor) and liquid phases for its operation. Heterogeneous photocatalysis utilization of light energy in the presence of solid catalyst makes it preferable for wastewater treatment as compared to homogenous process (Halmann, 1996). Semiconductor material applied as photocatalyst exists in the form of a powder suspended in water or fixed on a support material.

2.1.3 Principle of Heterogeneous photocatalysis

Metal semiconductor material plays a huge role in heterogeneous photocatalysis. They possess the specific electronic structure of the low energy valence band gap and a higher energy conduction band. The energy gap between the conduction band and valence band is called band gap energy. This energy gap falls in the UV-Visible region of the electromagnetic spectrum. Activation of semiconductor (Giolli *et al*., 2007) occurs via absorption of UV or Visible radiation, which results in promotion of the valence band (*VB*) electron to the conduction band (*CB*) with the generation of hole in the valence band (Mills *et al*., 1993) as depicted in Equation

2.1. The resulting hole is an oxidising agent and electron is a reducing agent. Both undergo recombination process at the surface or in the bulk of the particle within few nanoseconds.

$$SC + h\upsilon \rightarrow e^- + h^+ \quad 2.1$$

Both photo-generated electron hole pairs (e^-/h^+) initiate redox reactions, via oxidation of adsorbed water molecules and hydroxyl ions (electron donors) by photo-generated hole to give hydroxyl radicals as shown in Equation 2.2 & 2.3.

$$h^+ + OH^- \rightarrow OH^{\cdot} \quad 2.2$$

$$h^+ + H_2O \rightarrow OH^{\cdot} + H^+ \quad 2.3$$

Reduction of dissolved oxygen (electron acceptor) by the photogenerated electron results in super oxide anion radicals, which can lead to generation of peroxide (H_2O_2) via a series of redox reactions, which take place on oxidation of organic compounds.

$$O_2 + e^- \rightarrow O_2^{\cdot -} \quad 2.4$$

$$O_2^{\cdot -} + H^+ \rightarrow HO_2^{\cdot} \quad 2.5$$

$$O_2^{\cdot -} + H^+ + HO_2^{\cdot} \rightarrow H_2O_2 + O_2 \quad 2.6$$

The photo-generated H_2O_2 undergoes further decomposition on the catalyst surface in the presence of UV irradiation to yield the hydroxyl radicals. However, no significant contribution in generation of the hydroxyl radicals as compared in Equation 2.1 & 2.2.

$$H_2O_2 + e^{\cdot} \rightarrow 2HO^{\cdot} \quad 2.7$$

The superoxide and hydroxide radicals act as electron acceptors to prevent electrons and holes from recombining. In the presence of volatile organic compounds, hydroxyl, super anion radicals and hydrogen peroxide are strong oxidants capable of oxidative degradation reaction of these pollutants. Oxidation of organic compounds proceeds via free radical reactions, resulting in

several intermediates, which eventually yield total mineralization to carbon dioxide, water and inorganic ions (Guo *et al*., 2006) as depicted in Figure 2.1.

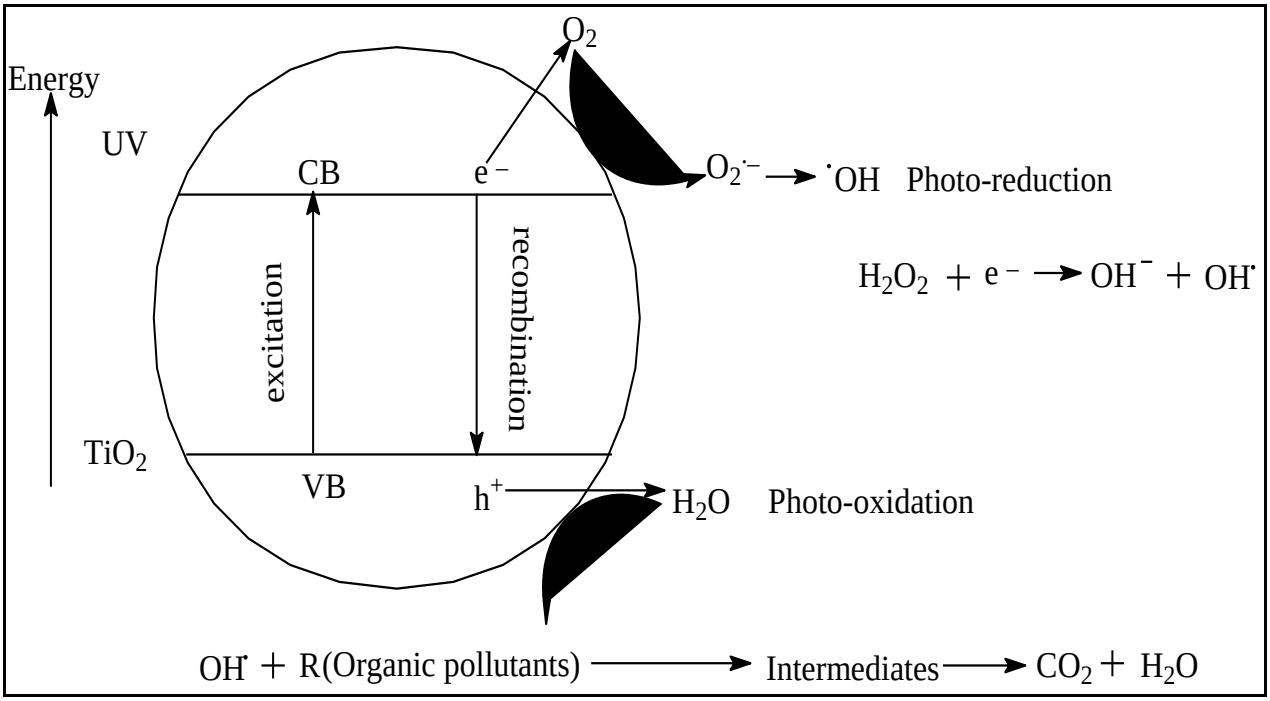

Figure 2. 1 Heterogenous photocatalysis on a semiconductor

2.2 Metal semiconductor for photocatalytic process

Metal semiconductor acts as photocatalyst in the overall reaction in the presence of light and it does not get consumed during reaction activity. Valence band of semiconductor must have higher oxidation potential than the material in consideration and stable over prolonged periods of time. Redox potential of the valence band and conductor band for different semiconductors varies between +4.0 and -1.5 volts versus normal hydrogen electrode (NHE). Metal oxides and sulphides represent classes of metal semiconductor applied for a photocatalytic process such as TiO_2, ZnO, ZrO_2, Fe_2O_3, CeO_2, WO_3, CdS, ZnS. An ideal photocatalyst must be (i) photoactive, (ii) biologically and chemically inert, (iii) excited in the visible and near UV light, (iv) photo stable (photo corrosion resistance) and (v) inexpensive and non-toxic (Bhatkhande *et al*., 2002). Band gap energies of employed metal semiconductors as photocatalyst are shown in Table 2.2.

Table 2. 2 Band gap and wavelength of Semiconductors

Semiconductor	Band gap (eV)	Wavelength (nm)
SnO_2	3.5	354
ZnS	3.7	335
ZnO	3.2	388
WO_3	2.7	459
TiO_2 (Anatase)	3.2	388
$SrTiO_3$	3.4	365
TiO_2 (Rutile)	3.0	413
CdS	2.4	517
Fe_2O_3	3.1	400
GaP	2.3	539
CdSe	1.7	729

Among these semiconductor materials applied for degradation organic compounds, TiO_2 has shown promising attributes for environmental applications :(Dheaya Alrousan *et al.*, 2009 and Byrne *et al*., 1998). ZnO possesses similarities to TiO_2 but dissolves in acidic solutions and instability in illuminated aqueous solutions (Neppolian *et al*., 2002). CdS adsorb large fractions of the solar spectrum than TiO_2 and forms chemically surface bound intermediates, but gets degraded during repeated catalytic cycles (Beydoun *et al*., 1999).

2.2.1 Titanium dioxide (TiO_2) Semiconductor

TiO_2 possesses vital application in commercial AOPs. This is ascribed to its low toxicity, natural abundance, low cost, high photoconductivity and other versatile applications. TiO_2 was discovery by William Gregor, on Cornwall beach, England in 1790s. It exists either as sulphate or chlorine form depending on the manufacturer (Reck and Richards, 1999). The sulphate form (ilmenite) found in metamorphic rock is further transformed into iron and titanium sulfates via reaction with sulphuric acid. Titanium hydroxide is precipitated by hydrolysis, filtered and calcined at high temperature. These seed crystals from alkaline hydrolysis together with chlorine will generate titanium tetrachloride, which is purified to yield pure TiO_2. It can also be applied as white pigment in paints, plastic, sun blocking material, cosmetics and paper products ascribe to its non-toxicity and stability. They play active roles in bone implants as biocompatible material,

while their optical and biological attributes make them suitable as UV protection materials (Gasparro *et al*., 1998).

TiO_2 exhibit different photocatalytic activities towards organic compounds under similar conditions (Serpone *et al*., 1996). Such differences are ascribed to differences in morphology, crystal phase, specific area, particle aggregate size, presence of impurities and surface density of OH^- groups in the TiO_2 materials. Three polymorphs of TiO_2 are Anatase (tetragonal), rutile (tetragonal) and Brookite (orthorhombic). Aside from these crystalline forms, two high-pressure TiO_2 exists from rutile (TiO_2 (II) with PbO_2 structure) and TiO_2 (H) with the hollandite structure. These three polymorphs differ in their crystal structure by distortion of each TiO_2 octahedral and their assembly patterns (Beydoun *et al*., 1999). Anatase TiO_2 constitutes of octahedral connected by vertices and corresponds to tetragonal symmetry (Fig 2.2a). Rutile TiO_2 connected by edges and mainly used in white pigment in paint (Fig 2.2b). Brookite TiO_2 connected by both vertices and edges, orthorhombic crystalline structure (Fig 2.2c).

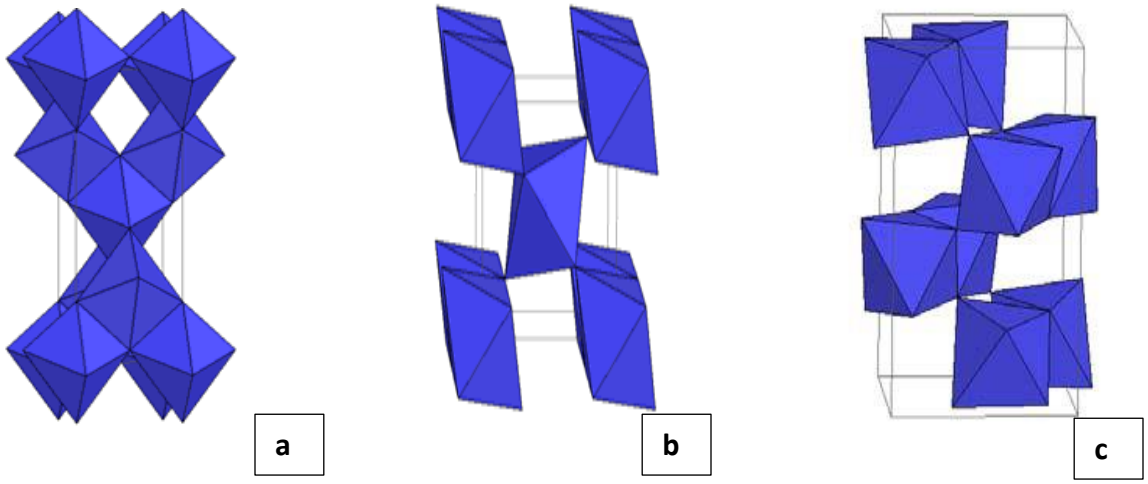

Figure 2. 2 Crystal structure of anatase (a) rutile (b) and brookite (c)

Anatase (3.2 eV) and rutile (3.0 eV) are widely applied in wastewater treatment, but anatase TiO_2 being more photoactive than rutile. Anatase is thermodynamically less stable than rutile, but its form kinectically favoured at lower temperature (< 600 ^oC), possess a high surface area and density for adsorption and catalysis activities.

2.2.2 Titanium dioxide preparation

TiO_2 can be prepared in the form of powder, crystals or thin films, liquid or gas phase method. Thin films are produced via gas phase methods, where main techniques include chemical vapour deposition (CVD), physical vapor deposition (PVD) (Giolli *et al*., 2007) and spray pyrolysis deposition (SPD) (Bellardita *et al*., 2007). New techniques based on vapor-phase deposition such as ion implantation (Bellardita *et al*., 2007), sputtering (Hidalgo *et al*., 2007), molecular beam epitaxy (Xie and Shang, 2007) and dynamic ion beam mixing (Andersson *et al*., 2007) offer control of film growth. They also produce pure materials but consumption of high energy is a disadvantage. Solution routes can also form thin films and powders, with the ability to produce homogenous materials, the formation of complex shapes and composite materials. Long time processing, expensive precursors and the presence of carbon impurities are part of challenges to these routes mentioned above.

TiO_2 liquid phase preparation includes precipitation and co-precipitation, solvothermal and hyrdothermal (Xie and Shang, 2007), microemulsion (Andersson *et al*., 2007), combustion and electrochemical synthesis (Kitamura *et al*., 2007 and Sankapal *et al*., 2006) and sol-gel method (Kolen´ko *et al*., 2005). Sol gel method has been widely employed for the synthesis of TiO_2 thin films, powders and membranes (Reddy *et al*., 2003).

2.2.3 Sol-Gel Method

Sol-gel method allows better control of texture, composition, homogeneity than crystallization or precipitation. The structural properties of final products can be controlled by adjusting the parameters i.e acidity, ageing temperature (Reddy *et al*., 2003). This method allows introduction of other solid phases into the TiO_2 matrix to form composites and also dopant species resulting in TiO_2-doped materials (Tong *et al*., 2008) with ease of control. This method is considered as “Chime douche” or soft chemical approach to metastable oxide material synthesis (Schubert and Hüsing, 2005). Sol-gel methods offer more prospects than other techniques by operating in mild chemical conditions, hydrolysis and condensation are catalysed by acids and bases. Sol-gel materials found applications as catalyst, ceramic fibres, electroceramic powders, insulating materials, high purity glasses. These processing options allow unique access to multicomponent oxide systems. Highly porous and nanocrystalline materials can be obtained via this process. Pore size and mechanical strength is achieved via controlled ageing and drying conditions.

A sol known as stable suspension of colloidal solid particles or polymers in a liquid, can be amorphous or crystalline. A gel is made up of porous, three-dimensionally continuous solid network surrounding and supporting a continuous liquid phase (wet gel). In colloidal gels, the network is made up of agglomeration of dense colloidal particles, while polymeric gels possess a polymeric sub-structure comprises of aggregation of sub-colloidal chemical units. The Sol-gel method employs two routes for TiO_2 precursor : the non-alkoxide (inorganic) and the alkoxide (organic) route. The non-alkoxide rate applies inorganic salts such as nitrates, chlorides, acetates, carbonates, acetyacetonates and the additional step of removal of inorganic anion is required (Sivakumar *et al*., 2004). The alkoxide route (widely employed) uses metal alkoxides like titanium ethoxide, titanium isopropoxide and titanium -n- butoxide as precursors.

The alkoxide route involves formation of TiO_2 sol or gel, or precipitation by hydrolysis and condensation of titanium alkoxides. However, hydrolysis and condensation steps are separated for desirable control of solid material and acid catalysis can be employed for this separation. Acid catalysis increase hydrolysis rates resulting in formation of crystalline powders from fully hydrolysed precursors. Base catalysis promote condensation to obtain amorphous powders, possessing unhydrolyzed alkoxide ligands. These reaction are preceded by thermal treatment to remove the organic part and promotes crystallization either in anatase or rutile phase. TiO_2 can come in nanosizes structures like nanowires (Zhang *et al*., 2002), nanotubes (Macak *et al*., 2007), nanorods (Pan *et al.*, 2007) and nanoribbons (Pan *et al*., 2007).

$$Ti(OR)_4 + xH_2O \leftrightarrow Ti(OH)_{4-x}\,OH_x + xROH\ (Hydrolysis) \quad 2.8$$

$$Ti(OH)_{4-x}\,OH_x + Ti(OR)_4 \leftrightarrow (OR)_{4-x}\,TiO_x\,Ti(OR)_{4-x} + xROH\ (Condensation) \quad 2.9$$

2.3 Organic micro pollutant

Organic micro pollutants represent major challenges worldwide and are found in every part of the environment such as soil, groundwater, surface water and plants. Industrialization forms bulk of activities that pollutes water and air, due to their toxicity, carcinogenic and mutagenic impact of these compounds on ecosystem at large (Busca *et al*., 2008). Volatile organic compounds (VOCs) are chemical compounds that possess vapour pressure under normal conditions to vapourize and enter the ecosystem at will. Volatile organic compounds according

to European Union legislation represents organic compounds with boiling points within 50 to 250 ^{o}C measure at 101.3 kPa (Lim *et al*., 2008) and some of these VOCs (Table 2.3) have been degraded by TiO_2 in wastewater (Herrmann, 1999).

Table 2. 3 Volatile organic compounds degraded by TiO_2

Volatile Organic Compounds	Examples
Alkanes and Haloalkanes	Methane, isobutene, pentane, cyclohexane, chloromethane, tetrachloroethane.
Aliphatic alcohols	Methanol, isopropanol, cyclobutanol, glucose
Carboxylic acids	Formic, oxalic, malic, benzoic, salicyclic, phthalic, butanoic
Alkenes and Haloalkenes	Propene, cyclohexene, hexafluoropentene, 1,2-dichloroethylene, perchloroethene
Phenolic compounds	4-chlorophenol, 4-fluorophenol, pentachlorophenol
Dyes	Methylene blue, eosin B, methyl orange, rhodamine B

2.4 Factors affecting Photocatalysis

Photocatalysis involves complex participants such as water, organic substrate, photocatalyst, light and oxygen. However, operational parameters affect efficiency of the photocatalytic process. These factors include the pH of the medium, catalyst loading, substrate concentration, light intensity and oxygen pressure. Meanwhile, physical and chemical properties of photocatalyst may affect the efficiency in the photocatalytic process. TiO_2 crystal composition surface area, crystalline dimensions and the presence of surface hydroxyl groups influence the efficiency of the photocatalyst in the reaction process and are discussed briefly below:

(i) **Catalyst loading** represents the amount of TiO_2, which is directly proportional to overall photocatalytic reaction rate. The reaction rate becomes independent of the mass of catalyst above a certain amount. This corresponds to a maximum amount of

TiO_2 that all particles are totally illuminated. Most photoreactors are operated at the catalyst concentration that guarantees efficient photons absorption (Herrmann, 2005) and prevents dark zones within the reactor.

(ii) **pH** depends on isoelectric point or surface charge of the photocatalyst and the substrate employed, which in turn affects the adsorption process. The variation of pH affects TiO_2 surface speciation due to the point of zero charge which lies in the range of 4.5-7.0 (Herrmann, 2005). Under acidic or alkaline situations, the surface of TiO_2 can be protonated or deprotonated respectively.

(iii) **Temperature** has little or no effect on the reaction process due to photonic activation. Though, increase in the reaction temperature (> 80 ^oC) promotes electron recombination of electron hole charges (Gaya and Abdullaha, 2008). Adsorption of the organic contaminants on TiO_2 surface at temperature (< 80 ^oC), results in the kinetics following Langmuir-Hinshelwood model. The absence of heating is cost efficient because water itself has high heat capacity.

(iv) **Dissolved oxygen** is strongly electrophilic in the photocatalytic process and its increase reduces unfavourable electron/hole recombination rates. Higher concentrations results in a downturn of the reaction rate, ascribed to TiO_2 surface highly hydroxylated. This furthers inhibits adsorption of pollutants at active sites.

(v) **Substrate concentration** with different initial concentration of organic pollutants requires different irradiation time for complete mineralization under the same operating conditions. High concentration of organic compounds could saturate the TiO_2 surface and block the UV light reaching the catalyst's surface.

(vi) **Light wavelength** must have sufficient energy to promote electron hole formation. Therefore, UV light with wavelength < 388 nm is required for activation of TiO_2, because the activation threshold of TiO_2 occurs at 388 nm.

(vii) **Light intensity** is proportional to radiant flux, forms major factor in reactor design and also a source of light. The degradation rates follow two distinct regimes with respect to radiant flux: a first-order regime for low photon flux and half-order regime for high

intensities (Ollis, 2005). Electron/hole pairs are consumed more rapidly by chemical reactions in first-order regime, electron/hole recombination dominates in the half-order regime.

2.4.1 TiO_2 structural properties

2.4.1.1 Crystal structure

It affects photodegradation efficiency and anatase TiO_2 is the most active polymorph as compared to rutile and brookite. Anatase TiO_2 high surface area contributes to its superior efficiency (Zhang *et al*., 1998) . The enhanced catalytic activity might results from the pore size distribution and crystal plane on which adsorption takes place.

2.4.1.2 Surface area

The surface area of a solid catalyst is directly related to the concentration of active sites for adsorption and reaction. A large surface area enhances the adsorption of organic compounds which promotes the reaction rate. Though the higher surface area is associated with large amounts of crystal lattice defects which can result in recombination of electron-hole pairs (Ayllón *et al*., 1999). There is a need for balance between surface area and crystallinity for maximum photoactivity.

2.4.1.3 Particle dimensions

Particle size and crystallinity dimension determine the activity of metal semiconductor in the overall reaction, which makes the recombination process dependent on them (Zhang *et al*., 1998). The physical and chemical attributes of metal semiconductor are changed when in nanometre-size range, as compared to bulk size dimensions (Li *et al*., 2004). Small variations in particle size affect the surface/bulk ratio, thereby changing the importance of volume and surface electron/hole recombination processes. Higher photocatalytic efficiency results from smaller particle size.

2.5 Kinetics and Photocatalytic reactor

Aside from chemical and physical factors that affects the reaction rates for enhanced photodegradation efficiency and optimization during degradation. The degradation rates of organic pollutants have been modelled by different kinetic models and Langmuir-Hinshelwood (L-H model) kinetics describe the reaction rates very well (Abdullah *et al*., 1990 and Matthews, 1990). The model is described below in Equation 2.10:

$$r = \frac{dC}{dt} = \frac{k \cdot K \cdot C}{1 + K \cdot C} \qquad 2.10$$

In an ideal situation, *C* is the bulk solute concentration; *k* is the reaction rate constant, *K* is the Langmuir adsorption constant and t is the time. The L-H rate constants applicable for comparison of reaction rate under different experimental conditions. The disappearance of reactant can be evaluated when other factors are held constants, once *k* and *K* have been evaluated. At lower concentrations, L-H model reduces to a pseudo first order expression in Equation 2.11 and applicable to many photocatalysis reactions (Gemeay *et al*., 2007).

$$In\left(\frac{C}{C_o}\right) = k \cdot K \cdot t = k_1 \cdot t \qquad 2.11$$

The organic pollutants in low concentration rate for the reaction rates to follow pseudo first order kinetics. However, the k reaction rate constant is dependent of UV intensity, pH, catalyst loading, geometry of the photo-reactor and initial concentration.

Photocatalytic reactors for wastewater treatment are made up of two configurations, i.e. slurry (Alfano *et al.*, 2000) and immobilised photo-reactor (Dionysiou *et al.*, 2000a and Dionysiou *et al*., 2000b). In the slurry reactors, TiO_2 particles are suspended in the contaminated water and mostly used in photocatalytic waste water treatment with higher photocatalytic activity. This reactor maintains fairly uniform catalyst distribution; minimize catalyst fouling effects and has no mass transfer limitations. Light scattering however lowers the efficiency of the treatment operation and post treatment for separation of nano-sized TiO_2 from wastewater is very costly (Gemeay *et al*., 2007) .

Immobilized photoreactors allow continuous use of photocatalyst, solving the issue of nano-sized TiO_2 post separation. In this reactor, catalyst is coated on the reactor wall round the light source or fixed to a support material. However, challenges of (i) mass transfer limitations, (ii) catalyst fouling or wash out, (iii) low surface to volume ratio and (iv) significant pressure drop limits its application.

2.6 Photocatalysis coupled with other operations

Heterogeneous photocatalysis has been combined with other physical or chemical processes to increase the overall photodegradation process. They result in increased photodegradation efficiency and decrease reaction time in respect to separated operations. They also reduce the cost of consumption of light energy, as found in heterogeneous photocatalysis with enormous light consumption. They are divided into two categories: operation that affects the catalytic process thus improving the efficiency, when coupled with ultrasonic irradiation, ozonation. The other operation that does not affect the catalytic rate thus improves overall reaction, when coupled with biological treatment, membrane reactor and membrane photo-reactor.

2.7 Surface modifications of TiO_2

The overall photocatalytic activity of the catalyst is determined by several factors such as its stability, efficiency, selectivity and wavelength response. The development of metal semiconductor materials capable of using natural sunlight for degradation of both organic and inorganic compounds is in vogue. However TiO_2 has always been employed for degradation of organic pollutants, but possess three limitations that affect its efficiency namely:

(a) Low photo-ionic yield of the degradation process;
(b) Wide band gap energy of 3.2 eV requiring excitation in the UV region for activation of the operation, which is less than 10% of the overall solar intensity (Linsebigler *et al*., 1995).
(c) Challenge of separation of photocatalyst from treated water poses a major constraint.

Furthermore, rapid aggregation of TiO_2 in solutions due to its smaller size and poor adsorbent for non-polar compounds are part of the challenges of TiO_2 application for degradation of organic contaminants in aqueous solution. In recent years, a great deal of activities has being performed in improving TiO_2 photocatalytic efficiency:

(i) Incorporation of energy levels in the band gap of TiO_2

(ii) Changing life time of charge carriers

(iii) Substitution of Ti^{4+} with cation of same size

(iv) Shifting of the conduction band and valence band to enable photo-excitation at lower energies.

These major activities can be achieved via catalyst modification by doping metal and non-metal ion into the TiO_2 lattice, dye photosensitization, deposition of noble metals, coupling with other semiconductors and addition of support materials.

2.7.1 TiO_2 Doping

In photocatalysis, the chemical composition of TiO_2 can be altered via doping with metals and non-metals to enhance the photocatalytic reaction. The main purpose of doping is to induce a batho-chromic shift (decrease of the band gap) which results in more visible light adsorption. The dopant ions can be adsorbed on the catalyst, incorporated into the interior of TiO_2, or form separate oxide phases. The dopant ions acts as the hole and electron traps, they occupy either as lattice (substitutional) or interstitial sites once inside the TiO_2 particle. A dopant ion will lengthen lifetime of generated charge carriers as an electron trap, resulting in enhanced photoactivity of catalyst. However, if electron is trapped in deep trapping site, lower redox potential can occur with decrease in photo-efficiency (Li and Li, 2002).

Concentration largely affects dopant in the TiO_2 matrix. An increase in concentration of dopant results in narrower space-charge regions and electron/hole pairs separated efficiently by the large electric field before recombination. The space-charge region becomes narrower and penetration of light into TiO_2 space-charge layer, when the concentration is higher. This further increase recombination of electron/hole in the catalyst especially when no driving force exists in separation. Heterocations of valences lower than Ti^{4+} (p-type dopants) act as electron acceptors which traps photoelectron and once negatively charged attract holes, thus forming recombination centres (Liu *et al*., 2008). On the contrast, Heterocations with valences higher than Ti^{4+} (n-type dopants) act as donor centres. Various metals have been doped with TiO_2 such as Sn^{4+}, Au^{3+}, Bi^{3+}, Mg^{2+} e.t.c (Cao *et al*., 2004 and Li and Li, 2002) and non-metals like B,

C, N, V and S also been doped into TiO_2 nanomaterial (Bettinelli *et al*., 2007 and Burda *et al*., 2003).

2.7.2 Metal deposition

Metal addition to the TiO_2 matrix also changes the photocatalytic process via alternation of semiconductor surface properties. The electron gets removed from the TiO_2 particle in the presence of each metal particle, when the work function of metal is higher than that of titania. This leads to the formation of a Schottky barrier at metal semiconductor surfaces, which leads to decrease in electron/hole recombination and efficient charge separation (Ayllón *et al*., 1999). This enhances reaction rates by accelerating the transfer of electrons to dissolved oxygen molecules, when metals are being deposited. This paves way for ease of deposition of group III metals and noble metals on the catalyst surface, also for enhanced electron transfer rates to oxygen and quantum yield. The enhancement of TiO_2 activity was discovered in photo-conversion of water into H_2 and O_2 employing the Pt/ TiO_2 system (Sato and White, 1980). That leads to further applications of other metals doping with TiO_2 such as Ag, Pd, Cr, Fe, Cu (Sobana *et al*., 2006, Kryukova *et al*., 2007).

2.7.3 Composite Semiconductors

They provide easier ways to increase photocatalytic process by increasing charge separation and extending energy range of photo-excitation of the system. This occurs via coupling a large band gap semiconductor with a smaller one with suitable potential energies. TiO_2/CdS represents a scenario, where a small portion of excitation energy exists for TiO_2 and large energy for excitation from the valence band for CdS in the conduction band. The photogenerated electrons in CdS are transferred into the TiO_2 matrix while holes remain in the CdS particle, which allows charge separation by isolating electrons and holes in two distinct materials at the same time. They also increase the photo response of photocatalyst in the visible (Bessekhouad *et al*., 2006).

Two cases are common: (i) only one semiconductor can be illuminated and (ii) the second case occurs when both metal semiconductors are illuminated. In the first scenario, a photoelectron generated on the active semiconductor with a more negative conduction band is injected into the conduction band of the inactivated metal semiconductor. The generated photo hole remains

on the activated one. Transfer of electrons and holes from one semiconductor to another occurs, in the case of both semiconductors illuminated. This results in accumulation of electron in the lower lying conduction band of one metal semiconductor, while accumulation of holes occurs at the other metal semiconductor (Lin *et al*., 2008). Composite metal semiconductor system exhibits higher degradation rates and widely employed in degradation of organic compounds in aqueous and gas phase such as TiO_2/CdS, TiO_2/SnO_2, TiO_2/ZnO (Bessekhouad *et al*., 2006, Lin *et al*., 2008).

2.7.4 Surface sensitization

Surface sensitization of wide band gap semiconductor through chemisorbed or physisorbed dyes/metal complexes will increase efficiency of excitation activity by extending its absorption in the visible region of the spectrum. They employ a wavelength range resulting from of excitation of the sensitizer proceeding with charge transfer between excited dye and semiconductor conduction band. The dye can act as donors or electron acceptor irrespective of its redox environment. This depends on favourable conduction band energy level of semiconductor in accordance with the oxidative energy level of the excited dye molecule. Here, the surface behaves as quencher by accepting electrons from excited dye molecule and in turn reduces organic molecules adsorbed on the surface. They can also react with surface adsorbed O_2 resulting in superoxide radical which furthers protonates to form the peroxide radicals. These radicals can initiate degradation of organic compounds aside from hydroxyl radicals. Common dyes employed as sensitizers include Erythrosin B dye (Kamat, 1993), Thionine (Patrick and Kamat, 1992), Thionine and Eosin (Chatterjee and Mahata, 2001c) and analogs of $Ru(bpy)_3^{2+}$ (Vlachopoulos *et al*., 1988).

2.7.5 TiO_2 composite catalysts

Vast photocatalytic degradation of organic compounds using photocatalyst is in the form of fine particles in liquid phase, but challenges of separation of TiO_2 from solution is a major issue that hinders TiO_2 industrial application. In avoiding the cost of removing the particles from treated water, immobilization of TiO_2 on the support layer with high activity and effective separation attributes constitutes major priority. Composite catalyst focused on increasing the illuminated specific catalyst area and to facilitate separation of catalyst. Immobilization also increases

adsorption capacity and surface area of photocatalyst; enhance photocatalytic activity through synergies of TiO_2 and the support material.

These composite materials can be obtained via coupling prepared TiO_2 with a support or by in situ generation. Spray coating, immobilization in a polymer matrix and electro-photo deposition represents techniques employed in coupling with prepared TiO_2. The in situ generation occurs via coating of support, wet chemical impregnation, and chemical vapourization of $TiCl_4$ e.t.c. High surface materials have been used as a support layer for TiO_2 in photocatalytic reaction. TiO_2 has been affixed to materials such as silica, glass (Mathews, 1987), stainless steel mesh (Yoshida *et al*., 1999), alumina (Torres *et al*., 2007), zeolites (Bhattacharyya *et al*., 2004), ceramics (Ménesi *et al*., 2008), activated carbon (Sheikh *et al*., 2004 and Tryba *et al*., 2003), carbon fibers (Liuxue *et al*., 2006 and Yuan *et al*., 2007).

However, zeolites with its intrinsic large surface area, internal pore volume, uniform pores and channel size are perfect host for immobilization of TiO_2 on their surface (Liu *et al*., 1993, Chen *et al*., 2002 and Corma and Garcia, 2004). Zeolites possess other attributes such as (i) full photochemical stability and chemical inertness; (ii) transparent to UV-Visible light above 250 nm, thus allowing penetration of light onto the solid powder; (iii) high adsorption for organic contaminants from solution at active sites of the photocatalyst; (iv) polarizing strength inside its pores by virtue of its different nature of internal charge balancing cations and size of the channels; (v) ability to act as electron acceptor or donor in the electron transfer process (Corma and Garcia, 2004). For enhanced activity of TiO_2-supported zeolites, several preparation techniques such as mechanical mixing or paper making techniques (Hashimoto *et al.*, 2001 and Ichiura *et al*., 2000), chemical vapour deposition (Ding *et al*., 2001) and cation exchange (Kim and Yoon, 2001) has been applied to create Ti-O-Si bonds.

2.8 Zeolites

Zeolites as synthesized or naturally occurring aluminosilicates of group IA and IIIA elements such as sodium, potassium, magnesium, calcium (Armenta *et al*., 2001) with three dimensional framework structure bearing AlO_4 and SiO_4 tetrahedral. The aluminosilicates is the most stable and defines the structure of zeolites. They are linked together by sharing of oxygen ions to form interconnected cages and channels. This framework structure contains channels or

interconnected voids that are occupied by cations and water molecules. The cations are mobile and undergo ion exchange. The water can be easily removed reversibly via application of heat.

Zeolite structural formula best shown in the crystallographic unit cell as:

$$Ma_{x/n}\ ((AlO_2)_x\ (SiO_2)_y\ (wH_2O)$$

M is the cation of valence of *n*, *w* is the number of water molecules; ratio *y/x* is for Si/Al ratio which depends on their structure. The sum *(x+y)* is the total number of tetrahedral in the unit cell. The [$(AlO_2)_x\ (SiO_2)_y$] represents the framework composition. However, zeolites in their empirical formula are best shown as:

$$M_{2/n}O.\ Al_2O_3.xSiO_2\ .\ yH_2O$$

In this oxide nature, *x* is generally equal to or greater than 2 since AlO_4 tetrahedra are joined only to SiO_4 tetrahedra, *n* is the cation valence. The primary building units are aluminium and silicon tetrahedral as shown below in Figure 2.3 (Breck, 1974).

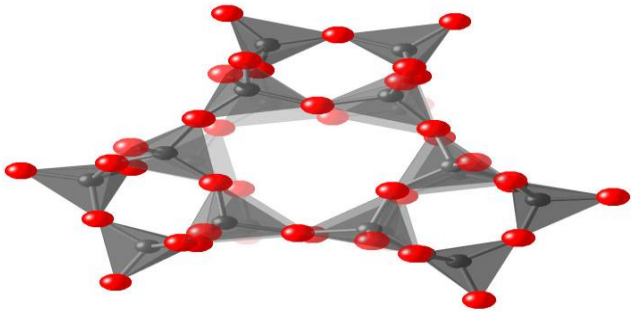

Figure 2. 3 An $[SiO_4]^{4-}$ or $[AlO_4]^{5-}$ tetrahedra (primary building unit)

Zeolites ability to behave as molecular sieves for separation of molecules based on size, configuration of the molecule relative to the size makes it superior over other crystalline inorganic oxide materials. Zeolites can also adsorb molecules with permanent dipole moment with selectivity as compared to other adsorbents. Zeolites possess vast application in ion

exchange reactions (waste water treatment) and also catalyse organic reactions, based on their high thermal stability and internal acidity.

Zeolites exist as natural and synthetic forms. Studies revealed that 150 kinds of synthetic zeolites exists and 45 different framework topologies for natural zeolites. However, use of synthetic zeolites are limited in areas of environmental application and cost effectiveness. Both natural and synthetic zeolite differs in so many ways such as:

- Natural zeolites occur through geological process, while synthetic manufactured from chemical materials with carbon footprint
- Natural zeolites possess higher silica to alumina ratio than synthetic zeolites
- Natural zeolites are resistant to acidic conditions, while synthetic ones ruptures in mildly acidic environments

These natural zeolite minerals are thermally stable and resistant to radiation (Faghihian *et al*., 1999) and properties of these natural zeolites depends on their geographic location, temperature and ash/water imparts different elemental composition in these different zeolites. Natural zeolites are attracting interest due to their layered or porous structure, lower cost and abundance in nature to synthetic zeolites (Li *et al*., 2005). For natural zeolites to be at par with synthetic ones, their physico-chemical properties have to be fine-tuned via ion exchange with simple inorganic salts and alkali bases, acid leaching, steaming and high temperature calcination (Cakicioglu-Ozkan and Ulku, 2005).

Dealumination or decationisation of natural zeolites influences exchange and removal of traces of Mg^{2+}, Na^{+}, Ca^{2+}, K^{+} embedded in the cavities of natural zeolites. Dealumination enhances reformation of pore structure, increases surface area of natural zeolites and contributes largely to removal of amorphous Al-species (Elaiopoulos *et al*., 2008). Dealumination influences breaking of Al–O bonds, as well as a loss of crystallinity, particularly at the low Si/Al ratios when treated with acid leaching. Some of the natural zeolite includes chabazite, clinoptilolite, analcime, phillipsite, ferrierite, heulandite and mordenite. Clinoptilolite is the most abundant among these natural zeolites and found in huge deposits around the world.

Clinoptilolite (CP) is the most abundant natural zeolite and member of heulandite group of natural zeolite, being isostructural with heulandite zeolite but differ in properties. Clinoptilolite

has higher Si/Al ratio > 4, while heulandite has Si/Al < 4 (Hernandez, 2000). Clinoptilolite possess higher thermal stability (> 500 ^{o}C) due to the bond between Si and O that is stronger than Al-O bonds, as compared to heulandite which undergoes structural collapse at 350 ^{o}C. Clinoptilolite in terms of cation content possess alkali cation dominant [(Na+K) > Ca], while heulandite have alkaline cation dominant [(Ca > (Na+K)] (Zhao *et al.*, 1998). Clinoptilolite contains less water as compared to heulandite (Smyth *et al*., 1990). Clinoptilolite chemical composition appropriately expressed as:

- Oxide formula: $(K,Na,1/2Ca)_2\ O{\cdot}Al_2O_3{\cdot}10SiO_2{\cdot}8H_2O$
- Idealized formula: $(K_2,Na_2,Ca)_3\ [(Al_6Si_{30}\ )O_{72}]{\cdot}24H_2O$

Though, exchangeable cations such as K^+, Na^+, Ca^{2+} and Mg^{2+} are the most common charge balancing cations present in the clinoptilolite, with small amount of Fe^{3+} found in the clinoptilolite mineral. Clinoptilolite atomic structure is based on three dimensional frameworks of silica and alumina tetrahedra. Each of the oxygen atoms in the tetrahedron is bonded to two adjacent silicon or aluminium ions linking them together. However, Si/Al ratio varies between 4 and 5.5, low silica members are enriched with calcium, while high silica clinoptilolite are enriched with potassium, sodium and magnesium.

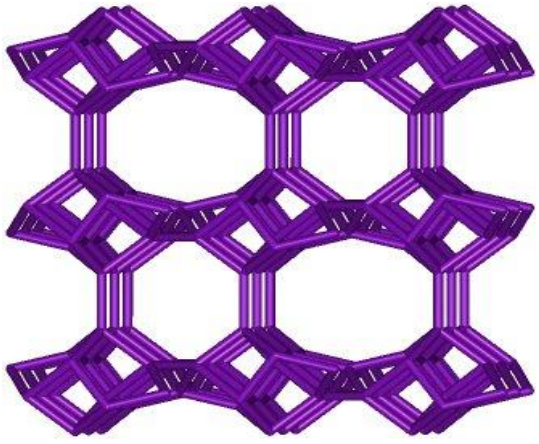

Figure 2. 4 Model framework structure of Clinoptilotile

Clinoptilolite found application in gas cleaning, waste water purification, agriculture and aquaculture, fertilizers, animal health and nourishment, gas separation and cleaning of

radioactive wastes. These applications rely on its adsorptive, ion exchange and catalytic properties.

2.9 Organic compounds employed in this present study.

Azo dyes represents 70% of dyes applied in major industries worldwide, especially among classes of dyes such as acidic, basic, neutral, disperse, direct and reactive (Fu and Viraraghavan, 2002). Approximately 15% of these dyes are being lost during synthesis and through waste water, which are toxic, carcinogenic (Cisneros *et al*., 2002) to human health and ecosystem at large. Decolourization of these dyes is of paramount before discharge into the environment. Azo dyes can be classified into monoazo, diazo, triazo according to the presence of one or more azo bonds.

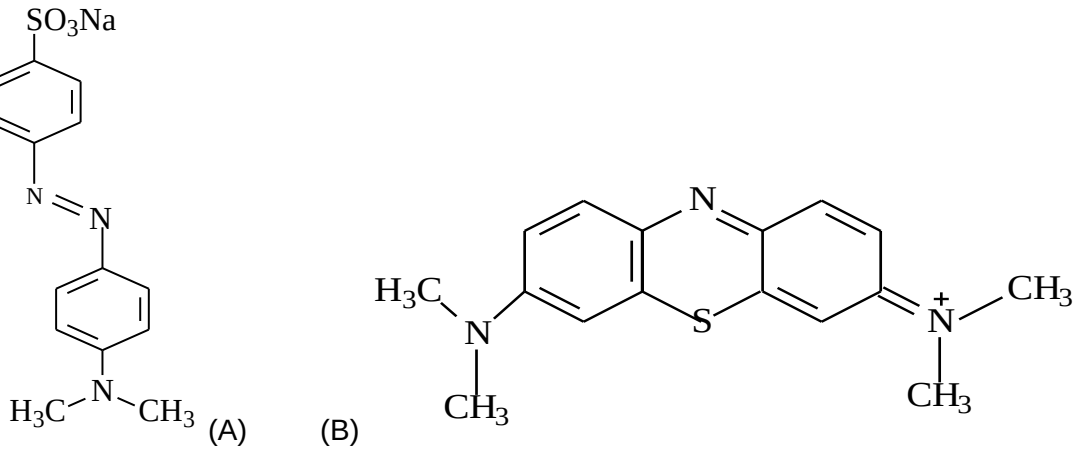

Figure 2. 5 Chemical structure of (a) Methyl orange and (b) Methylene blue

Methyl orange (MO) and Methylene blue (Bettinelli *et al*., 2007), azo dyes were chosen as our model organic compound to determine the photocatalytic efficiency of synthesized photocatalyst. The structure of the MO and MB are depicted respectively in Figure 2.5. The relative performance of supported photocatalyst to bare TiO_2 on degradation of mixture of MO and MB will be compared.

References

ABDULLAH, M., LOW, G. & MATTEWS, R. W. (1990) Effects of common inorganic anions on the rates of photocatalytic oxidation of organic carbon over illuminated titanium *J. Phys. Chem. B,* **94,** 6820-6825.

ALFANO, O. M., BAHNEMANN, D., CASSANO, A. E., DILLERT, R. & GOSLICH, R. (2000) Photocatalysis in water environments using artificial and solar light. *Catal. Today,* **58,** 199-230.

ANDERSSON, M., KISELEV, A., OSTERLUND, L. & PALMQVIST, A. E. C. (2007) Microemulsion mediated room-temperature synthesis of high-surface-area rutile and its photocatalytic performance. *J. Phys. Chem. B,* **111,** 6789-6797.

ARMENTA, G. A., RAMIREZ, G. H., LOYOLA, E. F., CASTANEDA, A. U., GONZALES, R. S., MUNOZ, C. T., LOPEZ, A. J. & CASTELLON, E. R. (2001) Adsorption kinetics of CO_2, O_2, N_2, and CH_4 in cation-exchanged clinoptilolite. *J. Phys. Chem. B,* **105,** 1313-1319.

AYLLÓN, J. A., FIGUERAS, A., GARELIK, S., SPIRKOVA, L., DURAND, J. & COT, L. (1999) Preparation of TiO_2 powder using titanium isopropoxide decomposition in a plasma enhanced chemical vapor deposition (PECVD) reactor. *J. Mater. Sci. Lett.,* **18,** 1319-1321.

BELLARDITA, M., ADDAMO, M., PAOLA, A. & PALMISANO, L. (2007) Photocatalytic behaviour of metal-loaded TiO_2 aqueous dispersions and films. *Chem. Phys.,* **339,** 94-103.

BESSEKHOUAD, Y., CHAOUI, N., TRZPIT, M., GHAZZAL, N., ROBERT, D. & WEBER, J. V. (2006) UV-vis versus visible degradation of Acid Orange II in a coupled CdS/TiO_2 semiconductors suspension. *J. Photochem. Photobiol. A: Chem.,* **183,** 218-224.

BETTINELLI, M., DALLACASA, V., FALCOMER, D., FORNASIERO, P., GOMBAC, V., MONTINI, T., ROMANÒ, L. & SPEGHINI, A. (2007) Photocatalytic activity of TiO_2 doped with boron and vanadium. *J. Hazard. Mater.,* **146,** 529-534.

BEYDOUN, D., AMAL, R., LOW, G. & M_CEVOY, S. (1999) Role of nanoparticles in photocatalysis. *J Nano. Res.,* **1,** 439-458.

BHATKHANDE, D. S., PANGARKAR, V. G. & BEENACKERS, A. (2002) Photocatalytic degradation for environmental applications a review. *J. Chem. Technol. Biotechnol.,* **77,** 102-116.

BHATTACHARYYA, A., KAWI, S. & RAY, M. B. (2004) Photocatalytic degradation of orange II by TiO_2 catalysts supported on adsorbents. *Catal. Today* **98,** 431-439.

BLUE PLANET NETWORK. (2006) The facts about the global drinking water crisis.

BRECK, D. W. (1974) Zeolite Molecular Sieves. *Wiley-Interscience Publication*.

BURDA, C., LOU, Y. B., CHEN, X. B., SAMIA, A. C. S., STOUT, J. & GOLE, J. L. (2003) Enhanced nitrogen doping in TiO_2 nanoparticles. *Nano Lett.,* **3,** 1049-1051.

BUSCA, G., BERARDINELLI, S., RESINI, C. & ARRIGHI, L. (2008) Technologies for the removal of phenol from fluid streams: a short review of recent developments. *J. Hazard. Mater.,* **16,** 265-288.

BYRNE, J. A., EGGINS, B. R., BROWN, N. M. D., MCKINNEY, B. & ROUSE, M. (1998) Immobilisation of TiO_2 powder for the treatment of polluted water. *Appl. Catal. B: Environ.,* **17,** 25-36.

CAKICIOGLU-OZKAN, F. U. & ULKU, S. (2005) The effect of HCl treatment on water vapour adsorption characteristics of Clinoptilolite rich natural zeolite.*Micro. Meso. Mater.,* **77,** 47.

CAO, Y. A., YANG, W. S., ZHANG, W. F., LIU, G. Z. & YUE, P. L. (2004) Improved photocatalytic activity of Sn^{4+} doped TiO_2 nanoparticulate films prepared by plasma-enhanced chemical vapor deposition. *New J. Chem.,* **28,** 218-222.

CHATTERJEE, D. & MAHATA, A. (2001) Demineralization of organic pollutants on the dye modified TiO_2 semiconductor particulate system using visible light. *Appl. Catal. B: Environ.,* **33,** 119-125.

CHEN, J., EBERLEIN, L. & LANGFORD, C. H. (2002) Pathways of phenol and benzene photooxidation using TiO_2 supported on a zeolite. *J. Photochem. Photobiol. A.,* **148,** 183-189.

CISNEROS, R. L., ESPINOZA, A. G. & LITTER, M. I. (2002) Photodegradation of an azo dye of the textile industry. *Chemosphere,* **49,** 393-9.

CORMA, A. & GARCIA, H. (2004) Zeolite-based photocatalysis. *Chem. Commun.***,** 1443-1459.

DHEAYA ALROUSAN, M. A., PATRICK DUNLOP, S. M., TRUDY MCMURRAY, A. & ANTHONY BYRNE, J. (2009) Photocatalytic inactivation of E. coli in surface water using immobilised nanoparticle TiO_2 films. *Wat. Res.,* **43,** 47-54.

DING, Z., HU, X., YUE, P. L., LU, G. Q. & GREENFIELD, P. F. (2001) Synthesis of anatase TiO_2 supported on porous solids by chemical vapor deposition. *Catal. Today,* **68,** 173-182.

DIONYSIOU, D. D., BALASUBRAMANIAN, G., SUIDAN, M. T., KHODADOUST, A. P., BAUDIN, I. & LAINE, J.-M. (2000) Rotating disk photocatalytic reactor: Development, characterization, and evaluation for the destruction of organic pollutants in water. *Wat. Res.,* 34, **11,** 2927-2940.

DIONYSIOU, D. D., KHODADOUST, A. P., KERN, A. M., SUIDAN, M. T., BAUDIN, I. & LAINE, J.-M. (2000) Continuous-mode photocatalytic degradation of chlorinated phenols and pesticides in water using a bench-scale TiO_2 rotating disk Reactor. *Appl. Catal. B: Environ.,* **24**, 139-155.

ELAIOPOULOS, K. P., PERRAKI, T. & GRIGOROPOULOU, H. (2008) Mineralogical study and porosimetry measurements of zeolites from Scaloma area, Thrace, Greece. *Microp. Meso. Mat.,* **112,** 441-449.

FAGHIHIAN, H., MARAGEH, M. G. & KAZEMIAN, H. (1999 The use of clinoptilolite and its sodium form for removal of radioactive cesium, and strontium from nuclear wastewater and Cu^{2+}, Ni^{2+} , Co^{2+}, Ba^{2+} form municipal wastewater. *Appl. Rad. Isotop.,* **50,** 655-660.

FU, Y. & VIRARAGHAVAN, T. (2002) Removal of Congo Red from an aqueous solution by fungus Aspergillus niger. *Adv. Env. Res.,* **7,** 239-47.

GASPARRO, F. P., MITCHNICK, M. & NASH, J. F. (1998) A Review of Sunscreen safety and efficacy. *Photo. Photobiol.,* **68,** 243-256.

GAYA, U. I. & ABDULLAHA, A. H. (2008) Heterogeneous photocatalytic degradation of organic contaminants over titanium dioxide: A review of fundamentals, progress and problems. *J. Photochem. Photobiol. C: Photochem. Rev.,* **9,** 1-12.

GEMEAY, A. H., GEHAD, R. E., GHRABAWY, E. & ZAKI, A. B. (2007) Kinetics of the oxidative decolorization of Reactive Blue-19 by acidic bromate in homogeneous and heterogeneous media. *Dyes and Pigments,* **73** 90-97.

GIOLLI, C., BORGIOLI, F., CREDI, A., FABIO, A. D., FOSSATI, A., MIRANDA, M. M., PARMEGGIANI, S., RIZZI, G., SCRIVANI, A., TROGLIO, S., TOLSTOGUZOV, A., ZOPPI, A. & BARDI, U. (2007) Characterization of TiO_2 coatings prepared by a modified electric arc-physical vapour deposition system. *Surf. Coat. Technol.,* **202,** 13-22.

GUO, Z., MA, R. & LI, G. (2006) Degradation of phenol by nanomaterial TiO_2 in wastewater. *Chem. Eng. J.,* **119,** 55-59.

HALMANN, M. M. (1996) Photodegradation of Water Pollutants. . *CRC Press***,** 301.

HASHIMOTO, K., WASADA, K., OSAKI, M., SHONO, E., ADACHI, K., TOUKAI, N., KOMINAMI, H. & KERA, Y. (2001) Photocatalytic oxidation of nitrogen catalytic oxidation of nitrogen oxides in the atmosphere. *Appl. Catal. B: Environ.,* **65,** 429-436.

HERNANDEZ, M. A. (2000) Nitrogen-sorption characterization of the microporous structure of clinoptilolite-type Zeolites. *J. Por. Mat.,* **7,** 443-454.

HERRMANN, J. H. (2005) Heterogeneous photocatalysis: State of the art and present applications. *Top. Catal.,* **34,** 49-65.

HERRMANN, J. M. (1999) Heterogeneous photocatalysis: Fundamentals and applications to the removal of various aqueous pollutants. *Catal.Today,* **53,** 115-129.

HIDALGO, M. C., AGUILAR, M., MAICU, M., NAVÍO, J. A. & COLÓN, G. (2007) Hydrothermal preparation of highly photoactive TiO_2 nanoparticles. *Catal. Today,* **129,** 50-58.

ICHIURA, H., KITAOKA, T. & TANAKA, H. (2000) Photocatalytic decomposition of VOC by Zeolite-TiO_2 composite sheet prepared using papermaking technique. Proceeding on environmentally friendly and emerging technologies for a suitable pulp and paper industry, Taiwan.

KAMAT, P. V. (1993) Photochemistry on non-reactive and reactive (semiconductor) surfaces. *Chemical Rev.,* **93,** 267-300.

KIM, Y. & YOON, M. (2001) TiO_2/Y-Zeolite encapsulating intramolecular charge transfer molecules: A new photocatalyst for photoreduction of methyl orange in aqueous medium. *J. Mol. Catal. A,* **168,** 257-263.

KITAMURA, Y., OKINAKA, N., SHIBAYAMA, T., MAHANEY, O. O. P., KUSANO, D., OHTANI, B. & AKIYAMA, T. (2007) Combustion synthesis of TiO_2 nanoparticles as photocatalyst. *Powder Technol.,* **176,** 93-98.

KOLEN´KO, Y. V., GARSHEV, A. V., CHURAGULOV, B. R., BOUJDAY, S., PORTES, P. & COLBEAU-JUSTIN, C. (2005) Photocatalytic activity of sol-gel derived titania converted into nanocrystalline powders by supercritical drying. *J. Photochem. Photobiol. A: Chem.,* **172,** 19-26.

KRYUKOVA, G. N., ZENKOVETS, G. A., SHUTILOV, A. A., WILDE, M., GÜNTHER, K., FASSLER, D. & RICHTER, K. (2007) Structural peculiarities of TiO_2 and Pt/TiO_2 catalysts for the photocatalytic oxidation of aqueous solution of Acid Orange 7 Dye upon ultraviolet light. *Appl. Catal. B: Environ.,* **71,** 169-176.

LI, F. B. & LI, X. Z. (2002) Photocatalytic properties of gold/gold ion-modified titanium dioxide for wastewater treatment. *Appl. Catal. A: Gen.,* **228,** 15-27.

LI, F. F., JIANG, Y. S., YU, L. X., YANG, Z. W., HOU, T. Y. & SUN, S. S. (2005) Surface effect of natural zeolite (clinoptilolite) on the photocatalytic activity of TiO_2. *Appl. Surf. Sci.,* **252,** 1410--1416.

LI, X., QUAN, X. & KUTAL, C. (2004) Synthesis and photocatalytic properties of quantum confined titanium dioxide nanoparticle. *Scr. Mater.,* **50,** 499-505.

LIM, M., RUDOLPH, V., ANPO, M. & LU, G. Q. (2008) Fluidized–bed photocatalytic degradation of airborne styrene. *Catal. Today,* **131,** 548-552.

LIN, C.-F., WU, C.-H. & ONN, Z.-N. (2008) Degradation of 4-chlorophenol in TiO_2, WO_3, SnO_2, TiO_2/WO_3 and TiO_2/SnO_2 systems. *J. Hazard. Mater.,* **154,** 1033-1039.

LINSEBIGLER, A. L., LU, G. Q. & YATES, J. T. (1995) Photocatalysis on TiO_2 surfaces - principles, mechanisms, and selected results. *Chem. Rev.,* **95,** 735-758.

LIU, X., IU, K.-K. & THOMAS, J. K. (1993) Preparation, characterisation and photoreactivity of titanium (IV) oxide encapsulated in zeolites. *J. Chem. Soc., Faraday Trans.,* **89,** 1861-1865.

LIU ZY, ZHANG XT, NISIMOTO S, MURAKAMI T & A., F. (2008) Efficient photocatalytic degradation of gaseous acetaldehyde by highly ordered TiO_2 nanotube arrays. *Environ Sci Technol,* **42,** 8547-51.

LIUXUE, Z., PENG, L. & ZHIXING, S. (2006) Photocatalysis anatase thin film coated PAN fibers prepared at low temperature. *Mater. Chem. Phys.,* **98,** 111-115.

MACAK, J. M., TSUCHIYA, H., GHICOV, A., YASUDA, K., HAHN, R., BAUER, S. & SCHMUKI, P. (2007) TiO_2 nanotubes: self-organized electrochemical formation, properties and applications. *Curr. Opin. Solid State Mat. Sci.,* **11,** 3-11.

MAHAMUNI, N. N. & PANDIT, A. B. (2006) Effect of additives on ultrasonic degradation of phenol. *Ultrasonic Sonochemistry,* **13** 165-174.

MALATO, S., BLANCO, J., VIDAL, A. & RICHTER, C. (2002) Photocatalysis with solar energy at a pilot-plant scale: an overview. *Appl. Catal. B: Environ.,* **37,** 1-15.

MATHEWS, R. W. (1987) Photooxidation of organic impurities in water using thin films of titanium dioxide. *J. Phys. Chem. B,* **91,** 3328-3333.

MATTHEWS, R. W. (1990) Purification of water with near UV illuminated suspensions of titanium dioxide. *Wat. Res.,* **24,** 653-660.

MÉNESI, J., KÖRÖSI, L., BAZSÓ, É., ZÖLLMER, V., RICHARDT, A. & DÉKÁNY, I. (2008) Photocatalytic oxidation of organic pollutants on titania-clay composites. *Chemosphere,* **70,** 538-542.

MILLS, A., DAVIES, R. H. & WORSLEY, D. (1993) Water purification by semiconductor photocatalysis. *Chem. Soc. Rev.,* **22,** 417-426.

NEPPOLIAN, B., CHOI, H. C., SAKTHIVEL, S., ARABINDOO, B. & MURUGESAN, V. (2002) Solar/UV-induced photocatalytic degradation of three commercial textile dyes. *J. Hazard. Mater.,* **89,** 303-317.

OLLIS, D. F. (2005) Kinetics of liquid phase photocatalyzed reactions: an illuminating approach. *J. Phys. Chem. B.,* **109,** 2439-2444.

PAN, K., ZHANG, Q., WANG, Q., LIU, Z., WANG, D., LI, J. & BAI, Y. (2007) The photoelectrochemical properties of dye-sensitized solar cells made with TiO_2 nanoribbons and nanorods. *Thin Solid Films,* **515,** 4058.

PATRICK, B. & KAMAT, P. V. (1992) Photophysics and photochemistry of quantized ZnO colloids. *Chem. Rev.,* **96,** 1423-1428.

PUCHER, P., BENMAMI, M., AZOUANI, R., KRAMMER, G., CHHOR, K., BOCQUET, J. F. & KANAEV, A. V. (2007) Nano-TiO_2 sols immobilized on porous silica as new efficient photocatalyst. *Appl. Catal. A: Gen.,* **332,** 297-303.

RECK, E. & RICHARDS, M. 1999. TiO_2 manufacture and life cycle analysis. *Pigm. Resin. Technol.,* **28,** 149-157.

REDDY, E. P., DAVYDOV, L. & SMIRNIOTIS, P. (2003) TiO_2-loaded zeolites and mesoporous materials in the sonophotocatalytic decomposition of aqueous organic pollutants: The role of the support. *Appl. Catal. B: Environ.,* **42,** 1-11.

SANKAPAL, B. R., SARTALE, S. D., LUX-STEINER, M. C. & ENNAOUI, A. (2006) Chemical and electrochemical synthesis of nanosized TiO_2 anatase for large-area photon conversion. *C. R. Chim.,* **9,** 702-707.

SATO, S. & WHITE, J. M. (1980) Photo-decomposition of water over Pt-TiO_2 catalysts. *Chem. Phys. Lett.,* **72,** 83-86.

SCHUBERT, U. & HÜSING, N. (2005) *Synthesis of inorganic materials*.

SERPONE, N., SAUVE, G., KOCH, G., TAHIRI, H., PICHAT, P., PICCININI, P., PELIZZETTI, P. & HIDAKA, H. (1996) Standadization protocol of process efficiencies and activation parameters in heterogeneous photocatalysis: Relative photonic efficiencies. *J. Photochem. Photobiol. A: Chem.,* **106,** 191-203.

SHEIKH, A. H., NEWMAN, A. P., AL-DAFFAEE, H., PHULL, S., CRESSWELL, N. & YORK, S. (2004) Deposition of anatase on the surface of activated carbon. *Surf. Coat. Technol.,* **187,** 284-292.

SIVAKUMAR, S., SIBU, C. P., MUKUNDAN, P., PILLAI, P. K. & WARRIER, K. G. K. (2004) Nanoporous titania-alumina mixed oxides - an alkoxide free sol-gel Nanoporous titania-alumina mixed oxides - an alkoxide free sol-gel. *Mater. Lett.,* **58,** 2664-2669.

SMYTH, J. R., SPAID, A. T. & BISH, D. L. (1990) Crystal structures of a natural and a Cs-exchanged clinoptilolite. *American Mineralogist,* **75,** 522-528.

SOBANA, N., MURUGANADHAM, M. & SWAMINATHAN, M. (2006) Nano-Ag particles doped TiO_2 for efficient photodegradation of direct azo dyes. *J. Mol. Catal. A: Chem.,* **258,** 124-132.

TONG, T., ZHANG, J., TIAN, B., CHEN, F. & HE, D. (2008) Preparation of Fe^{3+}-doped TiO_2 catalysts by controlled hydrolysis of titanium alkoxide and study on their photocatalytic activity for methyl orange degradation. *J. Hazard. Mater.,* **155,** 572-579.

TORRES, A. R., AZEVEDO, E. B., RESENDE, N. S. & DEZOTTI, M. (2007) A comparison between bulk and supported TiO_2 photocatalysts in the degradation of formic acid. *Braz. J. Chem. Eng.,* **24,** 185-192.

TRYBA, B., MORAWSKI, A. W. & INAGAKI, M. (2003) A new route for preparation of TiO_2-mounted activated carbon. *Appl. Catal. B: Environ.,* **46,** 203-208.

VLACHOPOULOS, N., LISKA, P., AUGUSTYNSKI, J. & GRATZEL, M. (1988) Very efficient visible light energy harvesting and conversion by spectral sensitization of high surface area polycrystalline titanium dioxide films. *J. Am. Chem. Soc.,* **110,** 1216-1218.

XIE, R. C. & SHANG, J. K. (2007) Morphological control in solvothermal synthesis of titanium oxide. *J. Mater. Sci.,* **42,** 6583-6589.

YOSHIDA, H., KAWASE, T., MIYASHITA, Y., MURATA, C., OOKA, C. & HATTORI, T. (1999) Effect of hydrothermal treatment of titania-pillared montmorillonite for photocatalytic degradation of dibutyl phthalate in water. *Chem. Lett.***,** 712-716.

YUAN, R., GUAN, R., LIU, P. & ZHENG, J. (2007) Photocatalytic treatment of wastewater from paper mill by TiO_2 loaded on activated carbon fibers. *Colloid Surf. A: Physicochem. Eng. Asp.,* **293,** 80-86.

ZHANG, Y. X., LI, G. H., JIN, Y. X., ZHANG, Y., ZHANG, J. & ZHANG, L. D. (2002) Hydrothermal synthesis and photoluminescence of TiO_2 nanowires. *Chem. Phys. Lett.,* **365,** 300-304.

ZHANG, Z., WANG, C.-C., ZAKARIA, R. & YING, J. Y. (1998) Role of particle size in nanocrystalline TiO_2-based photocatalysts. *J. Phys. Chem. B.,* **102,** 10871-10878.

ZHAO, D., CLEARE, K., OLIVER, C., INGRAM, C., COOK, D., SZOSTAK, R. & KEVAN, L. (1998) Characteristics of the synthetic heulandite-clinoptilolite family of zeolites. *Micro.Meso.Mat.,* **21,** 371-379.

CHAPTER THREE

EXPERIMENTAL AND METHODOLOGY

Introduction

In this chapter, materials and methods used during this study are highlighted with full description of the experimental setup and analytical procedure employed.

3.1 Materials

Natural Clinoptilolite ($(MgCaNa_2K_2)_{2.5}$ $(AlO_2)_7$ $(SiO_2)_{30}\cdot 21H_2O$), obtained from the Pratley Perlite mining company (South Africa) was applied as a support layer for TiO_2 with Si/Al ratio (5.5). Analytical grade of Titanium(IV)-n-butoxide (98% Aldrich), Methyl orange dye, Methylene blue all from Aldrich, while ethanol (99%), sodium chloride, ammonium chloride, silver nitrate, sodium sulphite, sodium carbonate, sodium nitrate, sodium sulphate all from Merck were used without any further purification. Sodium hydroxide and hydrochloric acid (Merck) were used to control pH of the methyl orange solution during irradiation activities. The physical properties of methyl orange (MO) and methylene blue (MB) are depicted in Table 3.1. Double distilled-deionized water was employed in preparation of solutions throughout the experiment.

Table 3. 1 Physical properties of Methyl Orange (MO) and Methylene Blue (MB)

	MO	MB
Molecular formula	$C_{14}H_{14}N_3NaO_3S$	$C_{16}H_{18}N_3SCl$
Molecular weight (g/mol)	327.33	319.85
Melting point (^oC)	300	110

3.2 Detailed preparation of photocatalyst

3.2.1 Preparation of dealuminated Clinoptilolite (HCP)

Natural Clinoptilolite was crushed in an agate mortar and sieved to less than 100 µm particle size fractions. For dealumination experiment, 20 g of sieved CP was added to 1M NH_4Cl solution, which was continuously stirred at 60-90 ^oC for 24 hrs to achieve the desired ion-exchange process (Kim, 2002). The resultant mixture was filtered, washed well with deionized water until the supernatant was neutral and free of chloride ions using silver nitrate. The obtained sample was air dried at 120-150 ^oC for 8 hrs. The sample was ground to fine powder and further calcined in the muffle oven at 550 ^oC for 8 hrs required for activation of the dealuminated Clinoptilolite (HCP) as described in Figure 3.1.

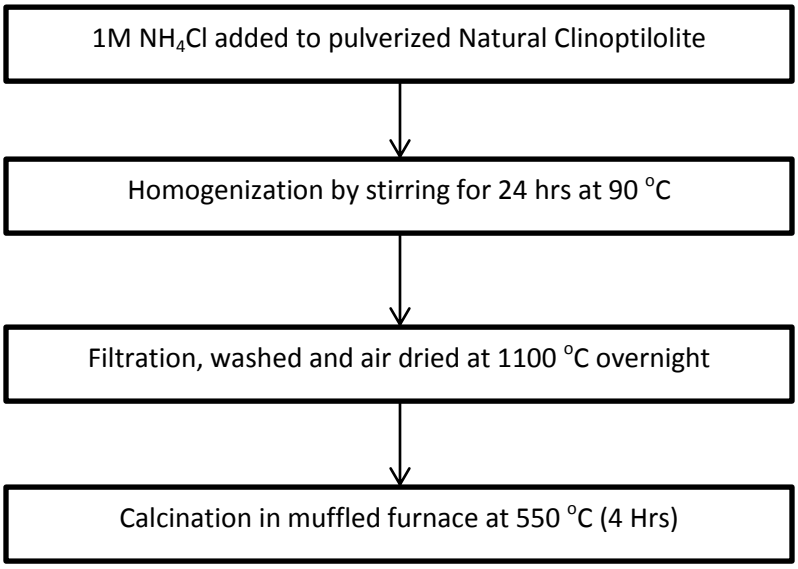

Figure 3. 1 Flow chart of detailed preparation of HCP

3.2.2 Preparation of supported photocatalyst (TiO_2/HCP) and pure TiO_2

TiO_2/HCP was synthesized via sol-gel process. Titanium(IV)-n-butoxide was added slowly to HCP suspended in ethanol solution, with vigorous stirring at room temperature for 3 hrs. A mixture of ethanol and water solution (1:1) was further added to hydrolyse Titanium(IV)-n-butoxide adsorbed on HCP under continuous stirring for 3 hrs. The preparation was dependent on loading of TiO_2 wt% on the dealuminated Clinoptilolite in aqueous solution (5 wt%, 7.5 wt%

and 10 wt%). The resultant mixture was filtered, washed with deionized water until the supernatant was neutral. The gel material was air dried in the oven at 110-120 ^{o}C overnight. The obtained solid was crushed to fine material and further calcined in a muffle oven at 550 ^{o}C for 4 hrs to achieve TiO_2/HCP, which was stored in the dark before the elucidation of prepared photocatalyst structure and photocatalytic activities on methyl orange. The same preparation procedure was applied to bare TiO_2 is applied via sol-gel process and calcined at 550 ^{o}C as shown in Figure 3.2.

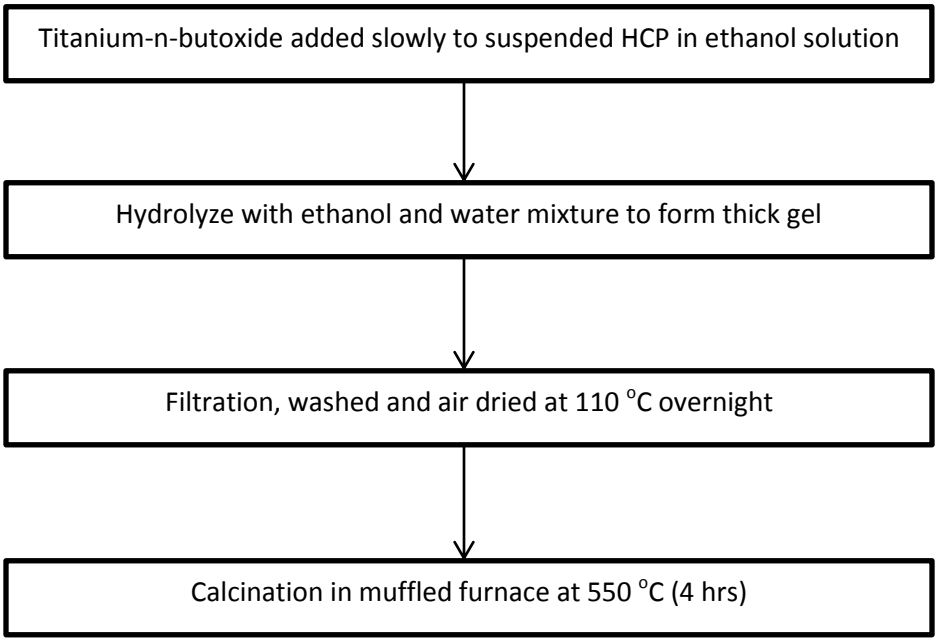

Figure 3. 2 Flow chart of detailed preparation of TiO_2/HCP

3.3 Characterization of synthesized photocatalyst

The synthesized photocatalyst were characterized using different analytical techniques such as Fourier transform infrared spectroscopy (FT-IR), X-ray diffraction (XRD) analysis, Scanning electron microscopy (SEM), Energy dispersive X-ray spectroscopy (EDAX), UV-VIS diffuse reflectance spectrophotometer (DRUV-VIS) and Thermal analysis (TGA-DSC). Ultraviolet-

visible spectroscopy (UV-VIS) was employed for the analysis of the organic model pollutants during photocatalytic degradation studies

3.3.1 XRD Analysis

The X-ray powder diffraction spectra of HCP and TiO_2/HCP were obtained using Bruker-AXS D8 Advance diffractometer, where Cu target Kα-ray (operating at 40 kV and 40 mA, λ = 0.15406 nm) was used as the X-ray source. The sample was ground into fine powder and a thin layer was prepared on a metal slide. The sample was placed on a sample holder inside the diffractometer. The divergence and convergence slit width was adjusted according to scanning range of 2 θ before scanning.

3.3.2 Fourier-transform infrared spectroscopy (FT-IR)

FT-IR was used to identify the functional groups present in the synthesized photocatalyst in the range of 600-4000 cm^{-1}. FT-IR spectra of synthesized photocatalyst samples bond vibrations were analysed on Fourier transform infrared spectrophotometer machine (Perkin Elmer spectrum 400).

3.3.3 SEM/EDAX analysis

The surface morphology of the supported and unsupported catalysts was examined using FEI Quanta Sirion microscope equipped with an EDAX system for Energy Dispersive Spectroscopic analysis, which was coated with a thin layer of gold film to avoid charging. Elemental analysis was performed with EDX (energy-dispersive X-ray spectroscopy) with the scanning electron microscope using a silicon detector operating at an accelerating voltage of 15 kV.

3.3.4 Thermal gravimetric analysis (TGA)

Thermal analysis was employed to estimate the mass of water evolved or absorbed in accordance to the weight loss. Thermal gravimetric analysis (TGA) was carried out using Perkin Elmer STA 6000 thermal simultaneous analyzer at a heating rate of 10 ^{o}C/min from 30 to 900 ^{o}C under 19.8 ml/mins in nitrogen purge stream.

3.3.5 DRUV-VIS

The samples were analyzed on a UV-vis spectrophotometer (Perkin Elmer Lambda 25) in the range of 200-900 nm, to determine the absorption spectral response of synthesized photocatalyst into the visible region.

3.4 Experimental Details of Photocatalytic degradation of model pollutants

The photocatalytic degradation efficiency of different compositions of HCP, TiO_2/HCP and pure TiO_2 was investigated in an aqueous suspension of the model pollutants.

Figure 3. 3 Pictorial diagram of Photoreactor

3.4.1 Experimental setup

The photocatalytic activities were measured via a decrease in concentration and absorbance of model organic pollutants in the reaction solution. Photocatalytic experiments were performed within a photocatalytic reactor system with cylindrical Pyrex glass cell with 1.0 L capacity, 10 cm diameter and 15 cm height (Figure 3.3). Irradiation experiment were done with Ace glass UV lamp (450 W), placed in a 5 cm diameter quartz tube and a magnetic stirrer applied for good

mixing of the solutions. All degradation activities were conducted at room temperature and there was no purging of oxygen during the photocatalytic activities. Subsequent irradiations after 30 minutes, 10 ml of aliquot were collected from irradiated solution, centrifuged at 100 rpm for 30 mins to separate the organic solution from the titania solid. This was further filtered using 0.45 µm microporous membrane filter and absorbance decrease of organic compounds was measured in the UV-Vis spectrophotometer (Perkin Elmer Lambda 25).

3.4.2 Experimental procedure

In case of photocatalytic activities, the required amount of catalyst was added in suspension to the aqueous solution of organic compounds employed in this study inside the photochemical reactor. The photodegradation experiment was performed at 50 ppm of Methyl orange at various loading wt%. For optimization of operational parameters of MO, experiments were conducted by varying initial MO concentration from 20 to 70 ppm. The pH of the solution was also monitored continuously, where the pH range was from 2-12 using hydrochloric acid (HCl) and sodium hydroxide (NaOH) as control. The effect of calcination temperature, inorganic ions and oxidant was conducted respectively.

Comparative degradation efficiency of photocatalyst was carried out using dye mixture of methyl orange and methylene blue (40 ppm). During each run, samples were taken from the photoreactor at relative time intervals. Degradation efficiency was done from absorbance of the model organic solution before and after photodegradation experiments, using UV-Vis spectrophotometer (Perkin Elmer Lamba 25).

References

KIM, J. K. (2002) Catalytic degradation of polypropylene: effect of dealumination of Clinoptilolite catalyst. *Polymer Degradation and Stability,* **75** 287-394.

LI, F. L. (2002) The enhancement of photodegradation efficiency using Pt-TiO_2 catalyst. *Chemosphere,* **48** 1103-1111.

CHAPTER FOUR

RESULTS AND DISCUSSIONS

4.1 Characterization of prepared photocatalyst

Raw Clinoptilolite (CP) was employed as our support layer and Titanium(IV)-n-butoxide was applied as our titania precursor throughout the experiment without any modification. The prepared photocatalyst is being characterized using analytical means.

4.1.1 XRD Analysis

X-ray powder diffraction method was used to assess the crystallinity of the supported and unsupported catalysts respectively. Judging from the XRD pattern of the CP as shown in Figure.4.1, it has no amorphous peak before loading of TiO_2. The patterns of diffraction peaks were similar between Raw CP, HCP and TiO_2/HCP. These means that CP cavities are not really affected by dealumination, which is ascribed to exceptional thermal stabilization of natural zeolites and also by incorporation of TiO_2 in the CP surface as a result of lower loading (Chuan *et al*., 2004 and Li *et al*., 2005).

The diffraction patterns of Raw CP, HCP and TiO_2/HCP are highly crystalline exhibiting reflections at 2θ values at 10^o, 11^o, 13^o, 17^o, 23^o, 30^o, 32^o which all corresponds to CP diffraction peaks. It's an established fact, 3 naturally occurring phases of TiO_2 exists: anatase, rutile and brokite. Calcination enhances crystallization of TiO_2 solid and accelerates transformation of amorphous TiO_2 phase into anatase or rutile phase. A peak of anatase exists at 2θ (25.2^o and 36.8^o), while the case of rutile peaks at 2θ (27.7^o and 36.6^o) respectively at calcination temperature of 550 ^{o}C.

There exists minute decrease in intensity of the peaks in the host-guest composite materials as compared to CP. These are ascribed to cation exchange and also the incorporation of TiO_2 in the HCP matrix during sol-gel process and dealumination activities (Reddy *et al*., 2003).

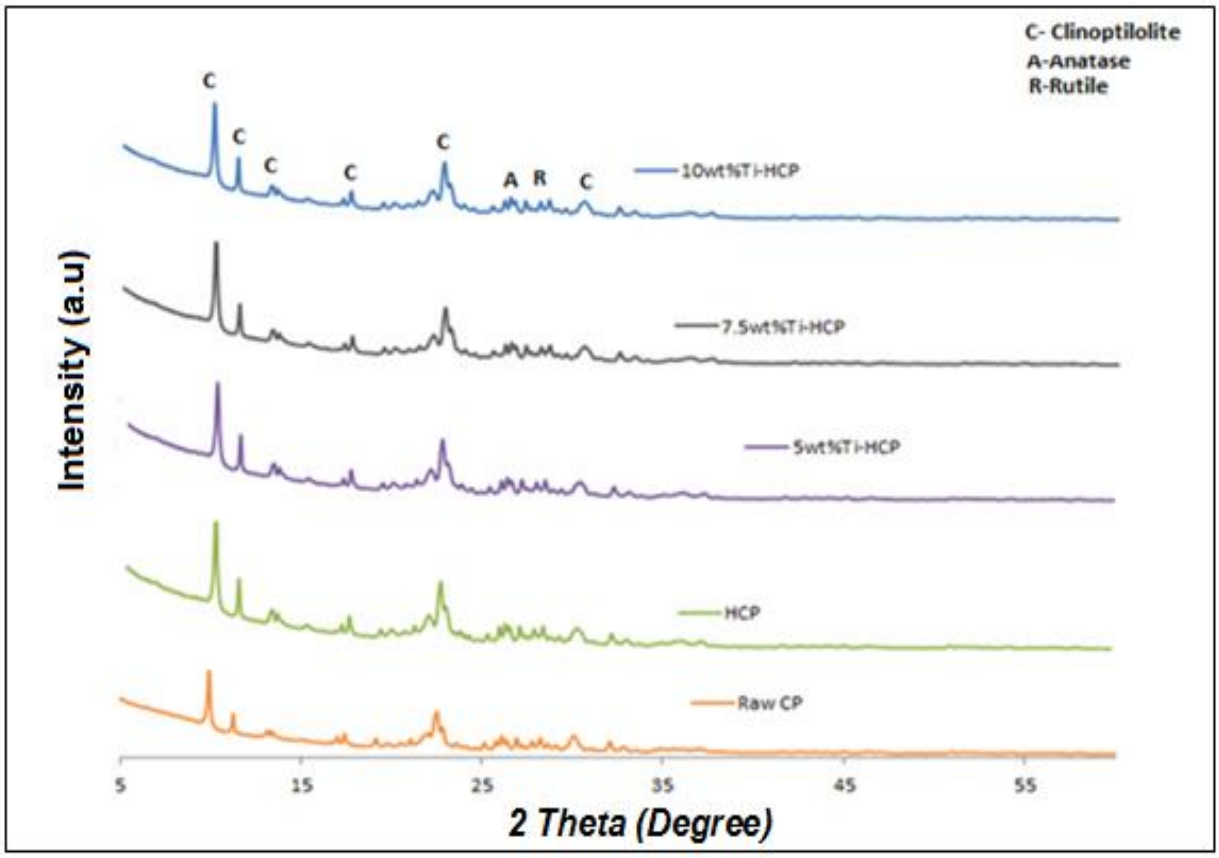

Figure 4. 1 X-Ray diffraction patterns of CP, HCP and TiO_2/HCP at 550 ^oC

4.1.2 SEM and EDAX Analysis

SEM analysis depicts the morphology texture of synthesized photocatalyst and images reveal partly distribution of TiO_2 particles on the HCP. The titania particles exist as clusters adsorbed on the HCP surface and pores respectively at magnification of 1000. TiO_2 nanoparticles are uniformly distributed on the HCP surface and no aggregation of Titania particles. EDAX reveals an elemental analysis of the sample, showing the presence and relative distribution of the Titania present on the HCP. The EDAX spectra obtained for the TiO_2/HCP catalyst indicates successful deposition of the titania nanoparticles on the CP surface. The observed Ti and O peaks were consistent with the formation of TiO_2 nanoparticles on the HCP. Both SEM and EDAX spectra in Figure 4.2 and 4.3 confirms loading of titania on the HCP matrix. The SEM and EDAX for 7.5 and 10 wt% TiO_2/HCP are depicted in Appendix 1 and 2 respectively.

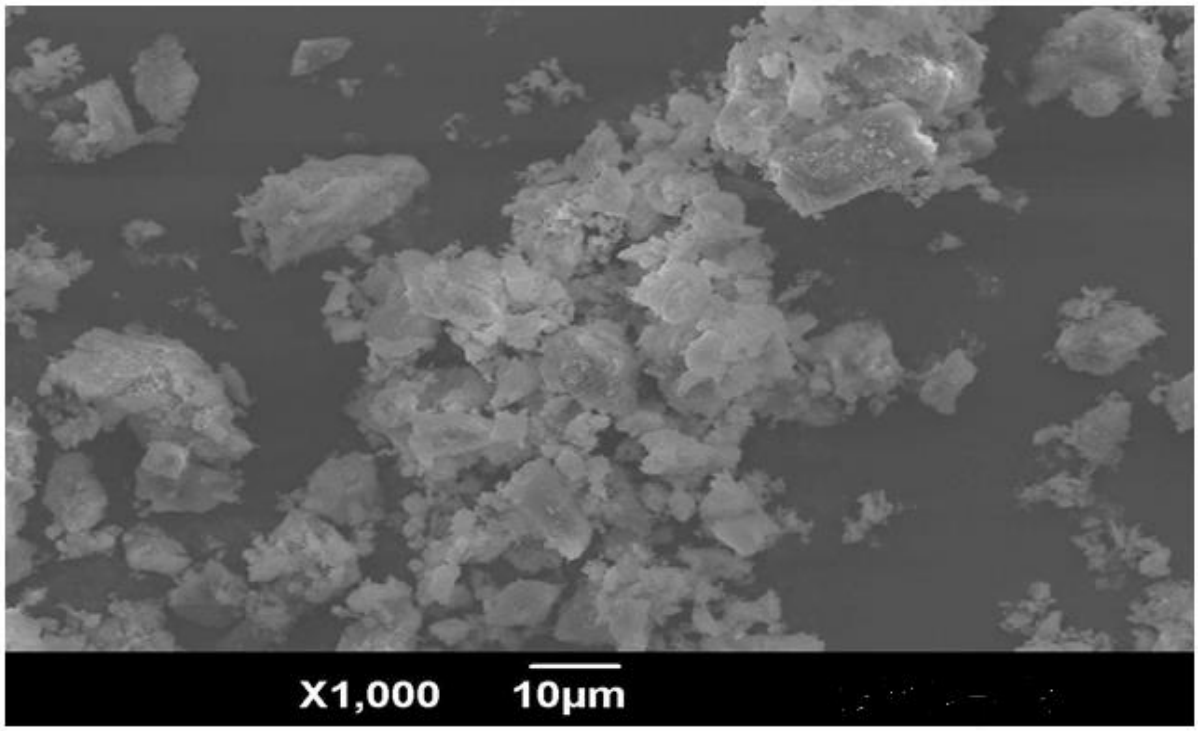

(a)

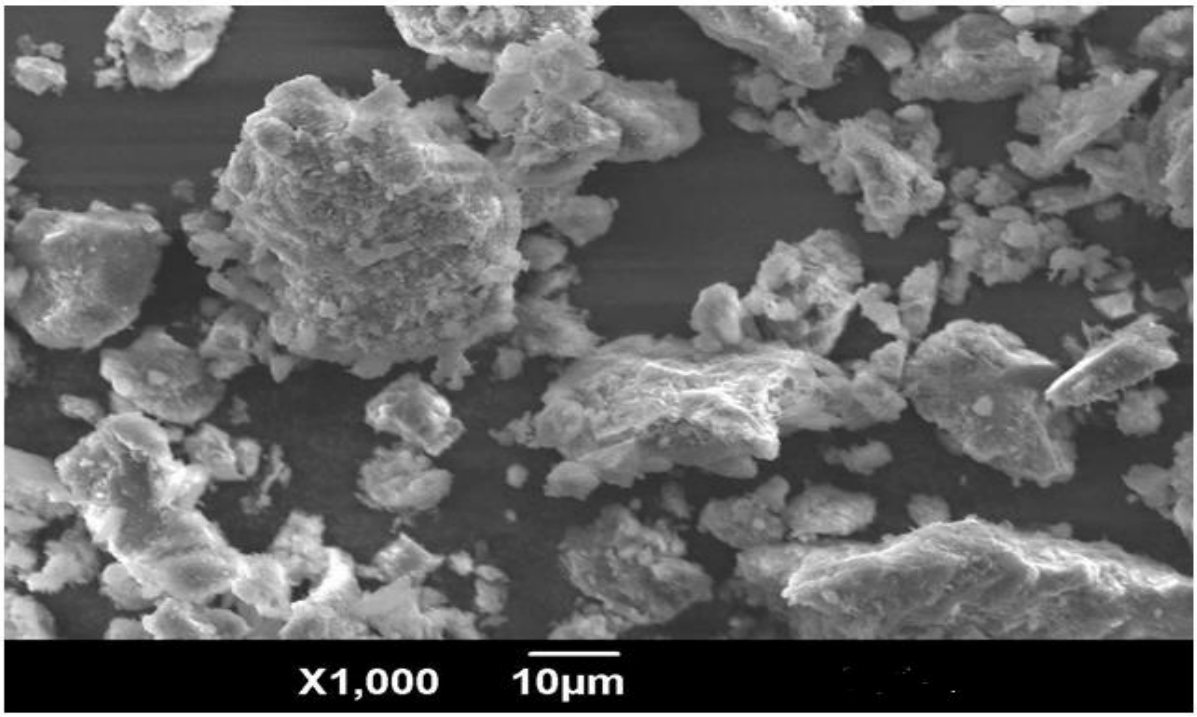

(b)

Figure 4. 2 SEM images of (a) HCP and (b) 5 wt% TiO_2/HCP

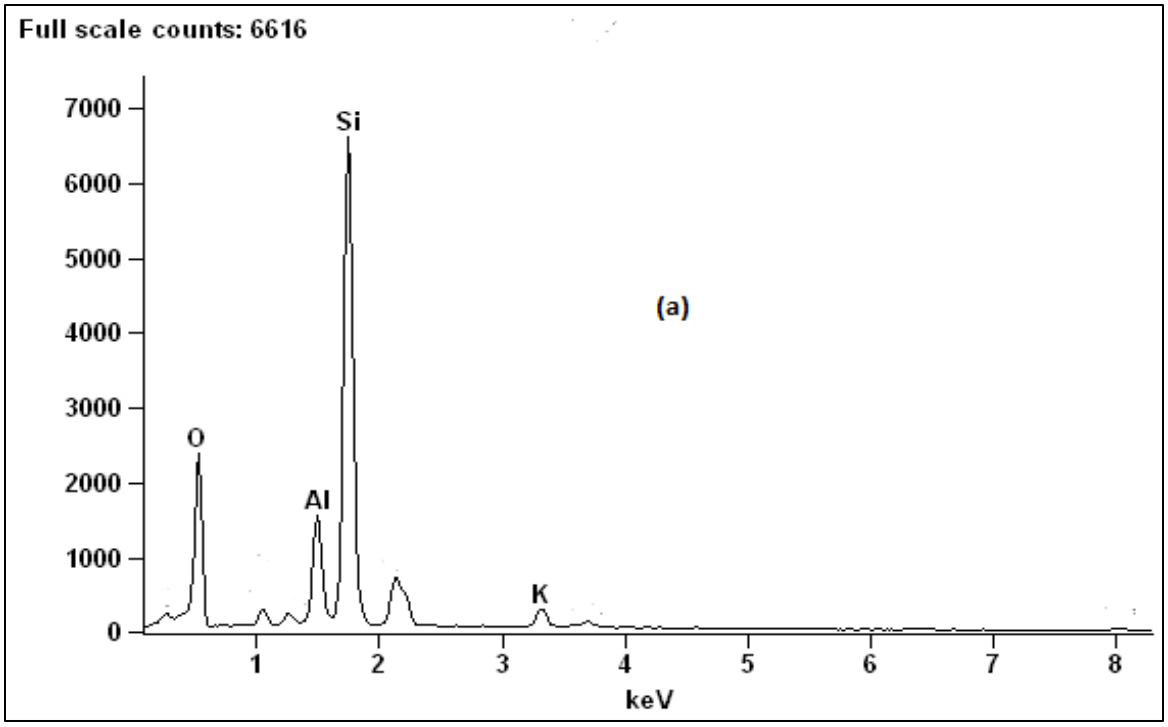

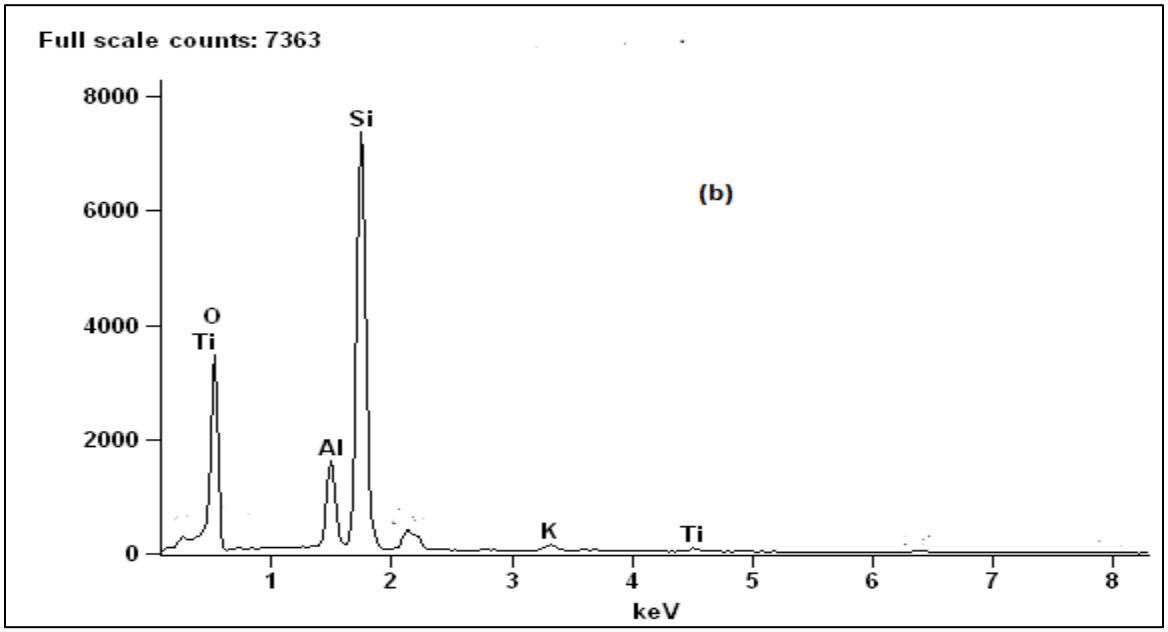

Figure 4. 3 EDAX of (a) HCP and (b) 5 wt% TiO_2/HCP

4.1.3 FTIR analysis

FTIR spectra of Raw CP, HCP and TiO_2/HCP as shown in Figure 4.4 reveals little shift in vibrational peaks, though the presence of hydroxyl stretching of CP at 3400 to 3500 cm^{-1} which decreases with calcination. The decrease also occurs with dehydration of CP and loading of TiO_2 on the HCP cavities. Sharp absorption peak at 1010-1100 cm^{-1} attributed to an asymmetrical stretching vibration band of Si(Al)-O in tetrahedral $Si(Al)O_4$ in CP, indicative CP structure will not decompose at 500 ^oC. Symmetrical stretching of T-O, T-O-T bonds in tetrahedral SiO_4 and AlO_4 pronounced at 790-800 cm^{-1} and distorted OH bending in CP at 1620-1640 cm^{-1}. Stretching vibrations of Ti-O-Si and Ti-O-Al at 960 cm^{-1} was not visible for TiO_2/HCP, ascribed to no chemical interaction between the TiO_2 and zeolite. This reveals that TiO_2 is partly impregnated in CP cavities was also observed by Sankararaman (Sankararaman *et al*., 1991). No replacement of Si sites with Ti was observed, and this in agreement with Tanaka And Chen (Tanaka *et al*., 2006 and Chen *et al*., 1999). The FTIR for 7.5 and 10 wt% TiO_2/HCP are depicted in Appendix 3 respectively. This largely ascribed to lower loading rate of TiO_2 on HCP and vibration peak of synthesized photocatalyst are shown in Table 4.1.

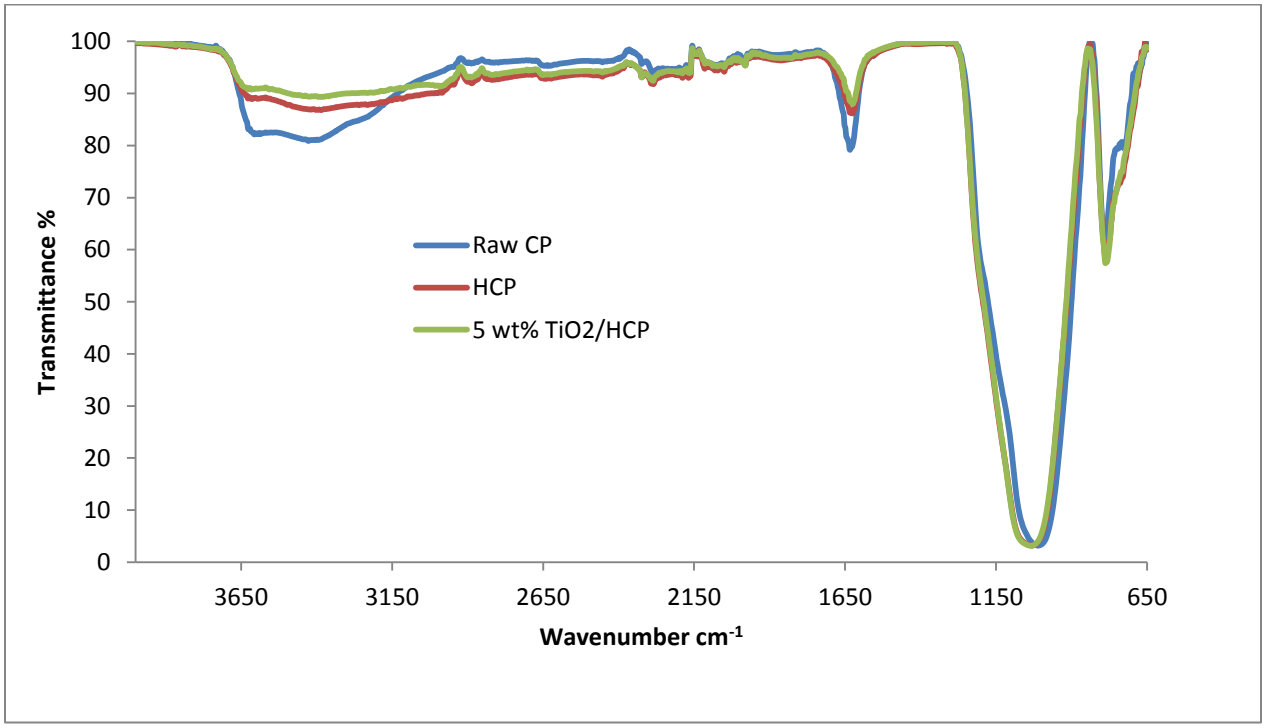

Figure 4. 4 FTIR of Raw CP, HCP and TiO_2/HCP

Table 4. 1 Vibrational bands of prepared photocatalyst

Vibration Bands	Raw CP	HCP	5 wt% TiO_2/HCP	7.5 wt% TiO_2/HCP	10 wt% TiO_2/HCP
Isolated OH stretching	3628	3678	3665	3656	3640
H-bonded OH stretching	3345	3462	3453	3449	3471
Distorted OH bending	1642	1663	1676	1633	1635
Asymmetric stretch	1075	1078	1070	1069	1056
Symmetric stretch	750	759	792	791	790

4.1.4 TGA analysis

The thermogravimetric analysis (TGA) pattern for Raw CP, HCP and TiO_2/HCP samples are shown in Figure 4.5 respectively. The TGA results are in relation to literature (Nezamzadeh-Ejhieh and Moeinirad, 2011) and water loss at 3 different temperatures attributed to exchangeable cations present in the zeolite. The weight loss in the Clinoptilolite centres around three forms: (i) physisorbed water (30-100 ^oC), (ii) water associated with exchangeable cations (100-300 ^oC), and (iii) water due to silanol nest that form hydrogen bond interaction with water (300-600 ^oC). The major weight loss occurred at 30-100 ^oC (2.90-3.66%) due to desorption of physisorbed water and hydroxyl species in CP cavities (Castaldi *et al*., 2005 and Garcia-Basabe *et al*., 2010), also weight loss at 100-300 ^oC (8.22-9.43%) ascribed to exchangeable cations respectively for Raw CP and HCP samples. However for 5 wt% TiO_2/HCP, increased weight loss occurs at the 30-100 ^oC (5.50%), 100-300 ^oC (10.46%) and finally at the 300-600 ^oC (12.16%) which is ascribed to the photocatalyst been affected considerably by heating. The percentage weight loss for the prepared photocatalysts at various loading is shown in Table 4.2, while the TGA plots for 7.5 and 10 wt% TiO_2/HCP is depicted in Appendix 4.

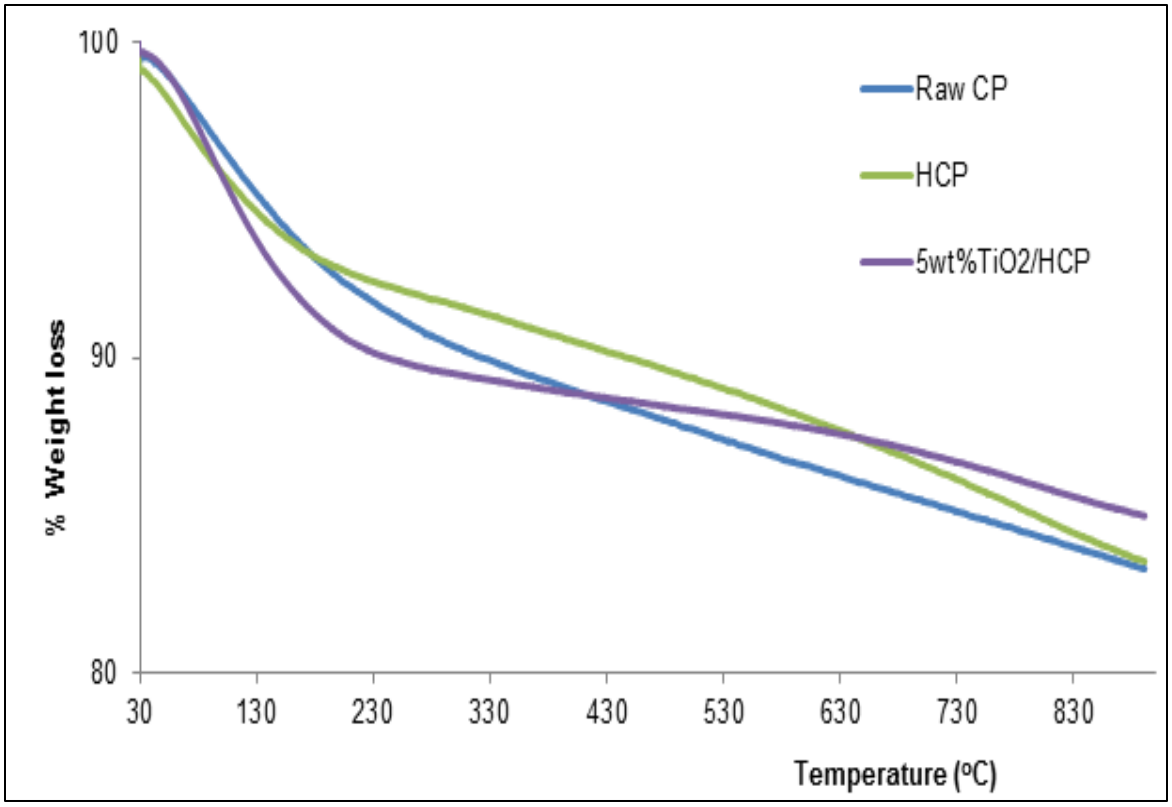

Figure 4. 5 TGA of (a) Raw CP, (b) HCP and (b) 5 wt% TiO_2/HCP

Table 4. 2 Percentage weight loss of prepared photocatalyst

Sample	Physisorbed Water (< 85 °C)	Exchange Cation with Water (100 °C--300 °C)	Hydrogen bond with Water (300—600 °C)	Total %Weight loss
Raw CP	2.90	8.22		11.92
HCP	3.66	9.43		13.09
5 wt% TiO_2/HCP	5.50	10.46	12.16	28.12
7.5 wt% TiO_2/HCP	4.26	10.51	12.22	26.99
10 wt% TiO_2/HCP	4.10	8.44	10.30	22.84

4.1.5 Diffuse Reflectance Spectroscopy

The spectral responses of prepared photocatalyst were investigated by UV-vis diffuse reflectance spectra (DRUV-VIS) are shown in Figure 4.6. There exists weak red shifting of absorption band of TiO_2/HCP into the visible light region from 400–700 nm. This absorption shift of TiO_2 is attributed to successful deposition of TiO_2 on HCP surface, which simultaneously reduces band gap energy of the composite photocatalyst. The mesoporous material (HCP) surface area increases due to fixing of TiO_2 and in turn reduces recombination of photogenerated electron hole pairs. The DRUV-VIS of calcined TiO_2/HCP at various calcination temperature is shown in Appendix 5.

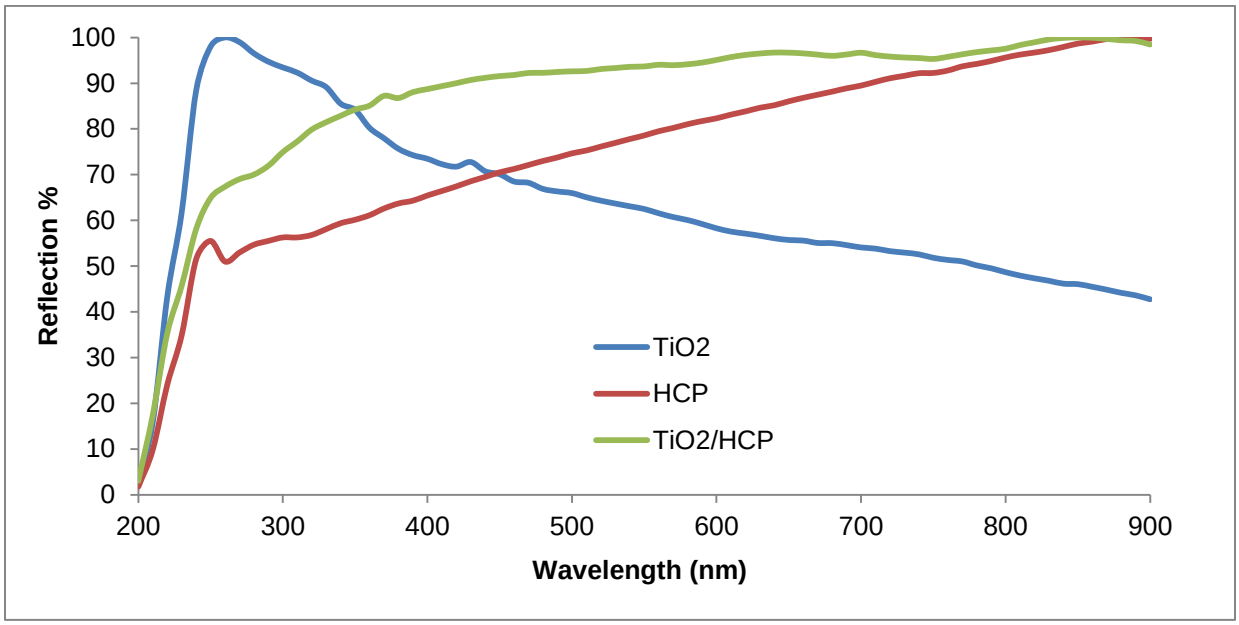

Figure 4. 6 DRUV-VIS of (a) Raw CP, (b) HCP and (b) TiO_2/HCP

4.2 Batch Adsorption and Photocatalytic degradation of MO

4.2.1 Adsorption of Methyl Orange (MO)

Studies revealed that photocatalyst surface properties such as its surface area, active sites and pore volume will greatly influence adsorption of molecules onto the catalyst surface. The

polarity, molecular weight and functional group present in the organic compounds will attract it to the catalyst surface also. Adsorption kinetics results of MO (anionic dye) using different catalyst were also determined, to depict distribution of the dye molecules between the liquid and solid phases at a definite temperature. Judging from Figure 4.7, adsorption properties occurred at lower loading of TiO_2 on HCP, as compared to higher loading. Though at 0 wt% (HCP) exhibit adsorption properties, which are ascribed to good dealumination of Clinoptilolite (CP) that enhances slight reduction of acidic sites on surface of CP, also increases its surface area and micropore size. There exists good electrostatic attraction between MO (being anionic dye) and HCP due to it being moderately acidic in nature.

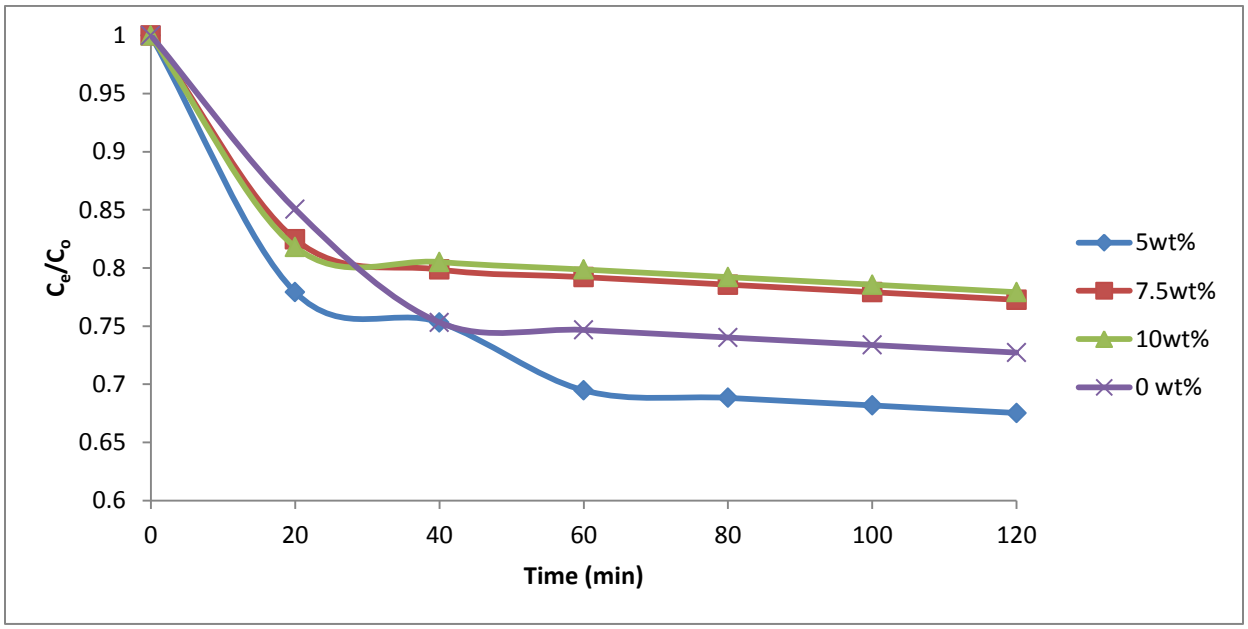

Figure 4. 7 Dark adsorption studies of photocatalyst on MO degradation

Adsorption increases with the loading of TiO_2 on support material, with optimum loading occurring 5 wt% loading of TiO_2.This is ascribed to electrostatic attraction between MO and positively charged TiO_2 on HCP, good dispersion of TiO_2 makes the support material (HCP) more acidic and increased higher surface area of HCP contributes to good adsorption of MO. Further increase in loading of TiO_2 might reduce the surface of the photocatalyst and results in lower adsorption of MO in solution. Basically, adsorption of MO on the HCP occurs via van der Waals force interactions, electrostatic interactions of methyl orange with extra framework cations presents in the HCP and increased surface area for adsorption of MO dye.

The determination of time vital for MO equilibrium adsorption was conducted at various photocatalyst loading and the amount of MO adsorption at equilibrium q_e (mg g^{-1}) can be calculated from the equation below:

$$qe = V\left(\frac{C_o - C_e}{W}\right) \quad 4.1$$

Where C_0 and C_e (mg/L) are the liquid-phase concentrations of dye at initial and equilibrium, respectively, V (L) is the volume of the solution and W (g) is the mass of photocatalyst used. From Figure 4.8, the amount of MO adsorbed is highest at lower loading of TiO_2, while the adsorption capacity drops as loading rate increases. An increase in loading rate will results in agglomeration of the photocatalyst in the solution, which furthers lead to adsorption in the interlayer space and decrease in the aggregation of MO adsorption at the external surface. The high loading rate will also results in increased viscosity and inhibits the diffusion of MO on the surface of TiO_2/HCP. The prepared photocatalyst showed exceptional adsorption capacity within 20 mins of MO adsorption almost achieved equilibrium at 30 mg/g.

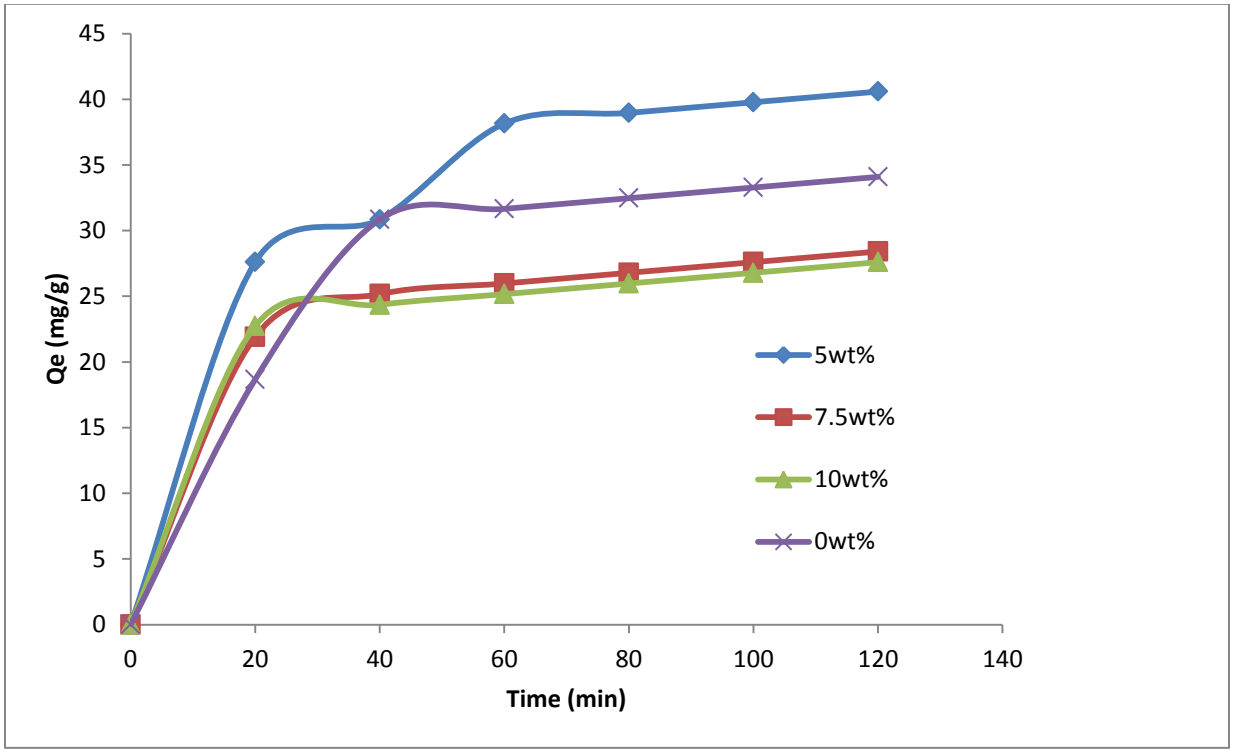

Figure 4. 8 Influence of loading rate on the adsorption of MO by TiO_2/HCP

4.2.2 Adsorption kinetic analysis

Adsorption is a physicochemical process that involves mass transfer of a solute from liquid phase to the adsorbent surface. The adsorption kinetics of MO onto TiO_2/HCP investigated in this study are the Lagergren pseudo-first order and pseudo-second-order model. The pseudo-first-order model can be expressed by the following linear form in Equation 4.2 below (Zhu *et al.*, 2010, Dogan *et al*., 2006).

$$In\,(Q_e - Q_t) = In\,Q_e - k_1 \cdot t/2.303 \qquad 4.2$$

where Q_e and Q_t (mg g^{-1}) are the amounts of adsorbed MO at equilibrium and at time *t*, respectively, k_1 (min^{-1}) is pseudo-first-order rate constant, and *t* (min) is contact time. k_1 can be determined from the slope of the plot of *In* $(Q_e - Q_t)$ versus *t.* The pseudo-second-order model (Wu, 2007, Ho and Chiang, 2001) can also be expressed in its linear form:

$$\frac{t}{q_t} = \frac{1}{k_2 \cdot q_e^2} + \frac{1}{q_e} \cdot t \qquad 4.3$$

where k_2 is the rate constant ($g \cdot mg^{-1} \cdot min^{-1}$) of pseudo-second order kinetic model for adsorption. The slope and intercept of the linear plots of *t/qt* against *t* yield the values of $\frac{1}{q_e}$ and $\frac{1}{k_2 \cdot q_e^2}$ from Equation 4.3.

The plots of Lagergren-first-order and pseudo-second-order kinetic models are depicted in Figures 4.9 and 4.10 for the loading rate of photocatalyst on MO adsorption, and corresponding values from the two models are listed in Table 4.3. It can be seen that the fitting of experimental data to the pseudo-first-order model was not so good, with rather low correlation coefficients values (R^2) and the experimental data does not obey the pseudo-first-order kinetic model. The linear plots of *t/qt* versus *t* with higher correlation coefficients than values obtained for pseudo first-order model, which indicates that the data exhibited a good compliance with pseudo-second-order kinetic equation. The adsorption kinetics of MO onto TiO_2/HCP photocatalyst follows the pseudo-second-order kinetic model judging from experimental and calculated q_e values. Similar observation is evident in comparison of the models on adsorption of MO at various loading rate in Appendix 6.

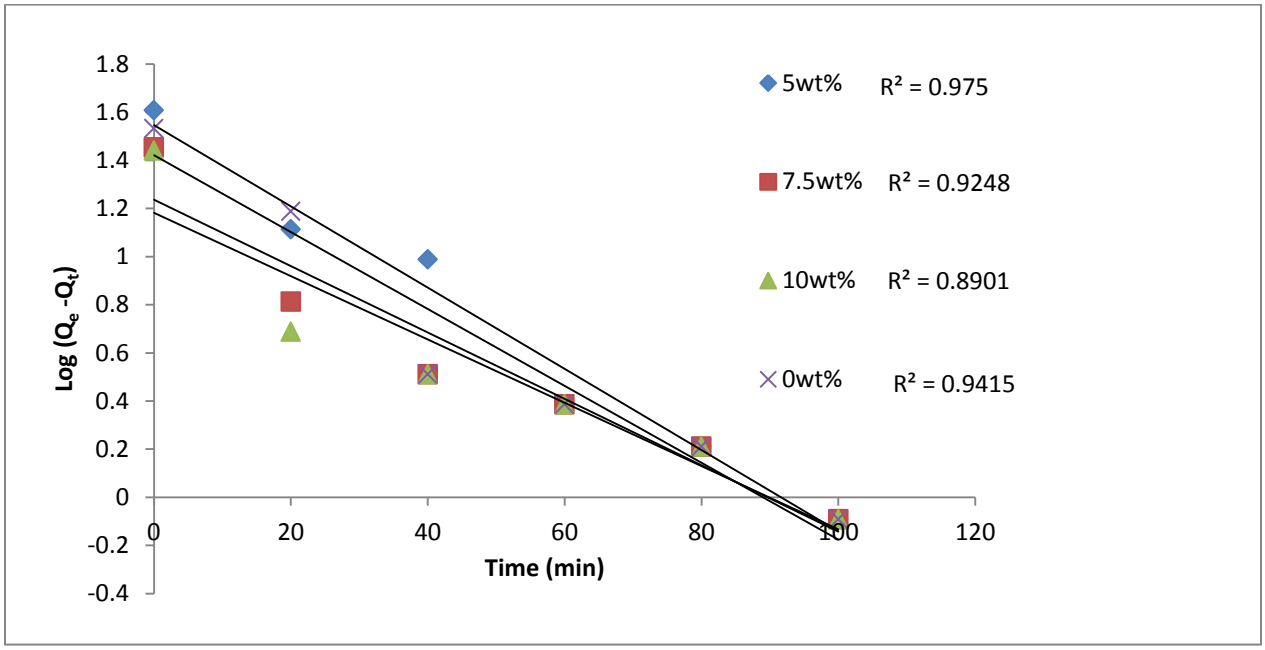

Figure 4. 9 Linear plot of pseudo first order kinetic model for MO adsorption

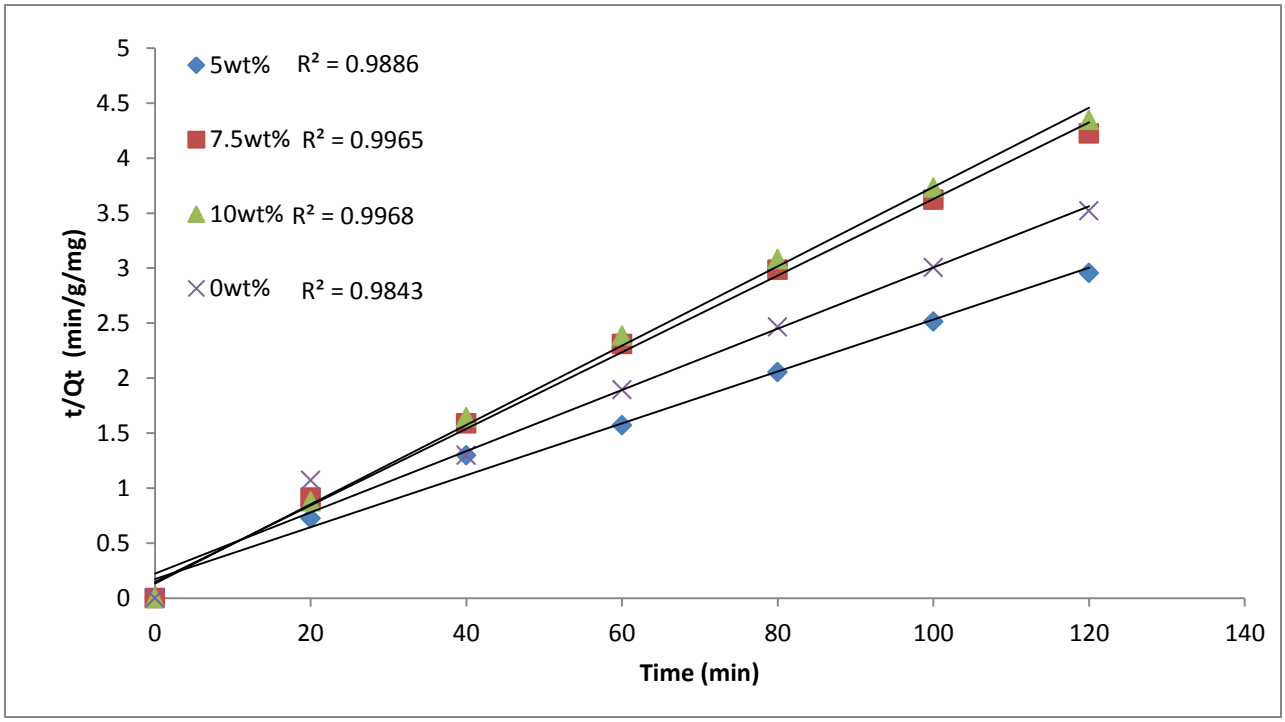

Figure 4. 10 Linear plot of pseudo second order kinetic model for MO adsorption

Table 4. 3 Adsorption kinetic model constants for MO adsorption at various loading

Loading %	Qe, exp (mg/g)	Pseudo first order		Pseudo second order	
		K_1 (min^{-1})	Q_e calculated	k_2 (g mg^{-1} min^{-1})	Q_e calculated
5 wt%	40.5844	0.0389	35.1489	0.0001721	39.9268
7.5 wt%	28.4091	0.0318	16.9946	0.0001779	27.7591
10 wt%	27.5974	0.0304	14.7414	0.0001726	26.8787
0 wt%	34.0909	0.0368	25.9867	0.0001719	33.7230

4.2.3 Photocatalytic degradation of Methyl Orange (MO)

Photocatalytic degradation experiments were conducted at different operating conditions by varying the effect of initial dye concentration, TiO_2 loading rate on HCP, pH, calcination temperature, inorganic anions, oxidant and recycling of photocatalyst. Throughout the experiments, the temperature was maintained at constant at 25 ^oC. In addition, comparative degradation efficiency experiments were also conducted among HCP, TiO_2 and TiO_2/HCP on a mixture of methyl orange and methylene blue. The dependency rate of reaction on degradation of MO and dye mixture kinetics was conducted using Langmuir-Hinshelwood model. Photocatalytic experiments were conducted here in the presence of UV radiation; degradation decrease was recorded in relation to decrease of wavelength and absorbance.

4.2.4 Effect of TiO_2 loading rate on MO degradation

In order to economize the process, the effect of TiO_2 loading must be optimized. TiO_2 loaded on HCP was employed by varying loading wt% at constant pH 8.0 during the photocatalytic treatment for its optimization. The photocatalytic degradation efficiency of photocatalyst on methyl orange increases from 29-88% (5 wt% TiO_2/HCP) maximal, as irradiation time increases from 30 mins to 270 mins, in the presence of photocatalyst at different TiO_2 loading and HCP possess lower degradation efficiency from 10-61%.

However, TiO_2/HCP poses highest degradation efficiency more than HCP (Figure 4.11), which is ascribed to its ability to gather methyl orange near to the TiO_2 surface where the degradation activities occur. The $OH^{\bullet}$ radical also on the TiO_2/HCP surface also assists in degradation of organic contaminant faster as compared to non-photoactive HCP. Other molecules such as O_2 and H_2O also contribute to degradation activities. These radical species occur from absorption of ultraviolet light on the photocatalyst surface. Electron-hole pair generation occurs on photocatalyst surface and oxygen traps the electron to prevent recombination of electron-hole pairs to form the super-oxides ($O_2^{\bullet-}$) and the $OH^{\bullet}$ radical from the holes reacts with H_2O adsorbed on photocatalyst surface (Vesely *et al*., 1991 and Chen and Liu, 2007).

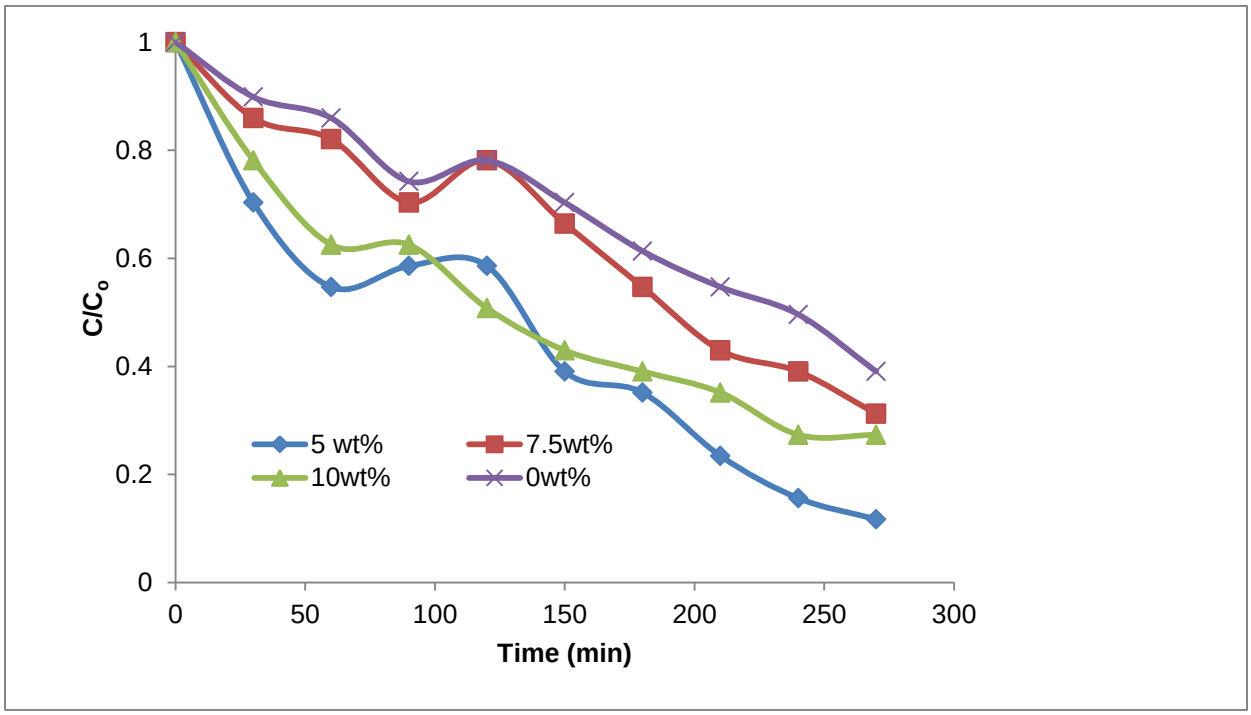

Figure 4. 11 Effect of loading wt% TiO_2 on HCP

In case of TiO_2 loading on HCP surface, 5 wt%TiO_2/HCP possesses optimum photodegradation efficiency (88%) at relative interval times as compared to 7.5 wt% (69%) and 10 wt% (73%) respectively. From observation, the efficiency of the photocatalytic process increases with increases in TiO_2 loading on HCP up to a certain limit, then becomes constant and starts to decrease after certain time.

The highest efficiency in 5 wt% TiO_2/HCP can be ascribed to fine dispersion of TiO_2 on HCP surface and increased active sites for degradation of Methyl orange chromophore. However, as the TiO_2 loading increases on the HCP surface (7.5-10 wt%), degradation efficiency drops which are ascribed to the agglomeration of TiO_2 particles on the HCP surface and decrease of the active site in the HCP (Wang, 2007). The pores in the HCP are also blocked, which leads to lower light penetration by ultraviolet light and reduces photoactivity as the TiO_2 loading increases further. The strong adsorptive properties of 5 wt% TiO_2/HCP also contribute to its enhanced photocatalytic degradation of methyl orange under ultraviolet light. In this present study, the optimum loading rate is 5 wt% TiO_2/HCP for a given concentration of 50 ppm of methyl orange solution.

4.2.5 Effect of Initial Methyl orange (MO) concentration

The pollutant concentration is a major parameter in wastewater treatment. The effect of initial dye concentration was being investigated on the photocatalytic degradation of MO after the optimization of catalyst loading rate. The initial dye concentration was varied during the photocatalytic treatment from 20 to 70 ppm, at constant pH of 8.0 and the catalyst dose of 100 mg.

There was a significant increase in efficiency (92-96%) from 20 ppm to 30 ppm, drastic decrease in photodegradation efficiency as initial MO concentration increases from 40-70 ppm, which is ascribed to the larger amount of methyl orange adsorbed on the surface of TiO_2 (Figure 4.12). They have inhibiting effect on the reaction of methyl orange molecules with $OH^{\cdot}$ radicals created on the photocatalyst surface. Reactive sites are reduced as a result of the occupation by the increased methyl orange concentration (cloudy and opaque) and in turn limit light penetration (photons) to reach the photocatalyst surface. Subsequently, the degradation activity is reduced, when fewer available $OH^{\cdot}$ radicals are required to oxidize more dye molecules. Maximal efficiency for the photocatalyst was obtained at 30 ppm of initial MO concentration. Formation of intermediate products during degradation of MO at high concentration will also result in lower photodegradation efficiency.

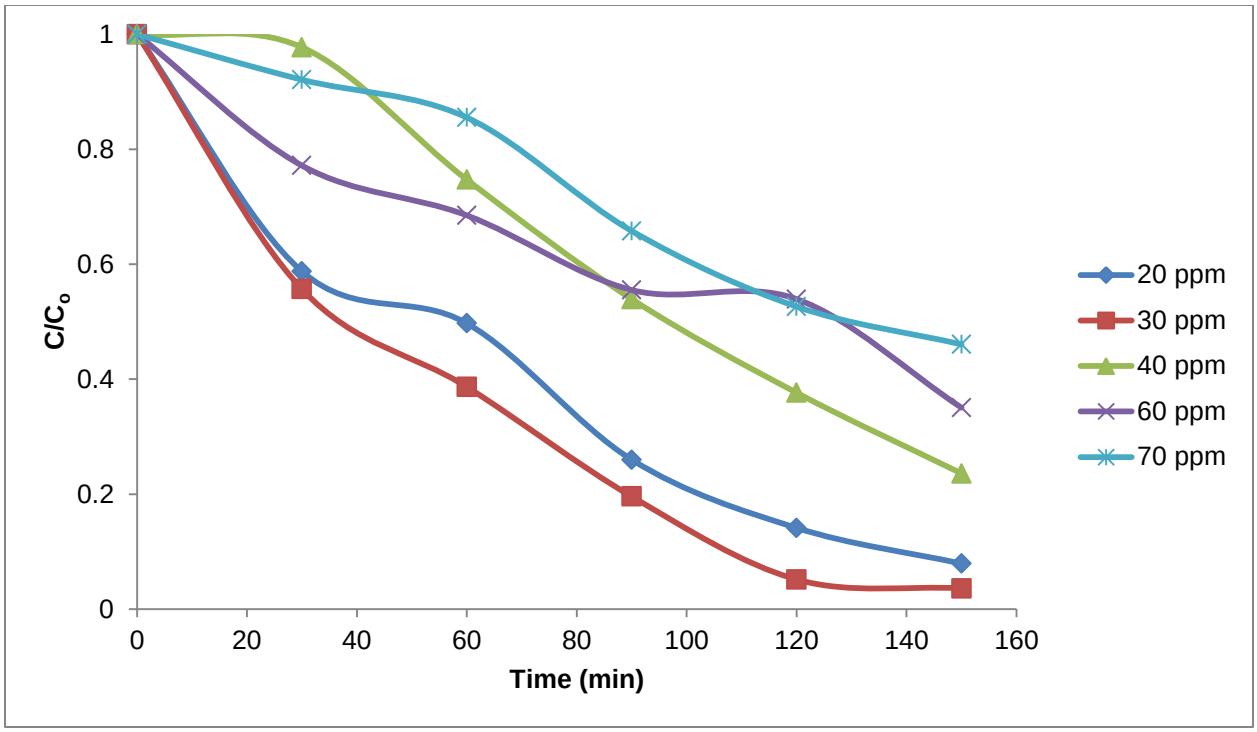

Figure 4. 12 Effect of initial MO concentration in the presence of TiO_2/HCP

4.2.6 Effect of pH on MO degradation

The pH value plays vital role in photocatalytic degradation efficiency of organic contaminants, in relation to hydroxyl and hydrogen ions affecting the photocatalyst surface area. The effect of pH on degradation of methyl orange was conducted in the pH range of 2-12 at 50 ppm MO with TiO_2/HCP. From Figure 4.13, photodegradation efficiency increases from 85% to 94% at pH of 2 to 4. A further increase from pH 6 upward results in a photodegradation efficiency decrease of methyl orange. The pH influences surface charge of TiO_2 and ionization state of ionizable organic molecules. The point of zero charge (pzc) of TiO_2 is 6.8. At pH values higher than pzc of TiO_2, the surface becomes negatively charged and vice versa for pH less than pzc of TiO_2:

$$pH < pzc: Ti - OH + H^+ \leftrightarrow TiOH_2^+ \quad 4.4$$

$$\mathrm{pH} > \mathrm{pzc}: \mathrm{Ti} - \mathrm{OH} + \mathrm{OH}^- \leftrightarrow \mathrm{TiO}^- + \mathrm{H_2O} \quad 4.5$$

In this present study, low pH makes TiO_2 positively charged in acidic medium, the positively charged TiO_2 surface adsorbs negatively charged methyl orange resulting in increased photocatalytic degradation of methyl orange (Xu and Langford, 2000). The negatively charged TiO_2 surface with negatively methyl orange creates a repulsive force resulting in a decrease in degradation efficiency of photocatalyst. Invariably different pH affects the surface charge density of TiO_2 catalyst (Rincon and Pulgarin, 2003).

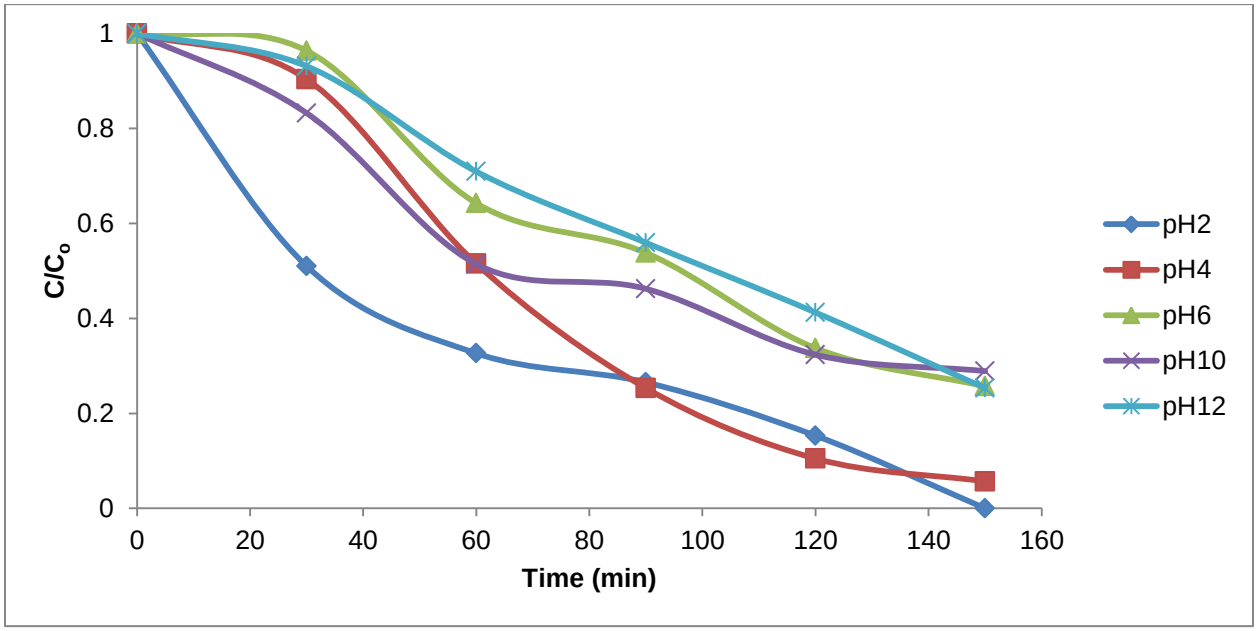

Figure 4. 13 Effect of pH on degradation rate of Methyl orange

4.2.7 Effect of calcination temperature on MO degradation

Photocatalyst structure affects photodegradation activities of organic contaminants; the samples were being calcined at different temperatures to depict different crystal structures. The effect of calcination temperature was performed in presence of TiO_2/HCP with Methyl orange within a temperature range of 423-973 K. From Figure 4.14, photodegradation efficiency increases with calcination temperature and maximal photocatalytic activity was obtained at 873 K with close activity at 423 K from 95-96%. This optimum calcination temperature is ascribed to the formation of anatase phase on the photocatalyst surface, which enhances degradation activities. Though as calcination temperature increases above 873 K, the photodegradation activities decreases to 84% as a result of formation of rutile phase and also accelerated

formation of TiO_2 particles on the surface of HCP. It also results in aggregation of TiO_2 and decrease in specific surface area of the particles.

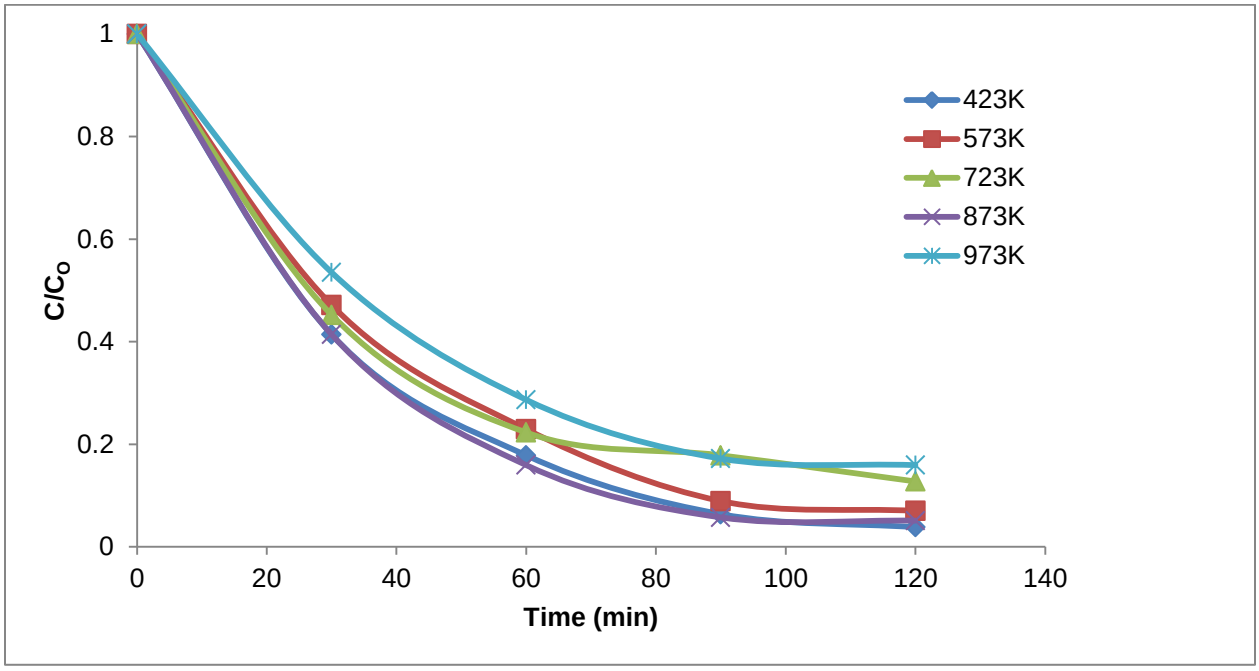

Figure 4. 14 Effect of calcination temperature on degradation rate of MO

4.2.8 Effect of inorganic anions on MO degradation

Inorganic anions coexist with dissolved organic and humic acid in wastewater (Wang *et al.*, 2004), studies revealed these substances can compete for active sites of photocatalyst. They can subsequently decrease photodegradation efficiency of photocatalyst on target organic contaminants. The effect of inorganic anions was conducted with 200 ppm of Cl^-, SO_4^{2-}, CO_3^{2-}, NO_3^- added as Sodium salts respectively, along with methyl orange solution (30 ppm, pH 4) in presence of TiO_2/HCP. From Figure 4.15, NO_3^- and SO_3^{2-} anions accelerate the degradation of methyl orange effectively, while the Cl^- deactivates the photocatalyst slightly with degradation efficiency decreasing $OH^{\bullet}$ radical generation increases in the solution upon absorption of UV by NO_3^-, which accelerates the degradation rate of methyl orange (Zhang *et al*., 2005).

$$NO_3^- + h\upsilon \rightarrow NO_2^- + O \qquad 4.6$$

$$NO_3^- + H_2O + h\upsilon \rightarrow NO_2^{\cdot} + OH^- + OH^{\cdot} \quad 4.7$$

However SO_4^{2-} and CO_3^{2-}, strongly deactivates the efficiency of the catalyst and decreases the photocatalytic activities on methyl orange.

$$SO_4^{2-} + h \rightarrow SO_4^- \quad 4.8$$

$$SO_4^{2-} + OH^{\cdot} \rightarrow SO_4^- + OH^- \quad 4.9$$

$$CO_3^{2-} + OH^{\cdot} \rightarrow HO^{\cdot} + CO_3^- \quad 4.10$$

This inhibitory effect of SO_4^{2-} and CO_3^{2-} can be ascribed to the reactions of anions with positive holes and hydroxyl radicals which in turn acting as h^+ and $OH^{\cdot}$ scavengers. These anions compete with methyl orange for oxidizing species and in turn prolong catalytic activities (Guillard *et al.*, 2003).

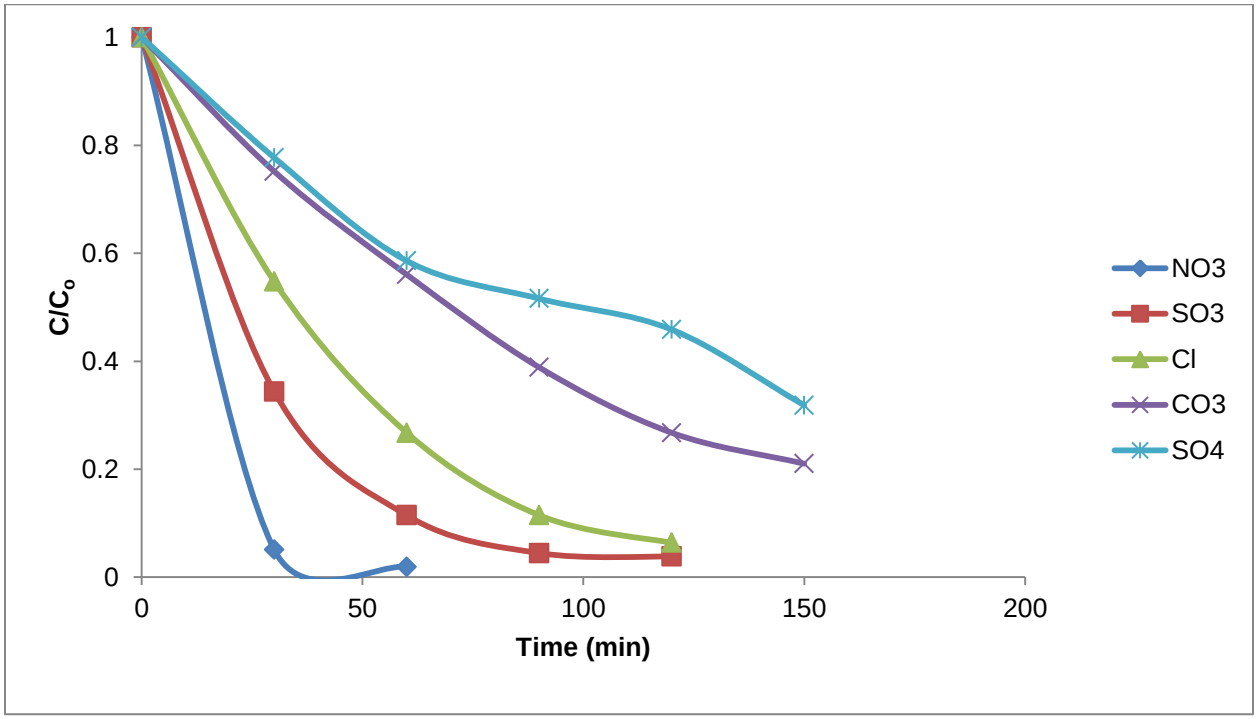

Figure 4. 15 Effect of inorganic ions on degradation rate of MO

4.2.9 Effect of oxidant on MO degradation

The effect of addition of H_2O_2 was studied for enhancing the elimination and breaking of bonds in MO dye chromophore. Electron acceptor such as H_2O_2 was added to Methyl orange (MO) solution and subjected to photodegradation activities in the presence of TiO_2/HCP. Their effect on the degradation of MO versus time is depicted in Figure 4.16, the experiment conducted with 50 ppm MO solution with pH 4 and different concentrations of H_2O_2. Enhanced degradation of MO increases with increasing mass of peroxide, with 15 mM possessing highest degradation efficiency (98%). Rapid generation of $OH^{\bullet}$ radical which enhances degradation of MO, in the presence of H_2O_2 with a combination of UV radiation (Irmak *et al*., 2004, Peternel *et al*., 2006).

$$H_2O_2 + h\upsilon \rightarrow 2OH^{\cdot} \quad (4.11)$$

$OH^{\cdot}$ radical is the strongest oxidant after fluoride (Andreozzi *et al*., 1999) and active radical that oxidize organic contaminants rapidly into mineralized products on the surface of the photocatalyst illuminated by UV light. Irrespective of added H_2O_2 concentration of MO solution, the following reactions take place:

$$OH^{\cdot} + OH^{\cdot} \rightarrow H_2O_2 \quad (4.12)$$

$$H_2O_2 + OH^{\cdot} \rightarrow H_2O + HO_2^{\cdot} \quad (4.13)$$

$$HO_2^{\cdot} + OH^{\cdot} \rightarrow H_2O + O_2^{\cdot} \quad (4.14)$$

Rapid degradation activities of MO in the presence of H_2O_2 are ascribed to trapping of electrons by H_2O_2, which in turn reduces recombination of electron-hole pairs and leads to rapid generation of $O_2^{\cdot-}$, $HOO^{\cdot}$, $OH^{\bullet}$ on the photocatalyst surface. Though, H_2O_2 in high concentration might lead to decrease in the degradation activities which are ascribed to exhaustion of $OH^{\bullet}$ in the solution (Huang, 1993).

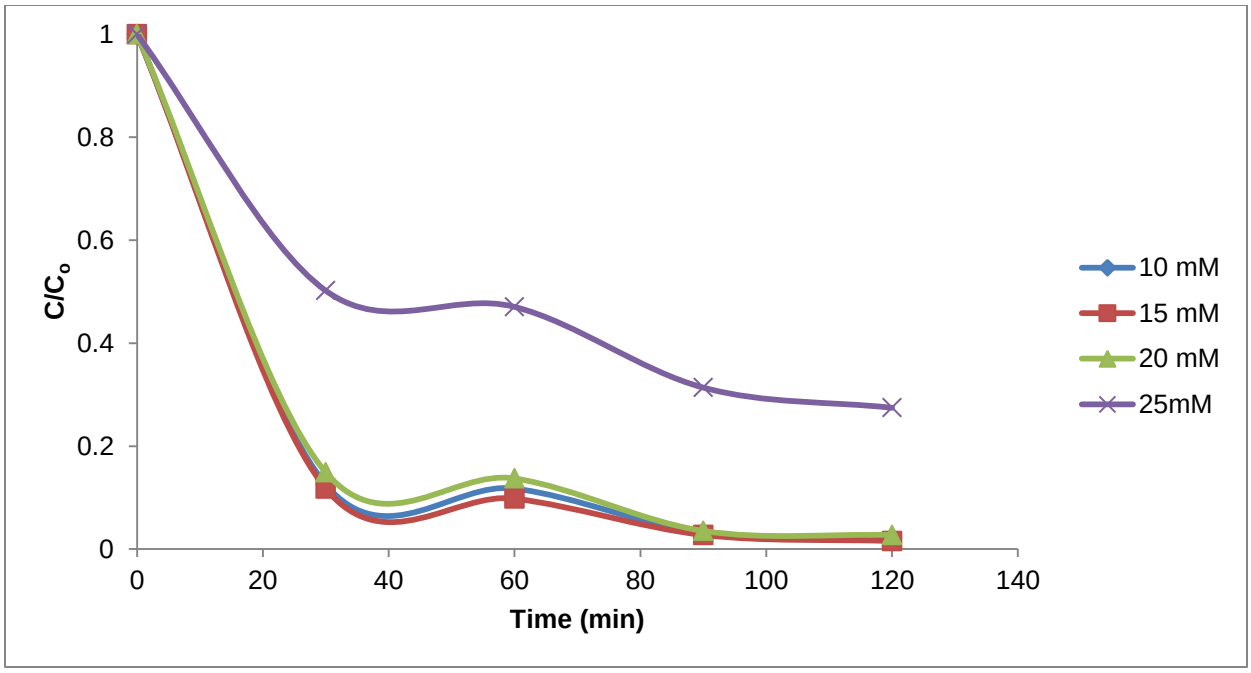

Figure 4. 16 Effect of peroxide on degradation rate of MO

4.2.10 Recycling of photocatalyst on MO degradation

Part of the challenges of applying titania material are the recycling, here recycling of the synthesized photocatalyst was aimed at practicability for other organic contaminants and for repeated cycles. Recycling of photocatalyst was conducted with TiO_2/HCP on degradation of methyl orange (20 ppm, pH 4) under ultraviolet light. The photocatalyst was recycled after filtration and heated at 110 ^{0}C at 2 hrs for every cycle. There was a considerable decrease in degradation efficiency as shown in Figure 4.17, from 92% to 48% after 3 cycles and maintaining 80% of initial activity. The decrease in degradation efficiency is attributed to loss of TiO_2 from HCP surface during filtration and washing process. Fouling can also result from the by-products form on the photocatalyst surface and heat treatment to assist in removing the by-products, which makes the photocatalyst surface refresh. However, heat treatment will also result in catalyst aggregation after several cycles and further decreases surface area resulting in low photocatalytic efficiency.

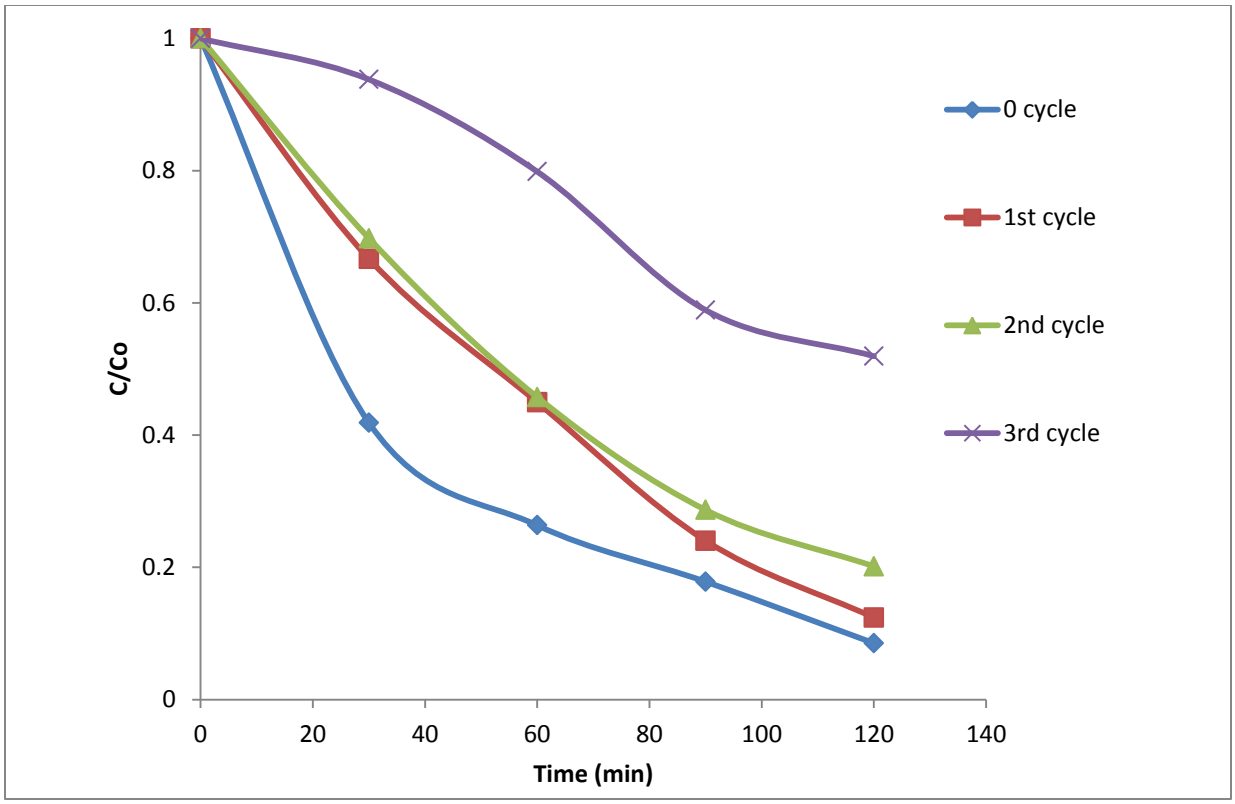

Figure 4. 17 Effect of recycling rate on degradation of MO

4.3 Comparison activities of the photocatalyst on dye mixtures

Decolourization of dye employing photocatalyst under UV light is very vital; however most attention has been on single dye components as compared to mixtures of dye molecules. Though, studies conducted by Robert *et al* depicts successful degradation of binary mixture of 4-hydroxybenzoic acid and benzamide without any change in the concentration of other molecules, under 2 parameters (pH and TiO_2 concentration) with improved selectivity (Robert *et al*., 2004). Gora *et al*. established kinetic analysis of the photocatalytic oxidation of a mixture of three herbicides (Gora *et al*., 2006). Gupta and his co-worker conducted photocatalytic degradation of a mixture of an anionic azo dye (methyl red) and a cationic triphenylmethane dye (crystal violet) in aqueous suspensions employing Ag^+ doped TiO_2 as photocatalyst under UV-light radiation (Gupta *et al*., 2006).

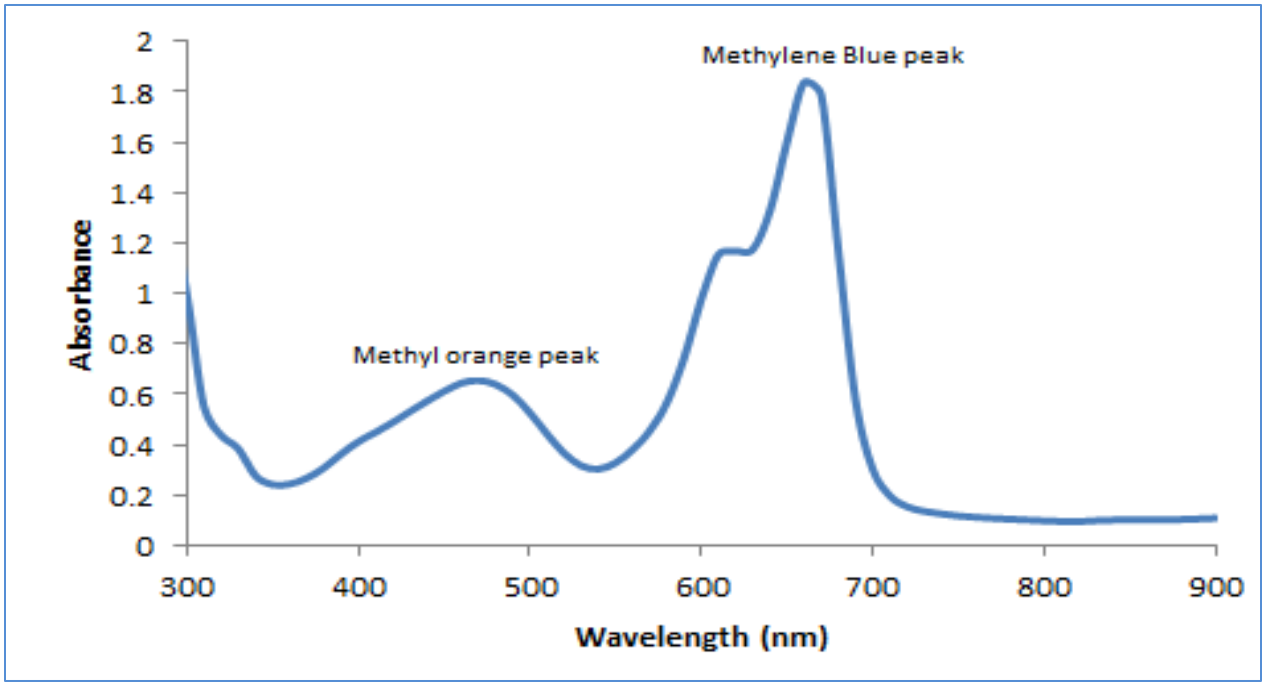

Figure 4. 18 Characteristic wavelengths of MO and MB

Here, comparative analysis is conducted on the photocatalyst prepared (HCP, TiO_2 and TiO_2/HCP) on a mixture of methyl orange (anionic dye) and methylene blue (cationic dye) in a single component under UV- irradiation. The mixture (40 ppm, pH 8) was conducted in the presence of a prepared catalyst (100 mg/L) under UV- radiation. From Figure 4.18, characteristic wavelength and absorbance is not affected by mixing both dyes together, with both dyes possessing their unique peaks for methyl orange (M0) and methylene blue (MB). The degradation of both dye mixtures was observed at a wavelength of 480 nm for MO and 661 nm for MB respectively in the visible region.

From Figure 4.19, TiO_2/HCP possesses highest degradation efficiency (93% for MB and 83% for MO) than HCP and TiO_2 due to fine dispersion of TiO_2 on HCP and in long run facilitate rapid breakdown of dye mixture in solution. This depicts that photocatalytic activity is accelerated when TiO_2 is immobilized on the HCP. The enhanced photocatalytic efficiency of TiO_2/HCP can also be attributed to good synergistic interaction between TiO_2 and HCP, which occurs from sol-gel synthesis of the photocatalyst.

However, HCP also possesses higher degradation efficiency (91% for MB and 76% for MO) more than TiO_2 (89% for MB and 75% for MO) due to good dealumination of natural CP, which increases the surface area and micropore size of the zeolite. HCP intrinsic properties as zeolites could have contributed to higher degradation rate more than TiO_2 such as good photochemical stability and active part in the electron transfer process. The transparency of HCP to UV radiation above 240 nm as compared to TiO_2, which utilizes 4% of sunlight radiation, might also be another factor for higher degradation of HCP than TiO_2.

However, MB degrades faster than MO when utilizing the catalyst under UV radiation in this comparative study as depicted in Figure 4.20. The analysis range on the UV-spectrophotometer was conducted between 200-900 nm, judging from characteristic reduction of wavelength and absorbance respectively of the dye mixtures. Prior to degradation activities, MB exhibits absorption wavelength at 661 nm due to the presence of the chromophore group (quinone) responsible for MB color. This chromophore is broken down to phenyl group, as well as absorption wavelength blue-shifted from 661-650 nm depicting rapid decrease in wavelength and conjugated bond in the presence of photocatalyst. For MO, absorption wavelength was in the visible region (480 nm) ascribed to the presence of chromophore (–N=N-) conjugated bond. The absorption spectrum of MO is blue shifted to 400 nm, as a result of breaking of the conjugated bond responsible for MO colour into –N=N- and less harmful metabolites.

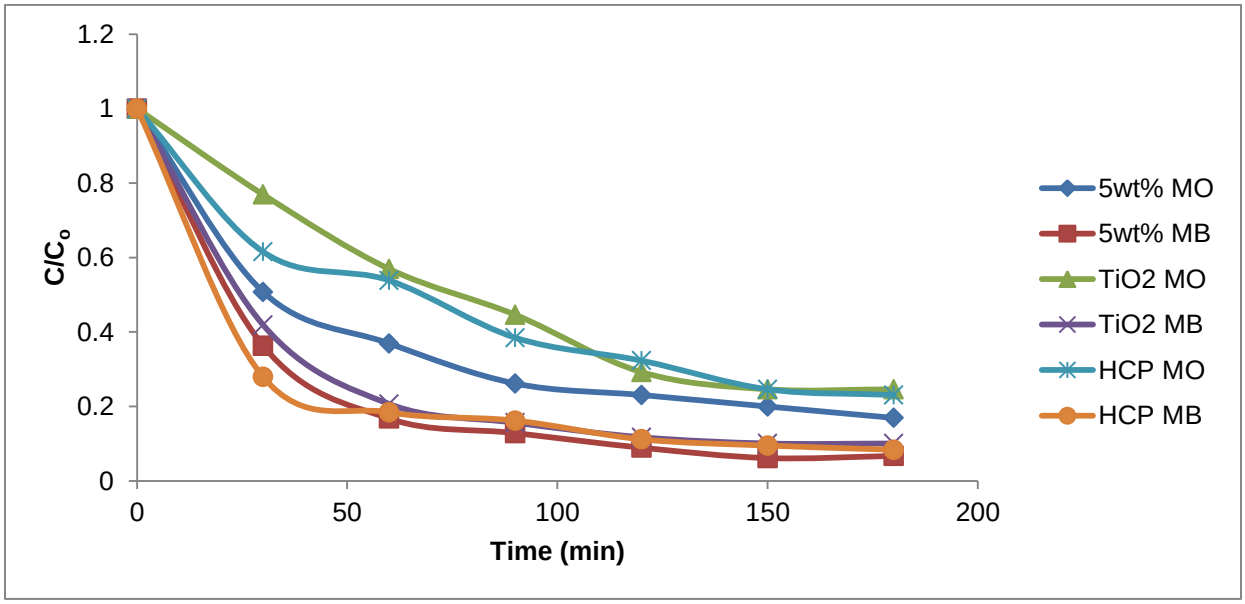

Figure 4. 19 Photodegradation of dye mixture in the presence photocatalyst

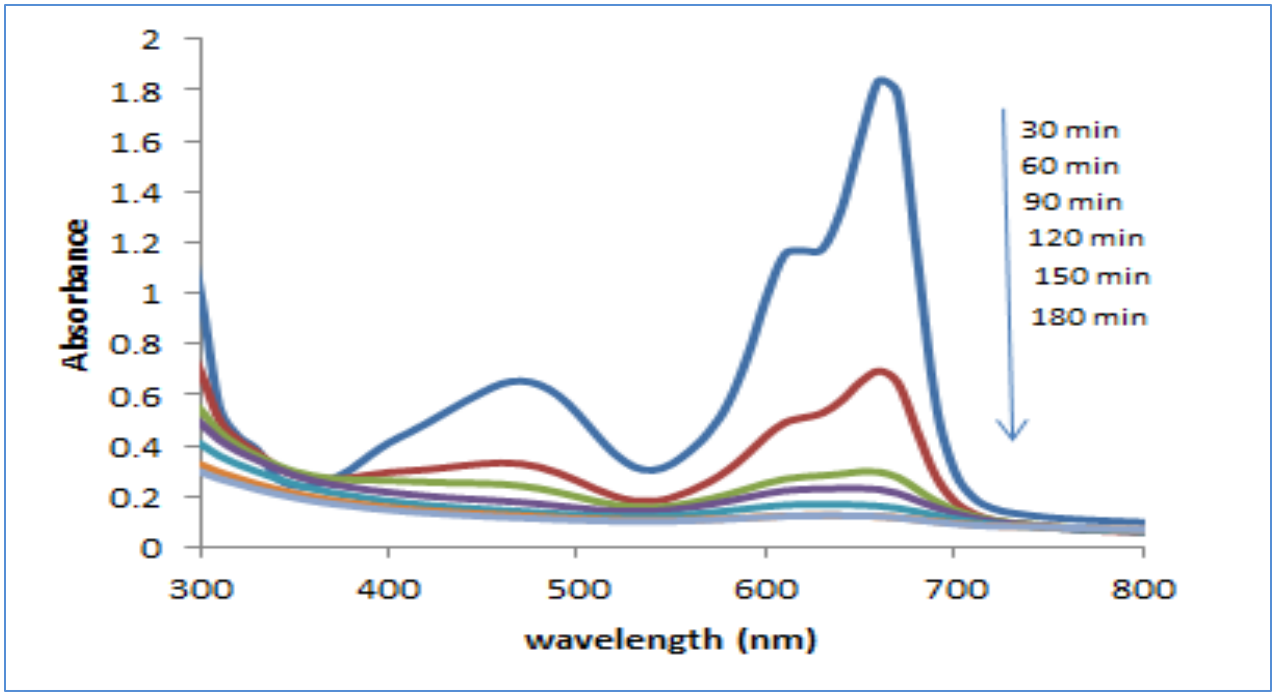

Figure 4. 20 UV-absorption spectra of dye mixture

4.4 Kinetics of photocatalytic degradation of Methyl orange and Dye mixture

Kinetic analysis enables the quantification of the photocatalytic process and comparison of the effect of different operational parameters such as effect of initial dye concentration, photocatalyst loading, pH, calcination temperature, anions, oxidant, the recycling period for Methyl orange (Konstantinou and Albanis, 2004) and comparative analysis on dye mixture. Langmuir Hinshelwood (L-H) kinetic model (Turchi and Ollis, 1990) has been applied to describe the dependency of photocatalytic reaction on concentration of organic pollutants as shown in Equation 4.15:

$$r = \frac{dC}{dt} = \frac{k \cdot K \cdot C}{1 + K \cdot C} \qquad 4.11$$

Where r is oxidation rate of the reactant (ppm min^{-1}), C_0 is initial concentration of the reactant (ppm), C_t is the concentration of the reactant at time t (ppm), t is irradiation time, k is the reaction rate constant (min^{-1}), and K is the Langmuir adsorption coefficient of the reactant onto

the catalyst particles (L mg^{-1}). The above equation is simplified into Zeroth (Equation 4.16) and pseudo first order reaction (Equation 4.17) as described below:

$$\boldsymbol{C_o - Ct = K_O \cdot t} \quad 4.16$$

$$\boldsymbol{In\left(\frac{C_t}{C_o}\right) = -K_1 \cdot t} \quad \mathbf{4}.17$$

However if the reaction follows second order kinetics, integration of Equation 4.15 will results into second order rate (Equation 4.18) as depicted below:

$$\boldsymbol{\frac{1}{C_t} - \frac{1}{C_o} = K_2 \cdot t} \quad 4.18$$

All the 3 order rates were tested for the operational parameters conducted in this study to determine which one fits well with degradation of organic pollutants employed in this study.

4.4.1 Loading rate kinetics

Studies reveal 3 crucial steps determine heterogeneous catalysis; adsorption of organics on the surface of the catalyst, followed by surface reaction on the catalyst surface and desorption of products from the catalyst surface. However, in terms of loading rate of TiO_2 on HCP surface affects the degradation rate of MO by making limiting reaction either as mass transfer or surface reaction.

At lower loading of TiO_2, UV-radiation penetrates the surface of the catalyst and its strong absorptive power accelerates rapid degradation of MO as compared of the higher loading of TiO_2. Basically at lower loading, the reaction step is surface reaction and at higher loading mass transfer becomes limiting step. The kinetic plot for the degradation of the methyl orange dye at different TiO_2 loading follows pseudo first order kinetics (Figure 4.21), but not for Zeroth and second order in the appendix (Appendix 7). The kinetic parameters are also depicted in Table 4.4.

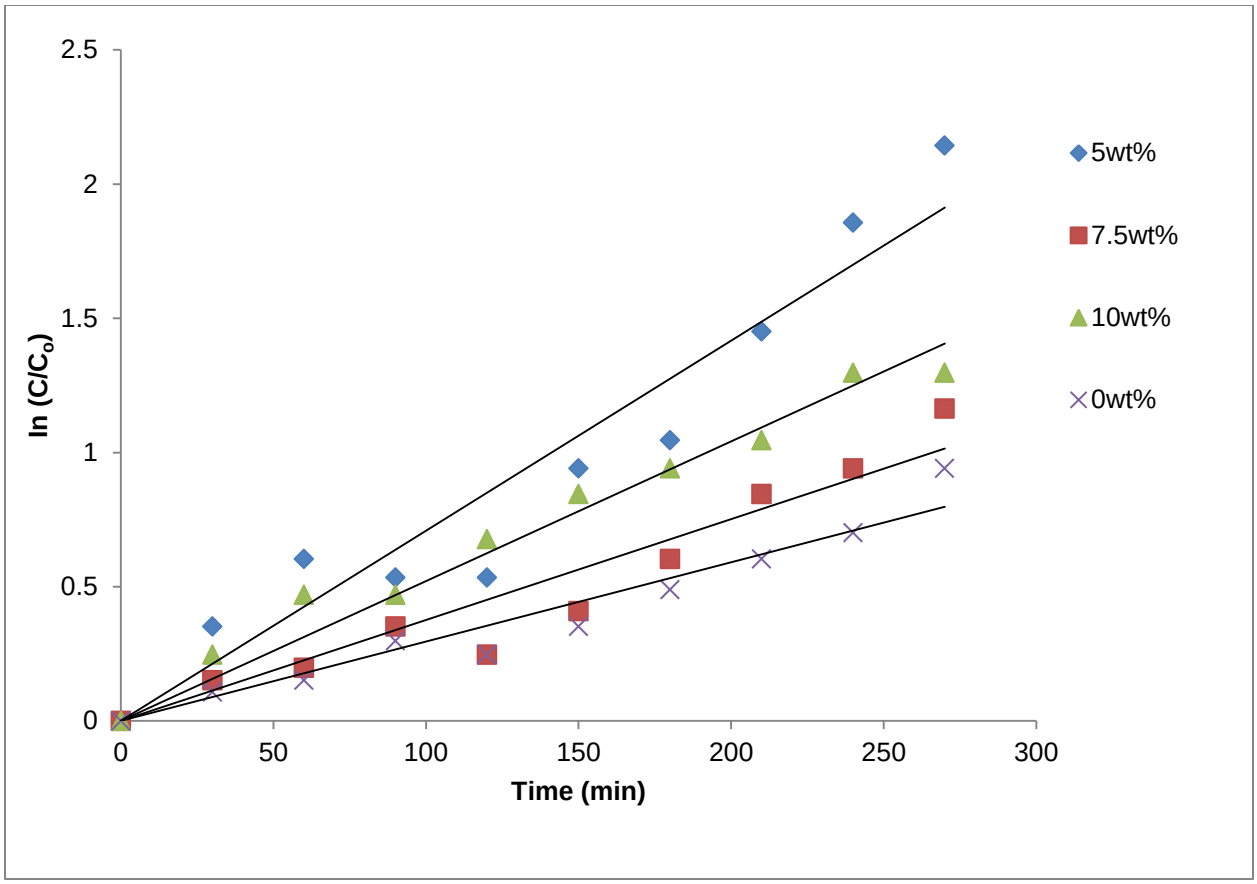

Figure 4. 21 Pseudo first order kinetics of MO degradation at loading of TiO_2

Table 4. 4 Kinetic model parameters of degradation of MO at different loading of TiO_2

	Zeroth Order		1st Order		2nd Order	
Catalyst	K (min^{-1})	R^2	K (min^{-1})	R^2	K (min^{-1})	R^2
0wt%	0.0034	0.9736	0.1128	0.9427	0.0001	0.8560
5wt%	0.0079	0.8301	0.1634	0.9271	0.0006	0.7307
7.5wt%	0.0043	0.9553	0.1273	0.9243	0.00016	0.8290
10wt%	0.0048	0.8017	0.1345	0.9669	0.00019	0.9617

4.4.2 Kinetics of other operational parameters and on dye mixture

L-H model describes the degradation of MO, especially at lower concentrations of MO the reaction is governed by a L-H model becoming a first order reaction rate and limiting step govern by mass transfer. However at higher concentration of MO, L-H model becomes Zeroth order reaction rate and limiting step govern by surface reaction. Generally, degradation of MO in the presence of the catalyst in this study could be interfaced process that obeys L-H model in Equation 4.19:

$$\frac{\mathbf{1}}{\boldsymbol{k_{app}}} = \frac{\mathbf{1}}{\boldsymbol{k \cdot K}} + \frac{\boldsymbol{C_o}}{\boldsymbol{k}} \qquad 4.12$$

Here *k* is the reaction rate constant and *K* is L-H constant, while the plot of $\frac{1}{k_{app}}$ against C_o is shown (Figure.4.22) degradation of MO by the catalyst is in line with the L-H model. The values for *K* (2.81 ppm^{-1}) was larger than *k* (-14.87 ppm min^{-1}) depicting reaction occurred in the bulk solution and also on the surface of the catalyst. The kinetic plot for the degradation of the methyl orange dye at different initial MO concentration follows pseudo first order kinetics (Figure 4.23), but not for Zeroth and second order in the appendix (Appendix 13).

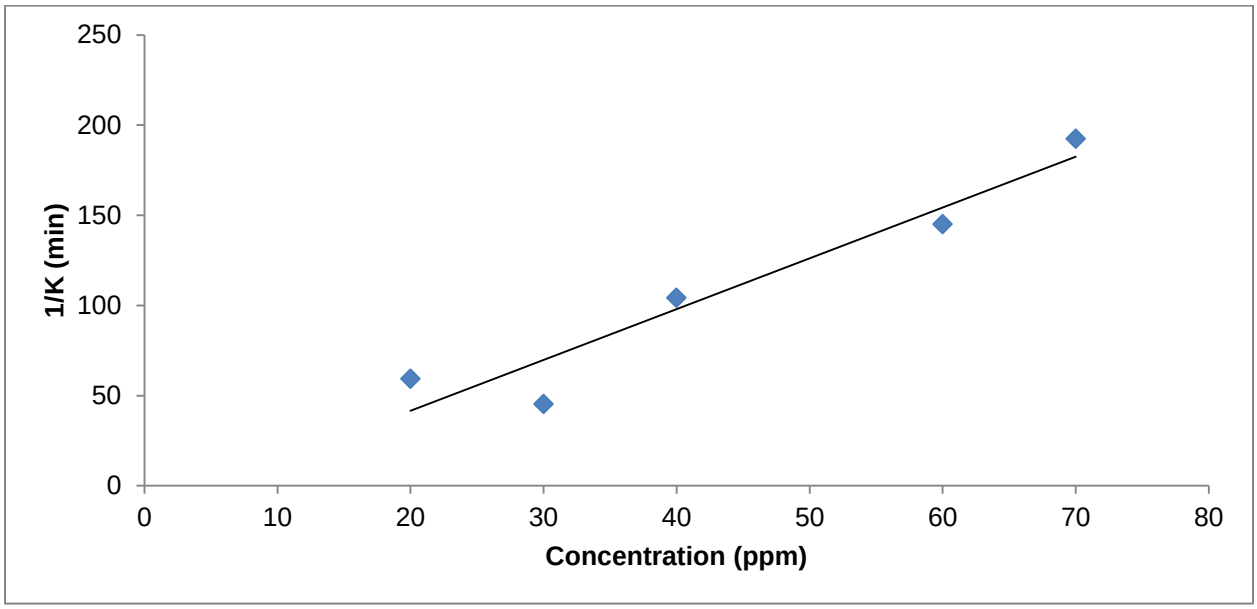

Figure 4. 22 Plot of $1/K_{app}$ versus C_o at different initial concentration of MO degradation

The kinetic parameters are also depicted in Table 4.5. The other operational parameters such as pH, calcination temperature, effect of anions and recycling period all follows the first order kinetic model, while oxidant and comparative analysis studies of prepared catalyst in the dye mixture follows Second order kinetic model.

Table 4. 5 Parameters of degradation of MO at different initial concentration of MO

C_o (ppm)	K (min^{-1})	r_o (ppm min^{-1})	% Degradation	$1/r_o$ (min ppm^{-1})	1/K (min)
20	0.0169	0.338	92.09	2.9586	59.1716
30	0.0221	0.663	96.39	1.5082	45.2488
40	0.0096	0.384	76.4	2.6041	104.1667
60	0.0069	0.414	64.96	2.4154	144.9275
70	0.0052	0.364	53.95	2.7472	192.3077

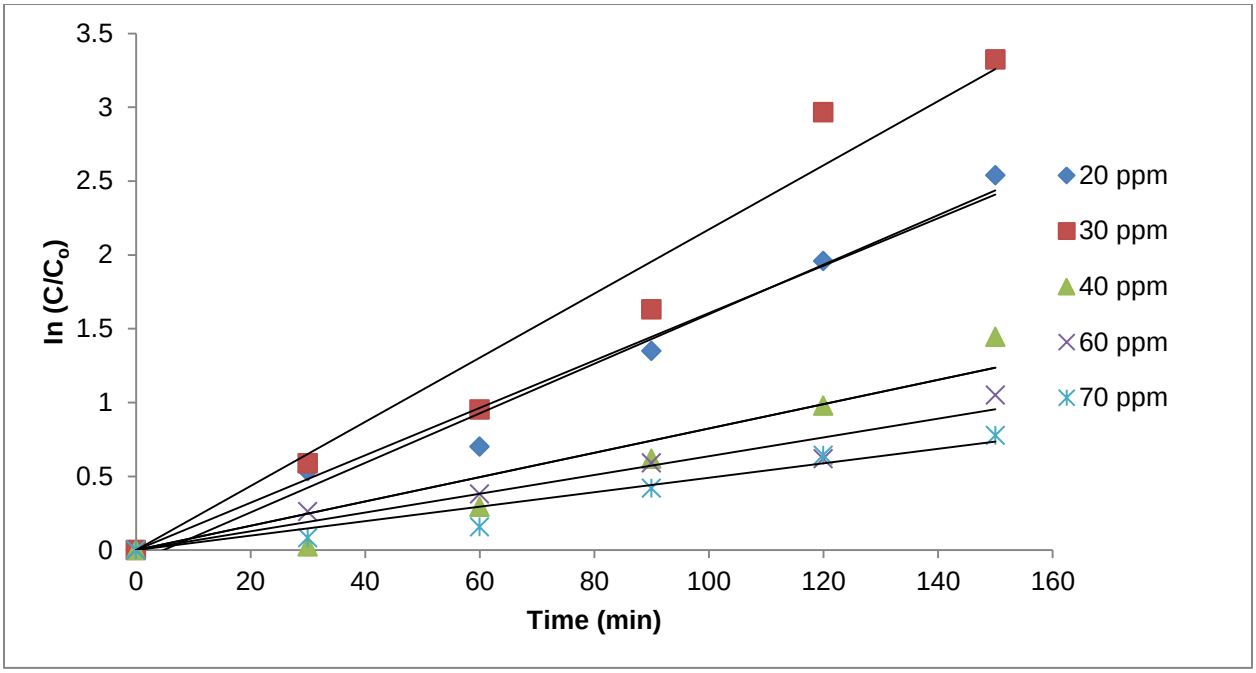

Figure 4. 23 Pseudo first order kinetics of MO degradation at various initial concentration

Table 4. 6 Kinetic model parameters of degradation of MO at different initial concentration

	Zeroth Order		1st Order		2nd Order	
Concentration	K (min^{-1})	R^2	K (min^{-1})	R^2	K (min^{-1})	R^2
20	0.1228	0.8700	0.0169	0.9780	0.0039	0.7769
30	0.1928	0.8261	0.0221	0.9585	0.0059	0.7385
40	0.2037	0.9611	0.0096	0.9079	0.0005	0.7824
60	0.2598	0.9242	0.0069	0.9453	0.0002	0.8682
70	0.2518	0.9674	0.0052	0.9439	0.0001	0.9046

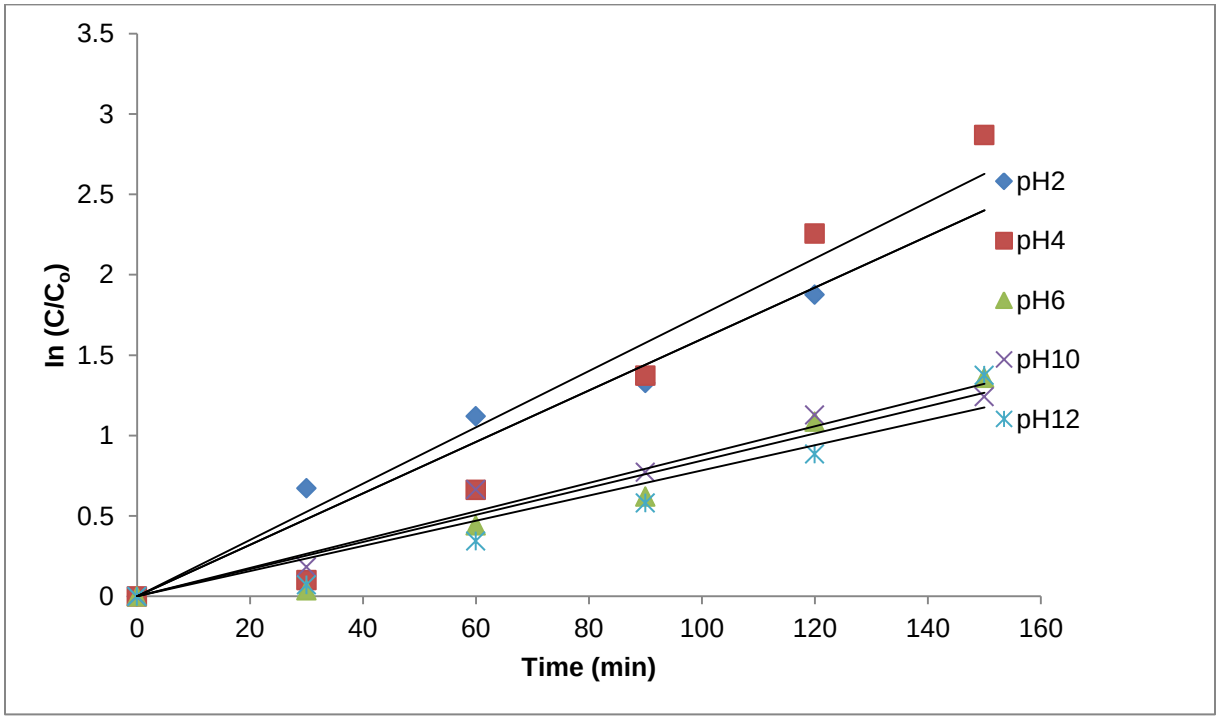

Figure 4. 24 Pseudo first order kinetics for degradation of MO at different pH

Table 4. 7 Kinetic model parameters of MO degradation at different pH

	Zeroth Order		1st Order		2nd Order	
pH	**K (min^{-1})**	**R^2**	**K (min^{-1})**	**R^2**	**K (min^{-1})**	**R^2**
2	0.3333	0.7490	0.0156	0.9613	0.0009	0.9218
4	0.3144	0.9450	0.0188	0.9339	0.0014	0.7217
6	0.2477	0.9601	0.0091	0.9442	0.0003	0.8586
10	0.2369	0.9039	0.0094	0.9700	0.0003	0.9616
12	0.2489	0.9853	0.0074	0.9263	0.0002	0.7892

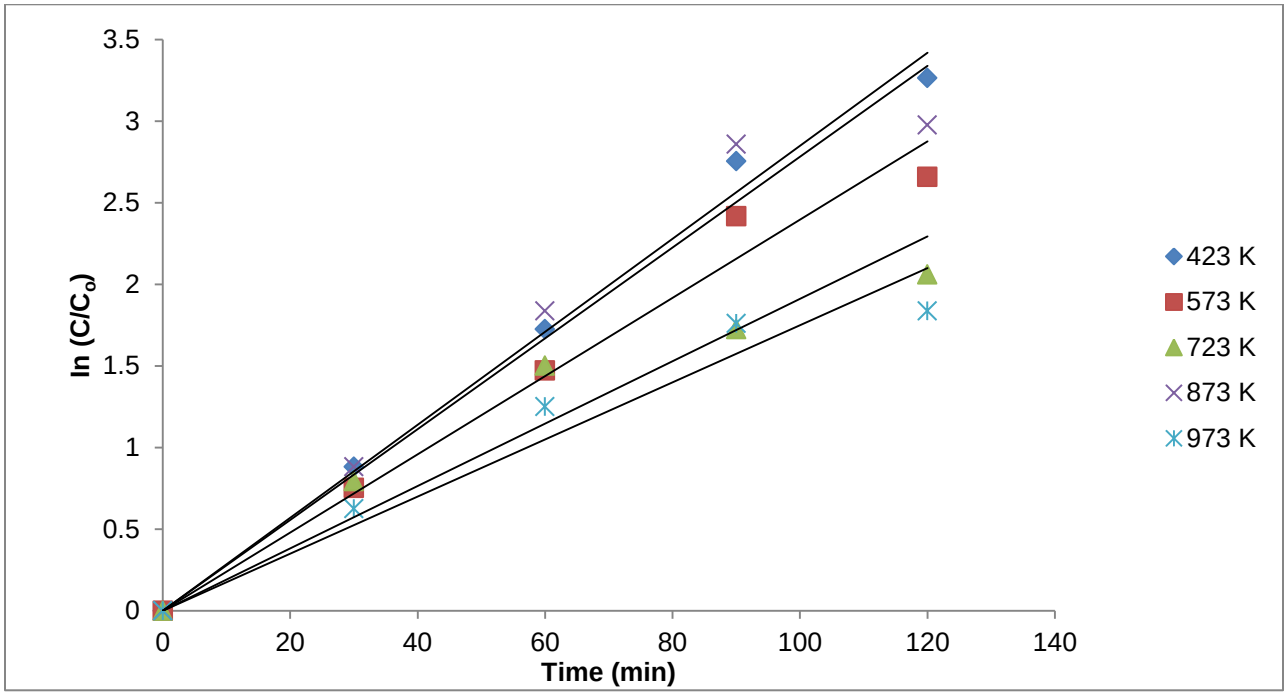

Figure 4. 25 Pseudo first order kinetics of MO degradation at different calcination temperature

Table 4. 8 Kinetic model parameters of MO degradation under different calcination temperature

Calcination Temperature	Zeroth Order K (min^{-1})	Zeroth Order R^2	1st Order K (min^{-1})	1st Order R^2	2nd Order K (min^{-1})	2nd Order R^2
423	0.1603	0.7029	0.0272	0.9915	0.0105	0.8500
573	0.1549	0.7535	0.0221	0.9765	0.0055	0.9011
723	0.1454	0.6590	0.0172	0.9158	0.0029	0.9862
873	0.1581	0.6796	0.0248	0.9561	0.0078	0.8914
973	0.1401	0.7557	0.0153	0.9371	0.0022	0.9611

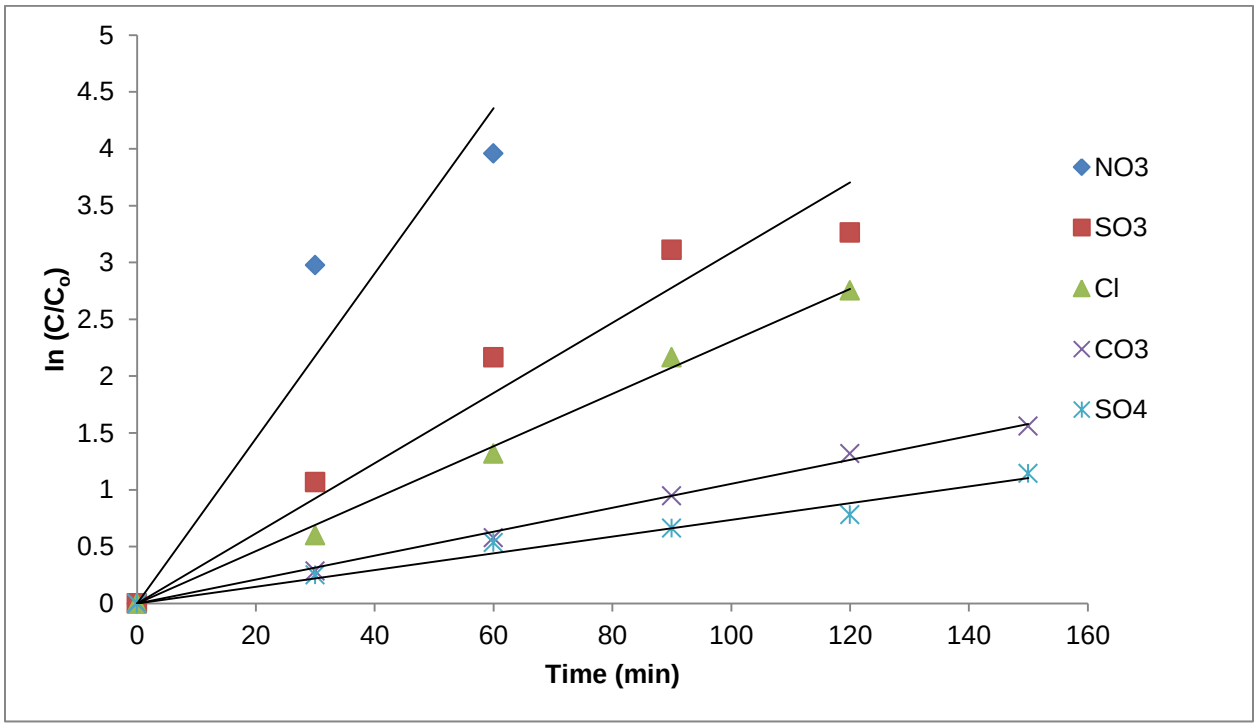

Figure 4. 26 Pseudo first order kinetics of MO degradation using different anions

Table 4. 9 Kinetic model parameters of MO degradation in presence of different anions

	Zeroth Order		1st Order		2nd Order	
Anions	**K (min^{-1})**	**R^2**	**K (min^{-1})**	**R^2**	**K (min^{-1})**	**R^2**
NO_3	0.3269	0.7292	0.0659	0.9062	0.0428	0.9706
SO_3	0.1603	0.5947	0.0272	0.9452	0.0119	0.8350
Cl	0.1561	0.8401	0.0229	0.9959	0.0061	0.8375
CO_3^{2-}	0.1053	0.9387	0.0104	0.9961	0.0013	0.9275
SO_4^{2-}	0.0909	0.9090	0.0076	0.9728	0.0007	0.9266

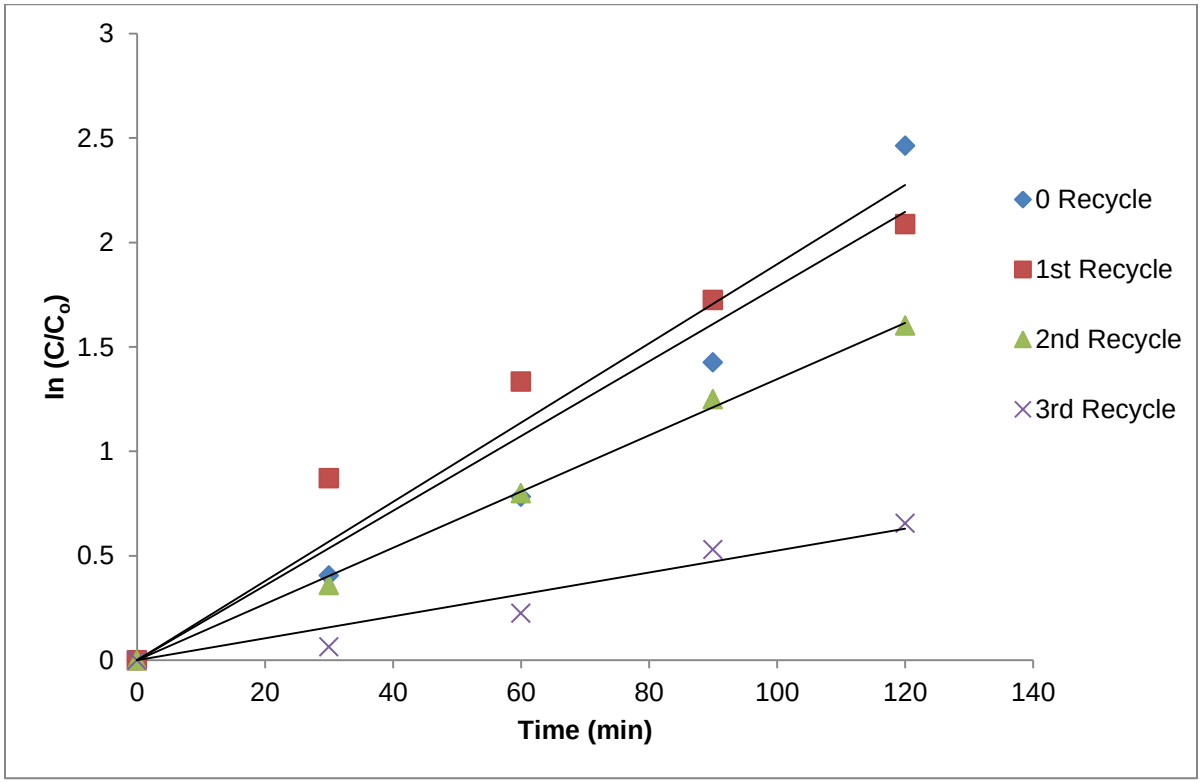

Figure 4. 27 Pseudo first order kinetics of MO degradation at different recycling rate

Table 4. 10 Kinetic model parameters of MO degradation at different recycling rate

	Zeroth Order		1st Order		2nd Order	
Recycle	**K (min^{-1})**	**R^2**	**K (min^{-1})**	**R^2**	**K (min^{-1})**	**R^2**
0 Rec	0.1525	0.6908	0.0205	0.9730	0.0045	0.8462
1 Rec	0.1459	0.9544	0.0174	0.9789	0.0029	0.8049
2 Rec	0.1331	0.9376	0.0133	0.9976	0.0017	0.9288
3 Rec	0.0801	0.9582	0.0055	0.9374	0.0004	0.9080

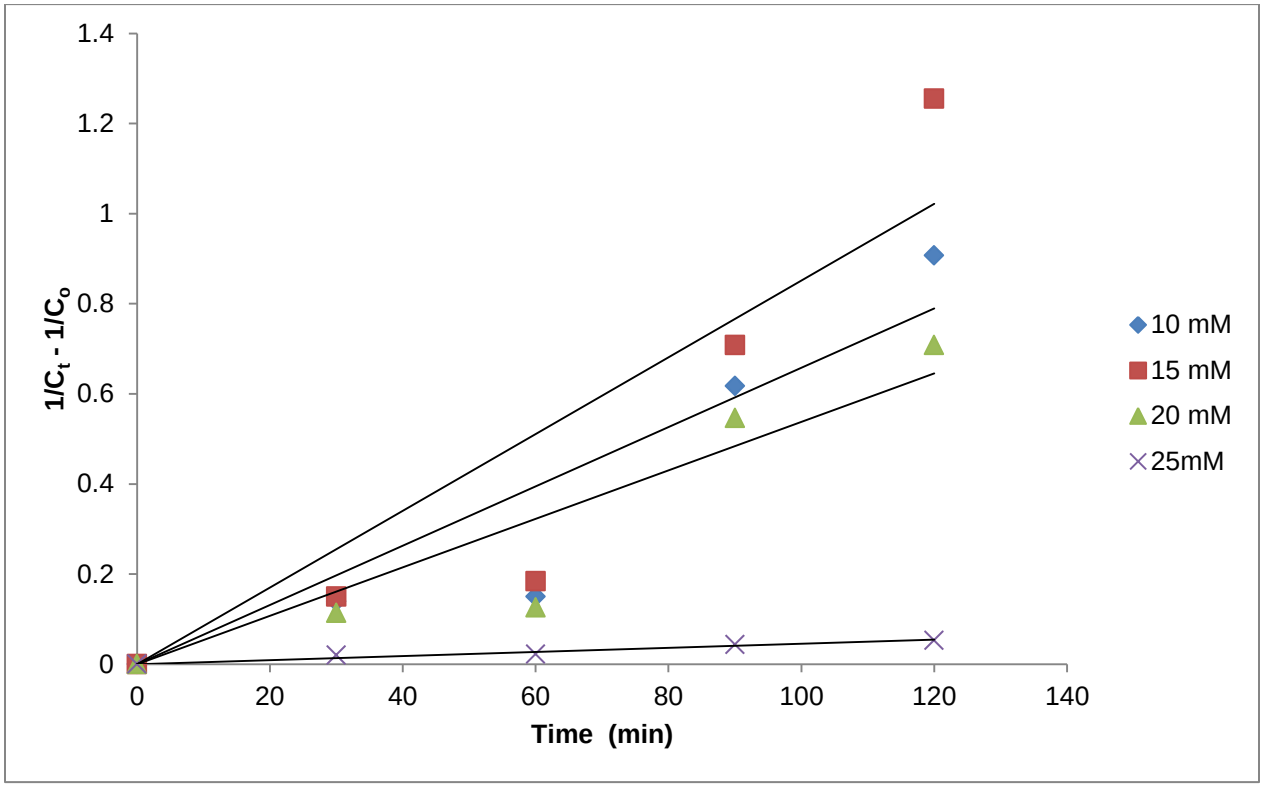

Figure 4. 28 Second order kinetics of MO degradation in presence of oxidant

Table 4. 11 Kinetic model parameters of MO degradation in presence of oxidant

	Zeroth Order		1st Order		2nd Order	
Oxidant	**K (min^{-1})**	**R^2**	**K (min^{-1})**	**R^2**	**K (min^{-1})**	**R^2**
10mM	0.4077	0.3431	0.0319	0.8842	0.0076	0.8678
15mM	0.4101	0.3324	0.0346	0.8600	0.0105	0.8370
20mM	0.4052	0.3753	0.0299	0.8667	0.0059	0.8721
25mM	0.3023	0.6734	0.0108	0.8658	0.0044	0.9587

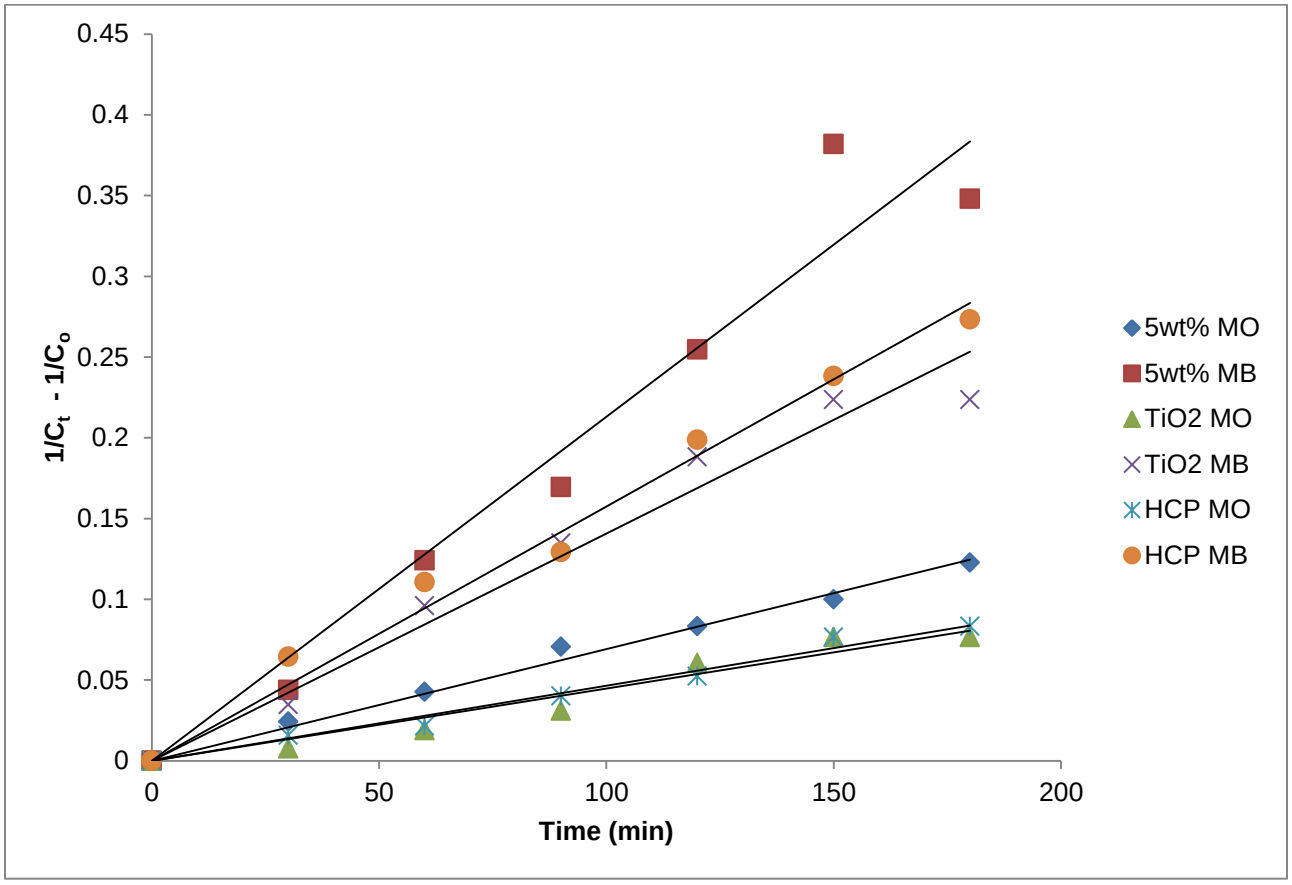

Figure 4. 29 Second order kinetics of dye mixture degradation using different catalyst

Table 4. 12 Kinetic model parameters of dye mixture degradation

	Zeroth Order		1st Order		2nd Order	
Catalyst	**K (min^{-1})**	**R^2**	**K (min^{-1})**	**R^2**	**K (min^{-1})**	**R^2**
5wt% MB	0.2073	0.2250	0.015	0.7950	0.0019	0.9528
5wt% MO	0.1846	0.4476	0.0099	0.8242	0.0007	0.9911
HCP MB	0.2036	0.0701	0.0138	0.6537	0.0015	0.9840
HCP MO	0.1709	0.7117	0.0081	0.9397	0.0004	0.9820
TiO_2 MB	0.1999	0.2785	0.0127	0.7503	0.0012	0.9654
TiO_2 MO	0.1675	0.8668	0.0077	0.9623	0.0004	0.9465

Kinetics (Pseudo first order) justifies consistent results in line with efficient photocatalytic degradation of MO was enhanced using TiO_2/HCP catalyst under visible light irradiation, in the presence of operational parameters discussed above. Though, effect of oxidant and comparative studies on dye mixture follows second order model. The apparent rate constants parameters in the highlighted tables agree with the initial observation during the degradation of MO, depicting good synergistic interaction when TiO_2 is immobilized on HCP surface.

References

ANDREOZZI, R. C., CAPRIA, V., INSOLA, A. & MAROTTA, R. (1999) Advanced oxidation processes (AOP) for water purification and recovery. *Catal. Today,* **53,** 51-59.

CASTALDI, P. S., SANTONA, L., COZZA, C., GIULIANO, V., ABBRUZZESE, C., NASTRO, V. & MELIS, P. (2005) Thermal and spectroscopic studies of zeolites exchanged with metal cations. *J. Mol. Struct.,* **734,** 99-105.

CHEN, H. M., MATSUMOTO, A., NISHIMIY, N. & TSUTSUMI, K. (1999) Preparation and characterization of TiO_2 incorporated Y-zeolite. *Coll. Surf. A. Physicochem. Eng. Aspects, **157**,* 157**,** 295.

CHEN, S. L. & LIU, Y. Z. (2007) Study on the photocatalytic degradation of glyphosate by TiO_2 photocatalyst. *Chemosphere,* **67,** 1010-1017.

CHUAN, X. H., HIRANO, M. & INAGAK, M. (2004) Preparation and photocatalytic performance of anatase-mounted natural porous silica, pumice, by hydrolysis under hydrothermal conditions. *Appl. Catal. B. Environ ,* **51,** 255-60.

DOGAN, M., ALKAN, M., DEMIRBAS, O., OZDEMIR, Y. & OZMETIN, C. (2006) Adsorption kinetics of maxilon blue GRL onto sepiolite from aqueous solutions. *Chem. Eng. J.,* **124,** 89-101.

GARCIA- BASABE, Y., RODRIGUEZ-IZNAGA, I., MENORVAL, L. C. D., LLEWELLYN, P., MAURIN, G., LEWIS, D. W., BINIONS, R., AUTIE, M. & RUIZ-SALVADOR, A. R. (2010) Step-wise dealumination of natural clinoptilolite : Structural and physicochemical characterization. *Micropor. Mesopor. Mater.,* **135,** 187.

GORA, A. T., TOEPFER, B., PUDDU, V. & LI PUMA, G. (2006) Photocatalytic oxidation of herbicides in single-component and multicomponent systems: Reaction kinetics analysis. *Appl. Catal. B: Environ.,* **65,** 1-10.

GUILLARD, C. L., LACHHEB, H., HOUAS, A., KSIBI, M., ELALOUI, E. & HERMANN, J. M. (2003) Influence of chemical structure of dyes, of pH and of inorganic salts on their photocatalytic degradation by TiO_2. Comparison of the efficiency of powder and supported TiO_2. *J. Photochem. Photobiol. A: Chem.,* **158,** 27.

GUPTA, A. P., PAL, A. & SAHOO, C. (2006) Photocatalytic degradation of a mixture of crystal violet (basic violet 3) and methyl red dye in aqueous suspensions using Ag^+ doped TiO_2. *Dyes and Pigments,* **69,** 224-232.

HO, Y. S. & CHIANG, C. C. (2001) Sorption studies of acid dye by mixed sorbents. *Adsorpt. J. Int. Adsorpt. Soc.,* **7,** 139-147.

HUANG, C. D. (1993) Advanced chemical oxidation: its present role and potential future in hazardous waste treatment. *Waste Management,* **13.**

IRMAK, S. K., KUSVURAN, E. & ERBATUR, O. (2004) Degradation of 4-chloro-2-methylphenol in aqueous solution by UV irradiation in the presence of titanium dioxide. *Appl. Catal. B: Environ.,* **54,** 85-91.

KONSTANTINOU, I. A. & ALBANIS, T. A. (2004) TiO_2-assisted photocatalytic degradation of azo dyes in aqueous solution: kinetic and mechanistic investigations: a review. *Appl. Catal. B: Environ.,* **49,** 1-14.

LI, F. F., JIANG, Y. S., YU, L. X., YANG, Z. W., HOU, T. Y. & SUN, S. S. (2005) Surface effect of natural zeolite (clinoptilolite) on the photocatalytic activity of TiO_2. *Appl. Surf. Sci.,* **252,** 1410-1416.

NEZAMZADEH-EJHIEH, A. M. & MOEINIRAD, S. (2011) Heterogeneous photocatalytic degradation of furfural using NiS-clinoptilolite zeolite. *Desalination,* **273,** 248-257.

PETERNEL, I. K., KOPRIVANAC, N. & KUSIC, H. (2006) UV-based processes for reactive azo dye mineralization. *Wat. Res.,* **40,** 525-532.

REDDY, E. D., DAVYDOV, L. & SMIRNIOTIS, P. (2003) TiO_2-loaded zeolites and mesoporous materials in the sonophotocatalysts: novel photocatalysts for the enhanced degradation p-chlorophenoxyacetic acid. *Appl. Catal. B. Environ.,* **42,** 1-11.

RINCON, A. P. & PULGARIN, C. (2003) Photocatalytical inactivation of E. coli: effect of (continuous-intermittent) light intensity and of (suspended-fixed) TiO_2 concentration. *Appl. Catal. B: Environ.,* **44,** 263--284.

ROBERT, D. P., PISCOPO, A. & WEBER, J. V. (2004) Selective solar photodegradation of organopollutant mixtures in water. *Solar Energy,* **77,** 553-558.

SANKARARAMAN, S. Y., YOON, K. B., YABE, T. & KOCHI, J. K. (1991) Control of back electron transfer from charge-transfer ion pairs by zeolite supercages. *J. Am. Chem. Soc.,* **113,** 1419-1421.

TANAKA, K. F., FUKUYOSHI, J., SEGAWA, H. & YOSHIDA, K. (2006) Improved photocatalytic activity of zeolite- and silica-incorporated TiO_2 film. *J. Hazard. Mater.,* **137,** 947-951.

TURCHI, C. O. & OLLIS, D. F. (1990) Photocatalytic degradation of organic water contaminants: mechanisms involving hydroxyl radical attack. *J. Catal.,* **122,** 178--192.

VESELY, M. C., CEPPAN, M. & LAPCIK, L. (1991) Photocatalytic degradation of hydroxyethylcellulose in aqueous Pt-TiO_2 suspension. *J. Photochem. Photobiol. A: Chem.,* **61,** 399-406.

WANG, C. C., LEE, C.K., LYU, M.D., JUANG, L.C. (2007) Photocatalytic degradation of C.I. Basic Violet 10 using TiO_2 catalysts supported by Y zeolite: An investigation of the effects of operational parameters. *J. Dyes and Pigments* **,** 1-8.

WANG, K. Z., ZHANG, J., LOU, L., YANG, S. & CHEN, Y. (2004) UV or visible light induced photodegradation of AO7 on TiO_2 particles: The influence of inorganic anions. *J.Photochem. Photobiol. A,* **164,** 201-207.

WU, C. (2007) Adsorption of reactive dye onto carbon nanotubes: equilibrium, kinetics and thermodynamics. *J. Hazard. Mater.,* **144,** 93-100.

XU, Y. L. & LANGFORD, C. H. (2000) Variation of Langmuir adsorption constant determined for TiO_2-photocatalyzed degradation of acetophenone under different light intensity. *J. Photochem.Photobiol. A: Chem.,* **133,** 67-71.

ZHANG, W. A., AN, T., CUI, M., SHENG, G. & FU, J. (2005) Effects of anions on the photocatalytic and photoelectrocatalytic degradation of reactive dye in a packed-bed reactor. *J. Chem. Technol. Biotechnol.,* **80,** 223-229.

ZHU, H. Y., JIANG, R., XIAO, L. & ZENG, G. M. (2010) Preparation, characterization, adsorption kinetics and thermodynamics of novel magnetic chitosan enwrapping nanosized [gamma]-Fe_2O_3 and multi-walled carbon nanotubes with enhanced adsorption properties for methyl orange. *Bioresour. Technol.,* **101,** 5063-5069.

CHAPTER FIVE

CONCLUSIONS AND RECOMMENDATIONS

5.1 Conclusions

From the scope of this dissertation, several conclusions were motivated in line with the preparation, characterization and application of synthesized photocatalyst in the photocatalytic degradation of model organic pollutant.

TiO_2 was successfully dispersed on HCP via sol-gel method and it exists as either nanoparticles or clusters on the dealuminated Clinoptilolite surface (HCP). Dealumination of CP was evident in HCP structure; though increase in surface area when TiO_2 was dispersed on HCP. Absorption band of TiO_2/HCP was slightly shifted to the visible region as shown in DRUV-VIS, emphasizing strong interaction between HCP and metal semiconductor phase.

However, the interface of TiO_2/HCP at different wt% loading on degradation of methyl orange in dark adsorption and photocatalytic activities was varied. TiO_2/HCP possessed enhanced photocatalytic activities on Methyl orange under the influence of different parameters such as loading rates, irradiation time, initial dye concentration, pH, calcination temperature, anions and H_2O_2 concentration as described:

- Among the different wt% loading of TiO_2 on HCP, 5 wt% exhibited optimum amount of loaded TiO_2 with highest adsorption and photodegradation efficiency among the catalyst prepared in this study.
- Photodegradation rate depends on initial concentration of MO and optimum photodegradation conducted at room temperature is favorable at initial MO concentration of 30 ppm.
- The pH motives a significant role in improving the photocatalytic degradation of organic contaminants. Photodegradation rate was optimized in acidic condition (pH 4).
- Catalysts calcined at 873 K exhibit fine crystallites of anatase and shows enhanced photodegradation efficiency than other calcination temperature.
- The addition of oxidant (H_2O_2) enhances photodegradation of methyl orange, they serves as electron acceptors and thus avoiding electron/hole recombination. Optimum H_2O_2 concentration at 15 mM.
- Removal efficiency in the presence of anions was greatly influenced by NO_3^-, SO_3^-, Cl^- but retarded by concentration of CO_3^{2-} and SO_4^{2-}.

- The photocatalyst possess good repeatability after 3 cycles, though loss in efficiency as a results of adsorbed particles, and changes in morphological properties.

Comparative analysis on prepared photocatalyst was conducted on dye mixture (MO & MB), with TiO_2/HCP exhibiting highest degradation activities more than HCP and TiO_2 alone respectively. Langmuir Hinshelwood model was applied to describe dependency of photocatalytic reaction on concentration of model organic pollutants. Kinetic studies depict the photocatalytic degradation of Methyl orange follows pseudo-first order reaction for all the operational parameters. The effect of oxidant and comparative analysis on the photocatalyst follow second order kinetic model.

5.2 Recommendation

This research work shows that TiO_2-supported dealuminated Clinoptilolite (HCP) is a viable photocatalyst that can applied for treatment of volatile organic compounds in wastewater. HCP high surface area assist in adsorption of dye molecule on the photocatalyst surface and further oxidizes them into mineralized products.

However, further work on synthesis of nano-composites materials that possess absorption in the visible region and low band gap energy in other to reduce electron-hole pair recombination via co-doping of metals or non-metal on TiO_2, dye sensitization on TiO_2 or application of other adsorbent that possess catalytic properties as immobilization support layer. The application of X-ray photoelectron spectroscopy (XPS) is vital for elucidation of surface elemental analysis and binding energy in synthesized photocatalyst.

The studies of mineralized products from degraded organic pollutants must be conducted via measure of “Total Organic Carbon (TOC), Chemical Oxygen Demand (COD) and Biological Oxygen Demand. Mineralized products must also be determined using analytical means through Gas Chromatography-Mass spectra (GC-MS), High Performance liquid Chromatography (HPLC) and Nuclear Magnetic Resonance (NMR).

APPENDICES

Appendix 1 Sem image of (a) 7.5 wt% TiO_2/HCP and (b) 10 wt% TiO_2/HCP

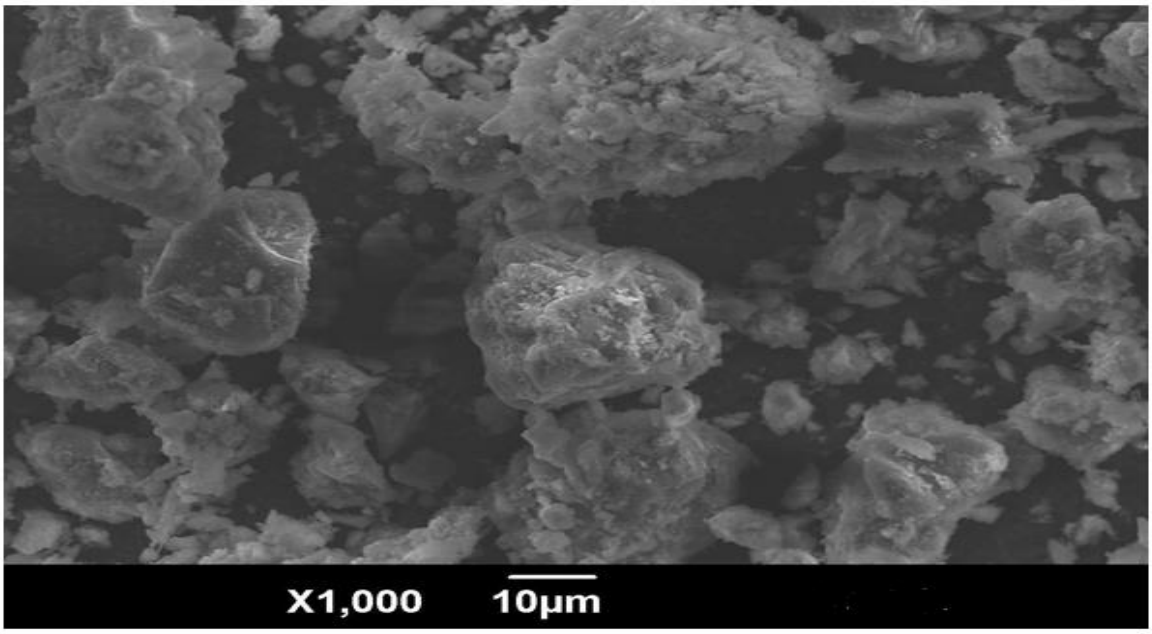

(a)

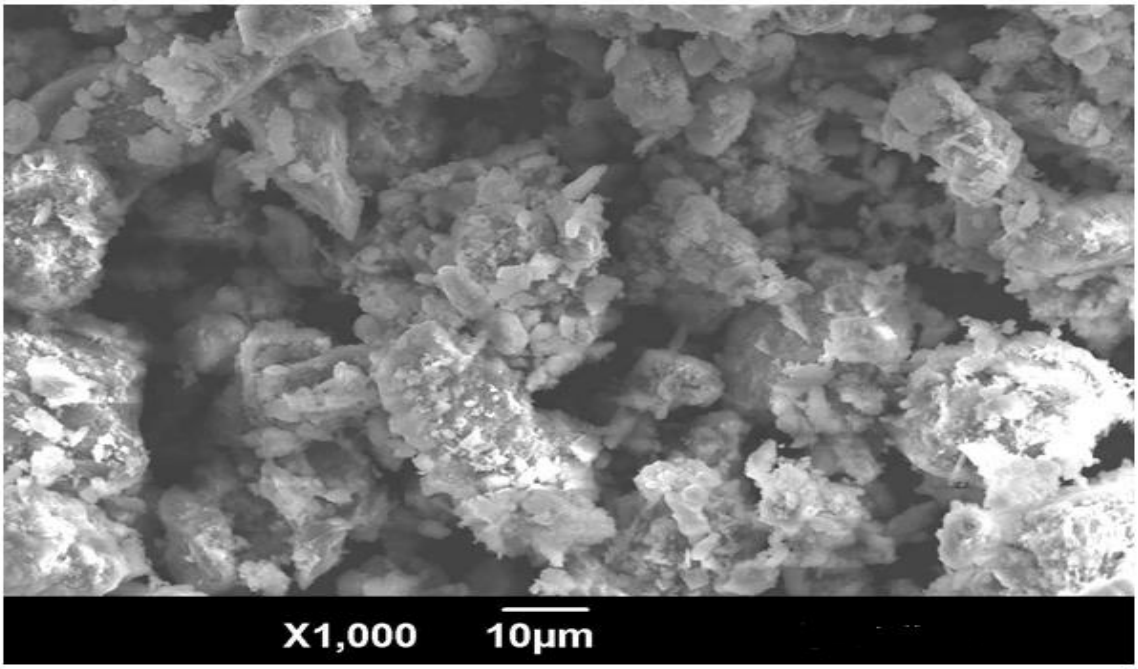

(b)

Appendix 2 EDAX of (a) 7.5 wt% TiO_2/HCP and (b) 10 wt% TiO_2/HCP

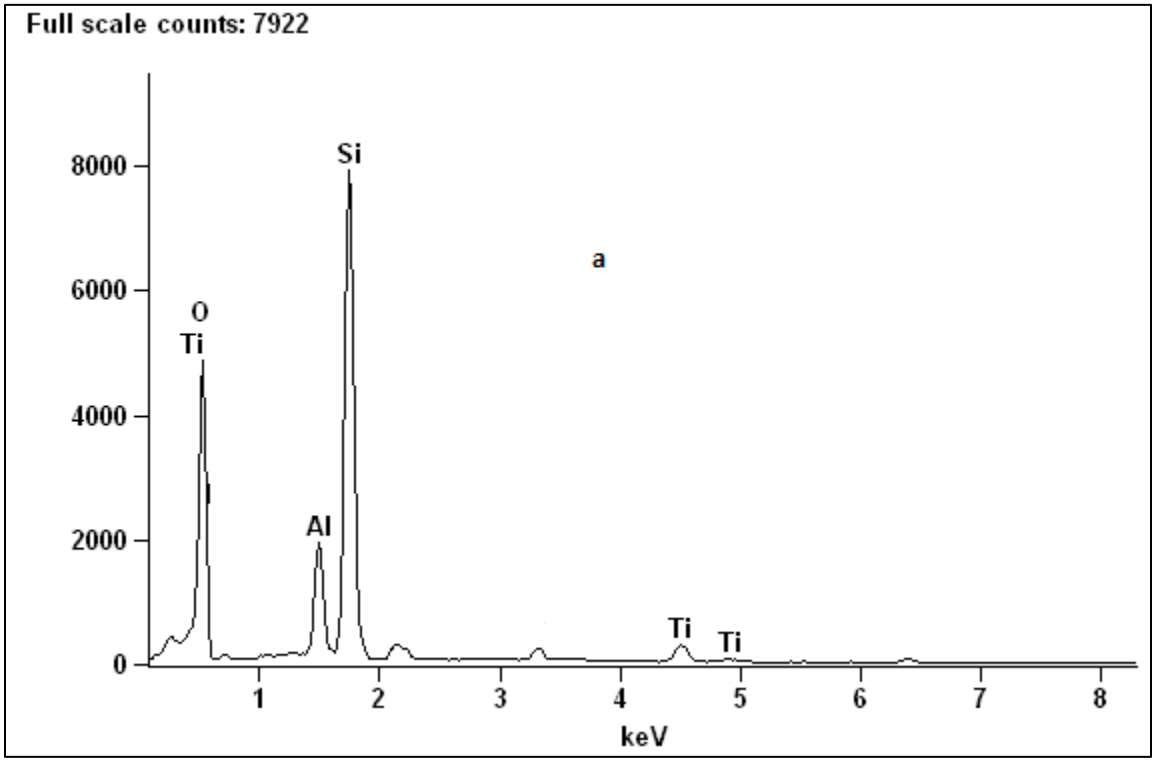

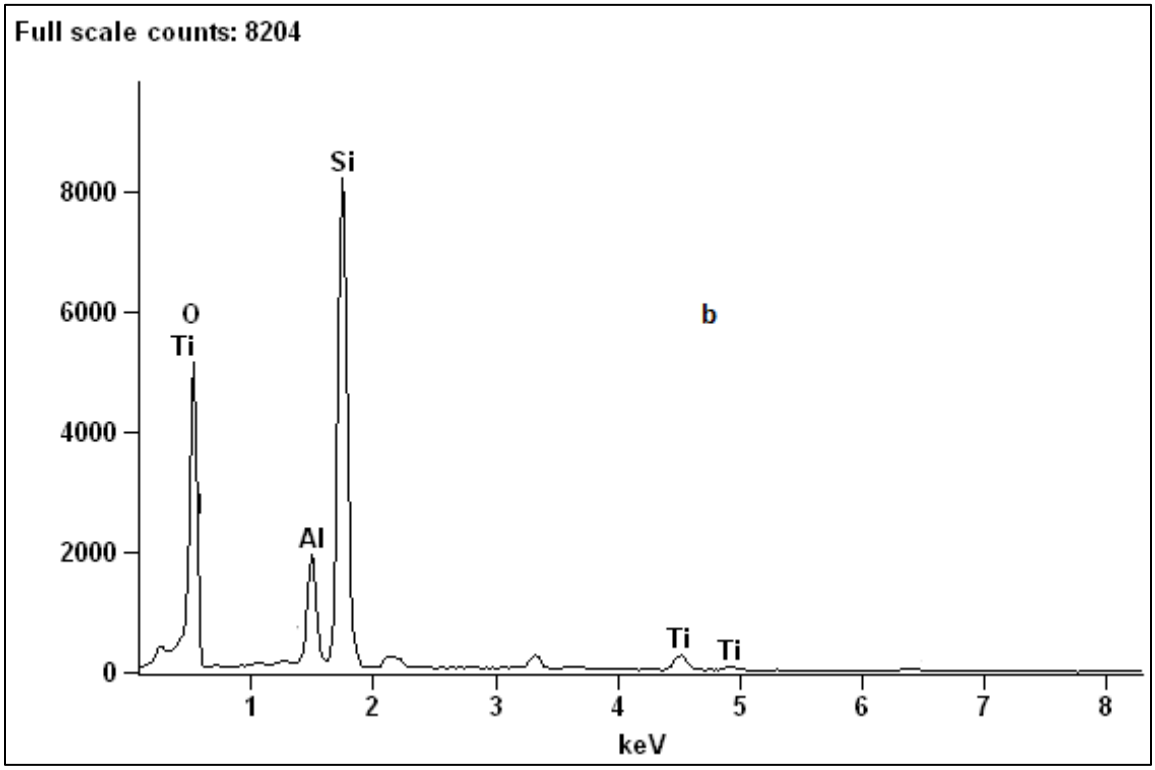

Appendix 3 FTIR of 7.5 wt% and 10 wt% TiO_2/HCP

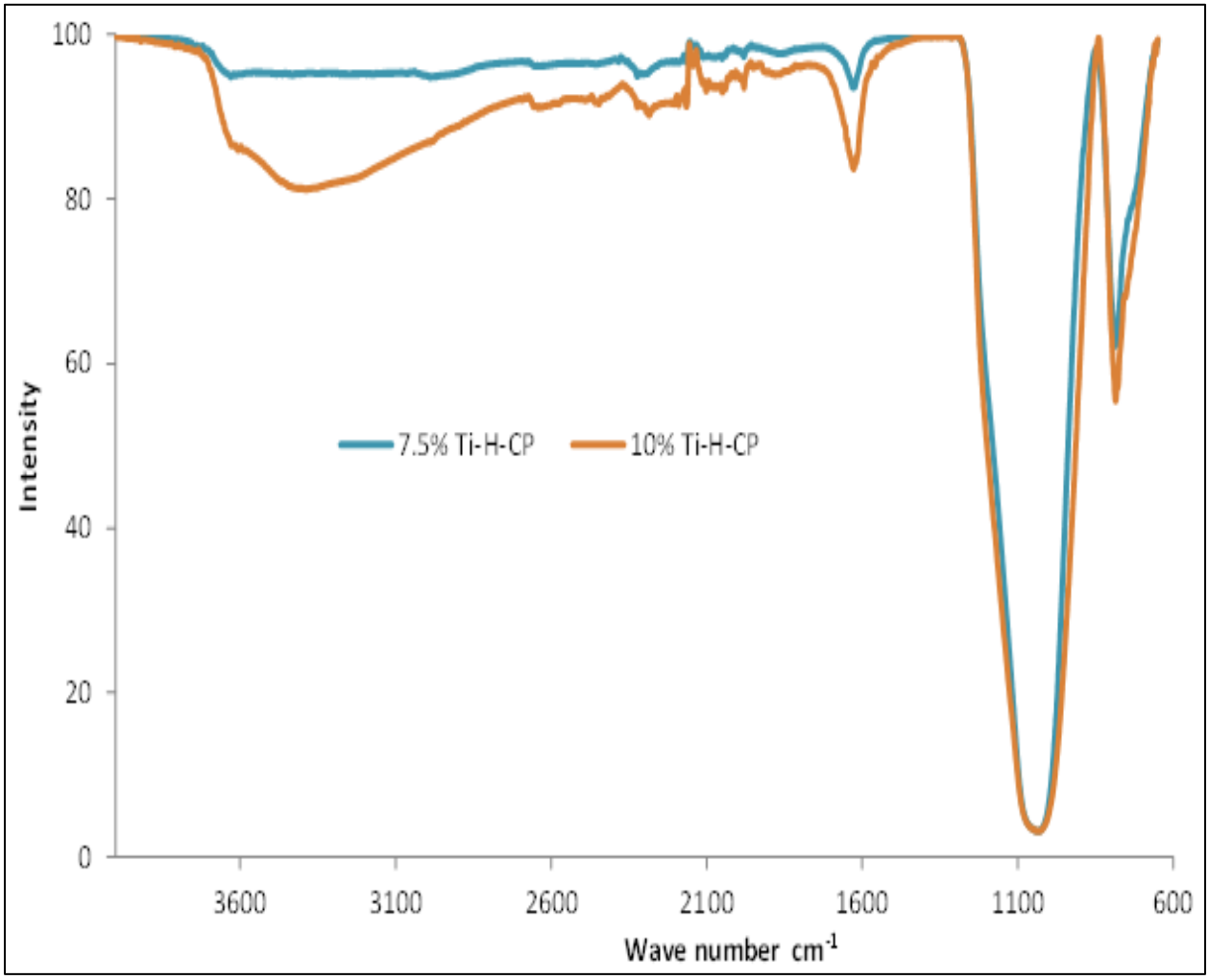

Appendix 4 TGA of 7.5 wt% and 10 wt% TiO_2/HCP

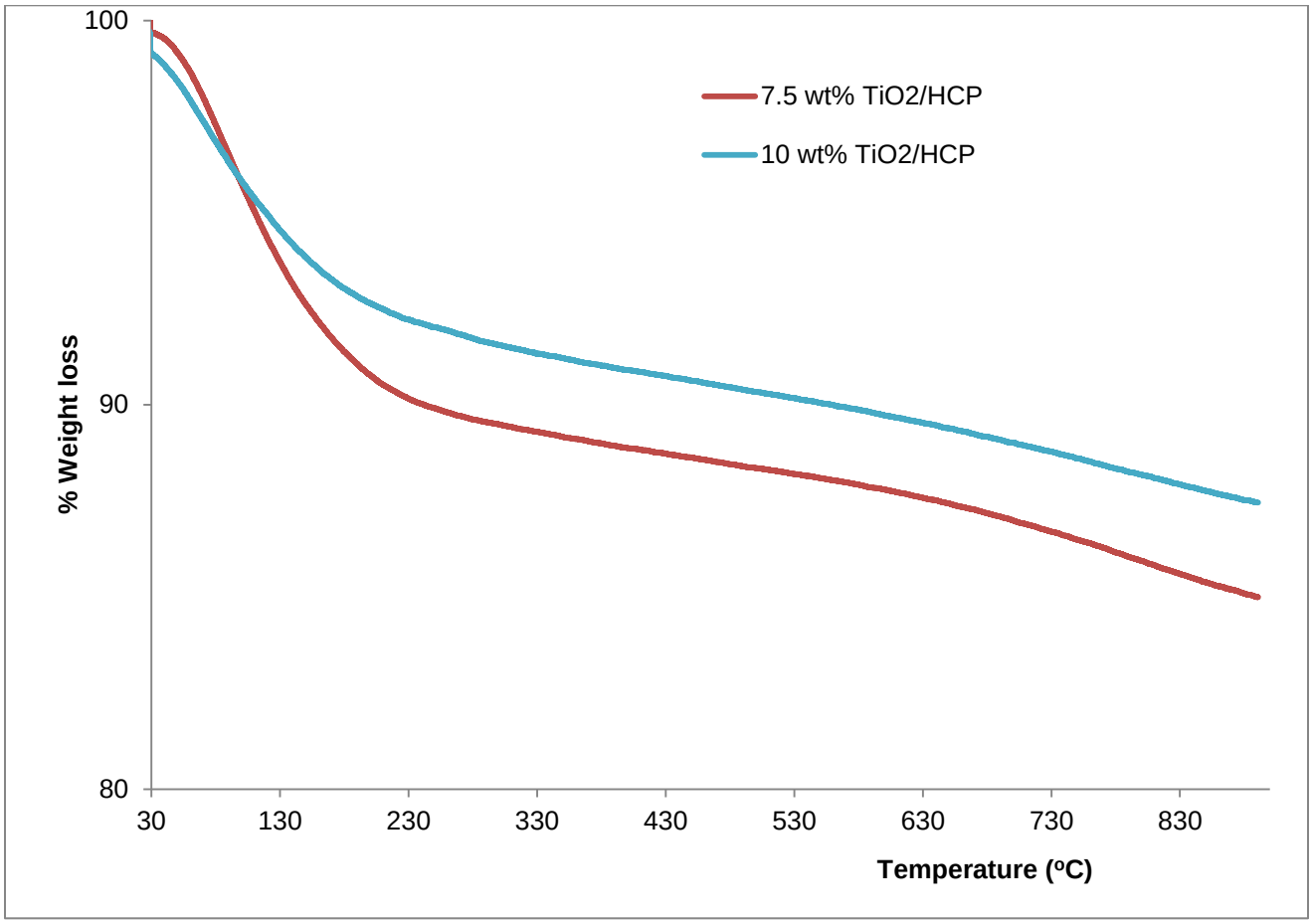

Appendix 5 DRUV-VIS Spectra of calcined photocatalyst at different temperature

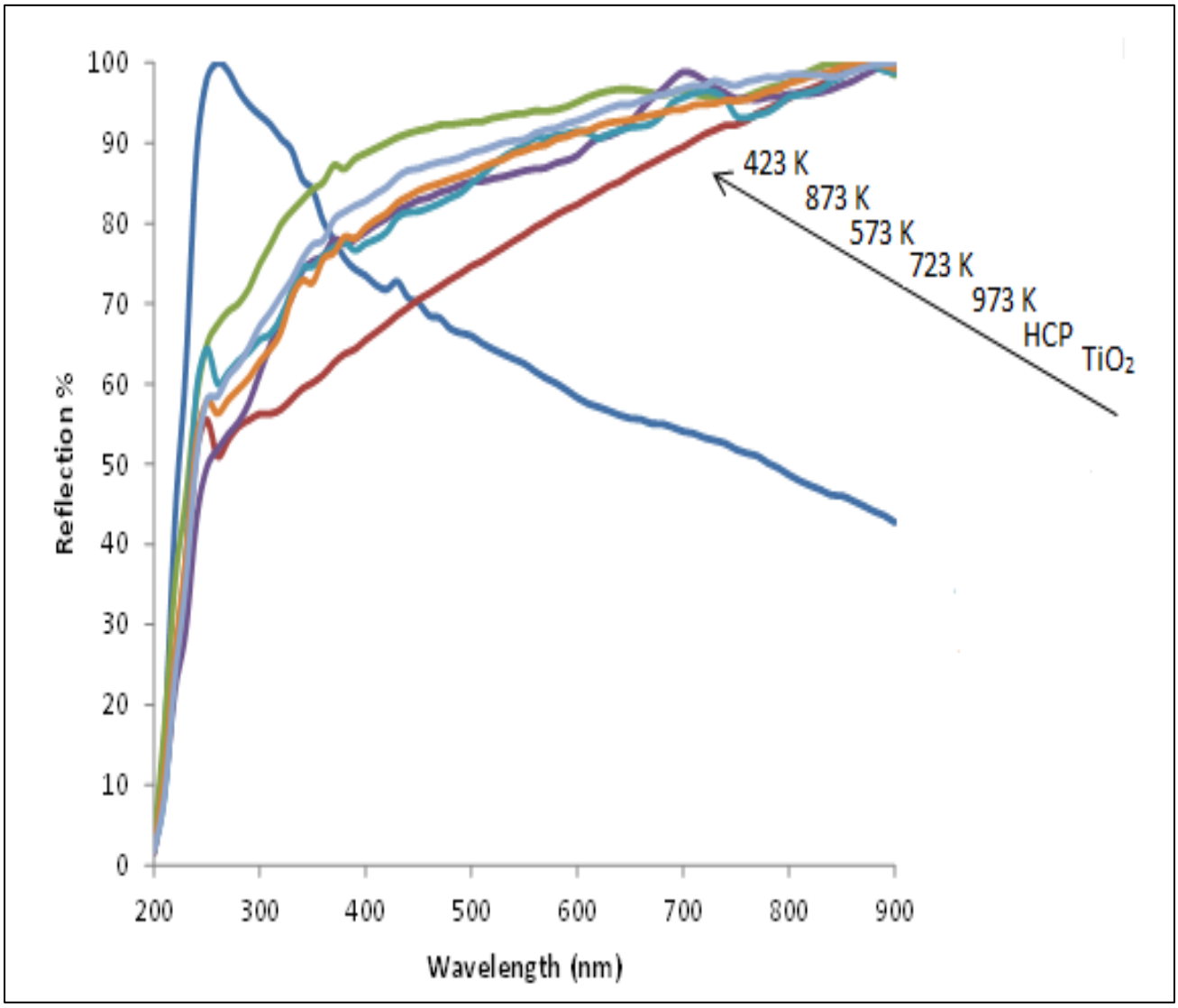

Appendix 6 Comparison of kinetic models for q_e for MO adsorption

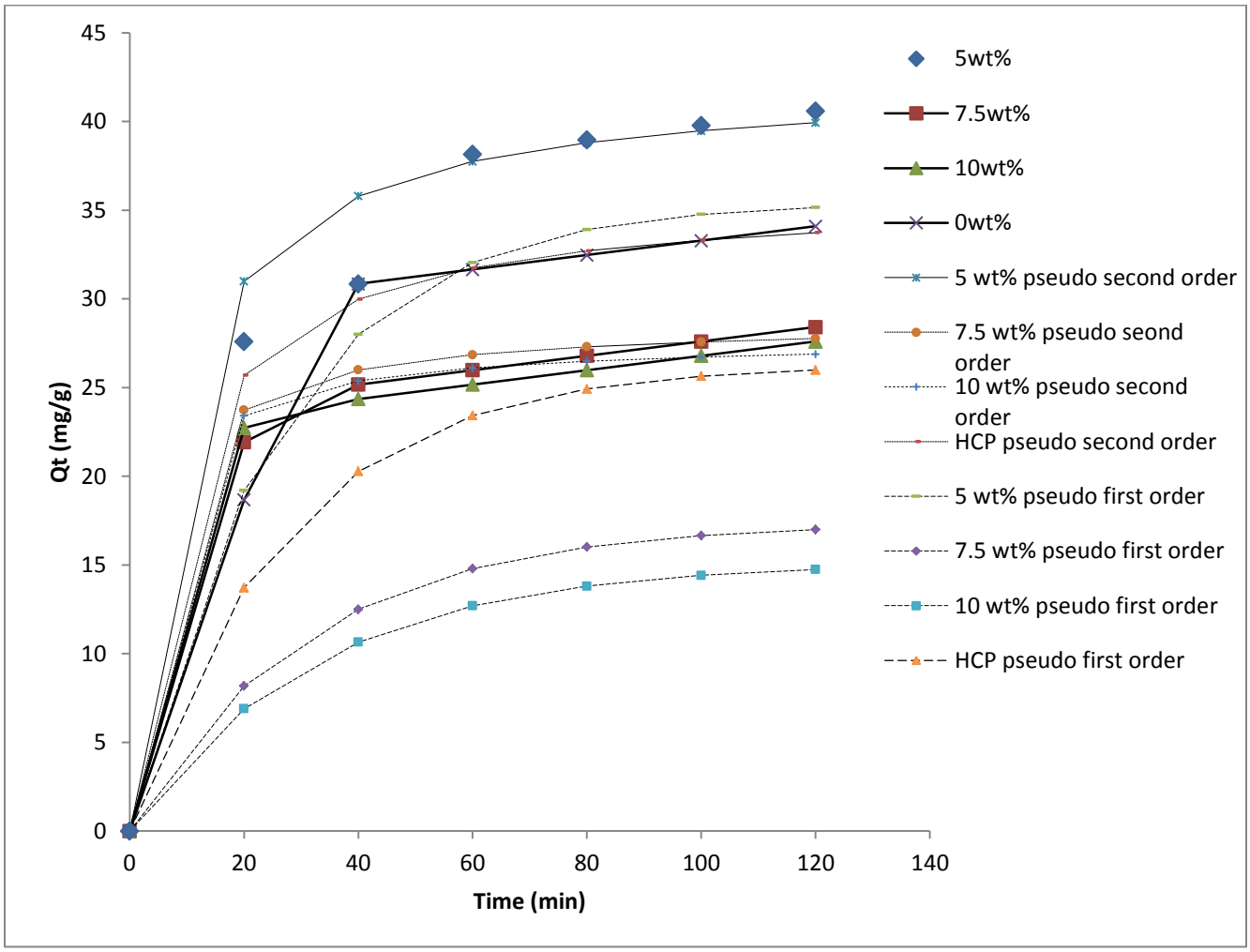

Appendix 7 Zeroth and Second order kinetics at different loading of TiO_2

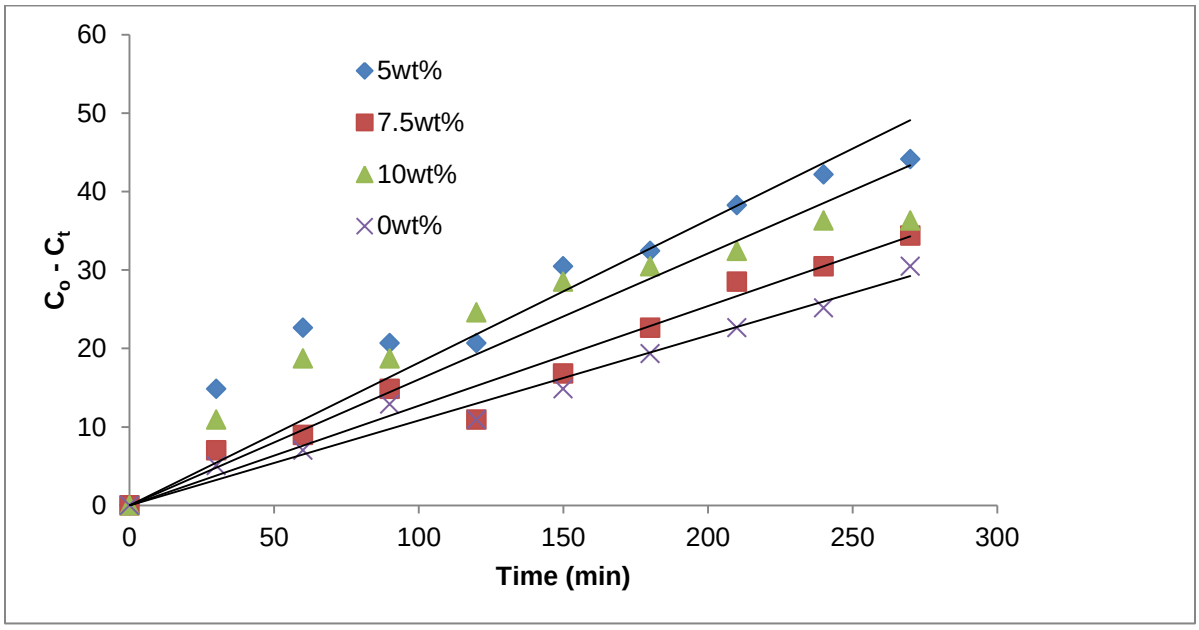

(a)

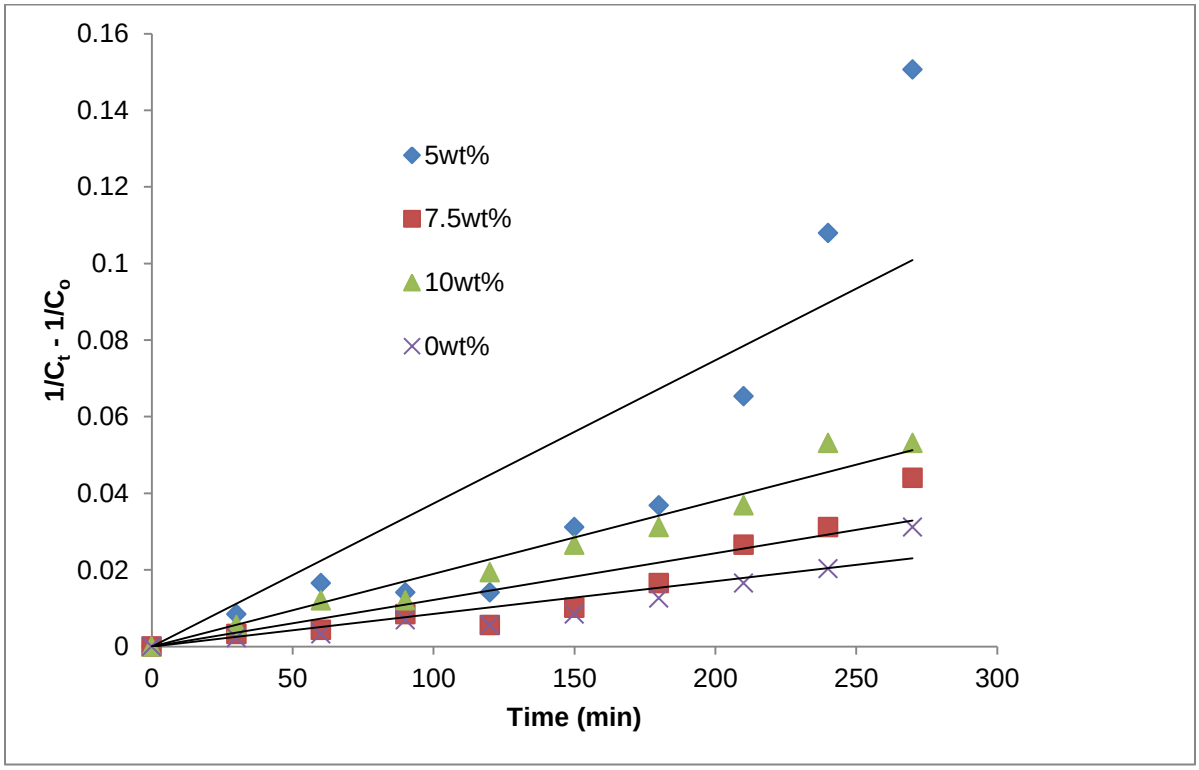

(b)

Appendix 8 Zeroth and second order kinetics at different initial concentration rate

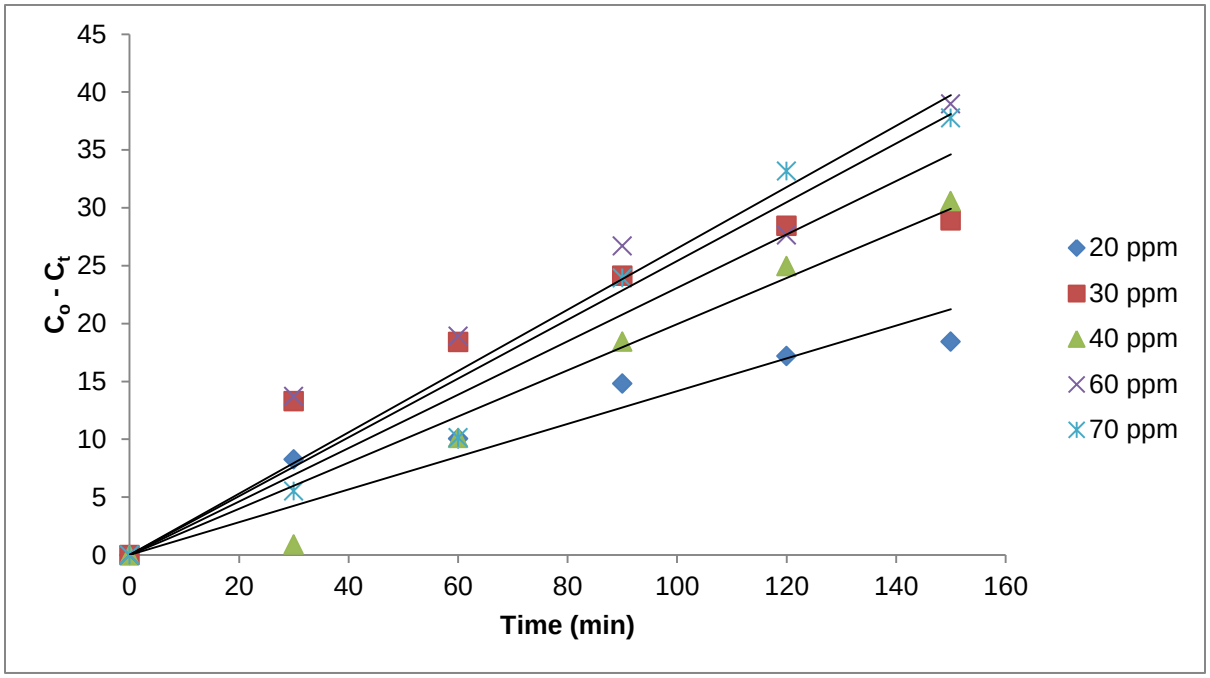

(a)

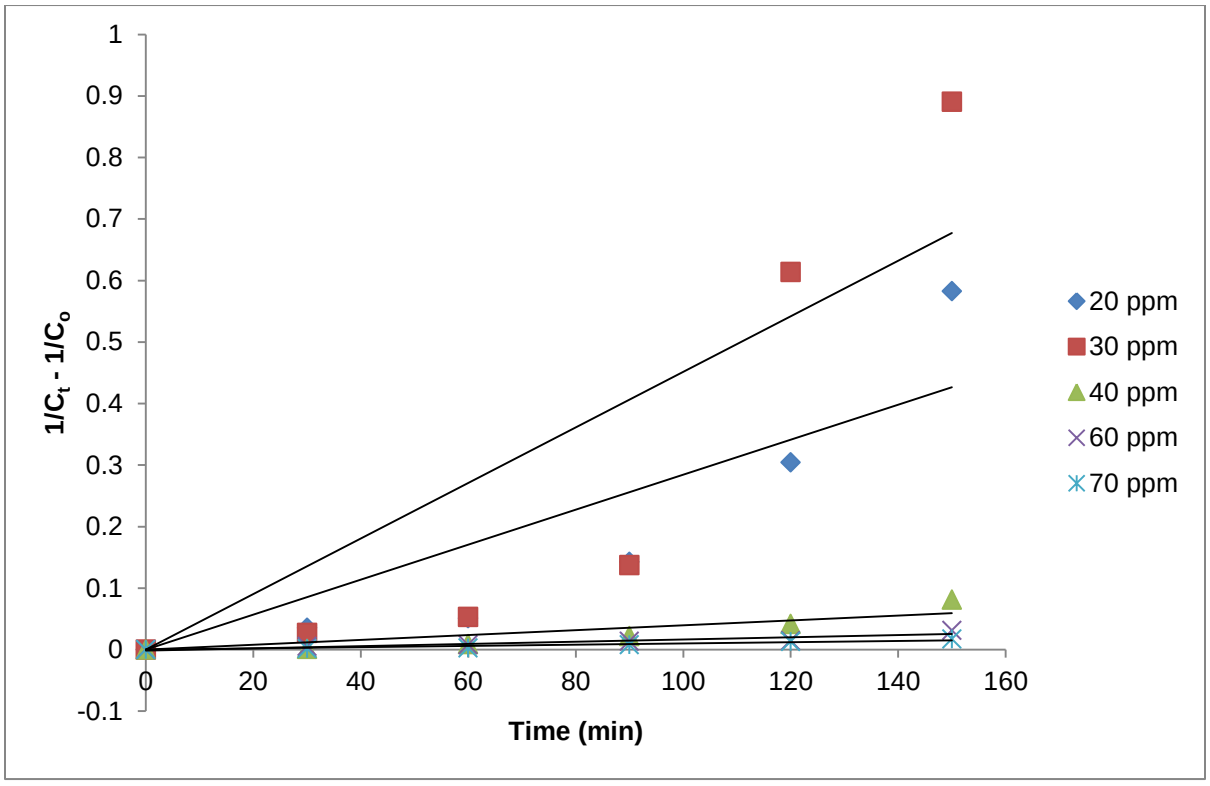

(b)

Appendix 9 Zeroth and second order kinetics at different pH

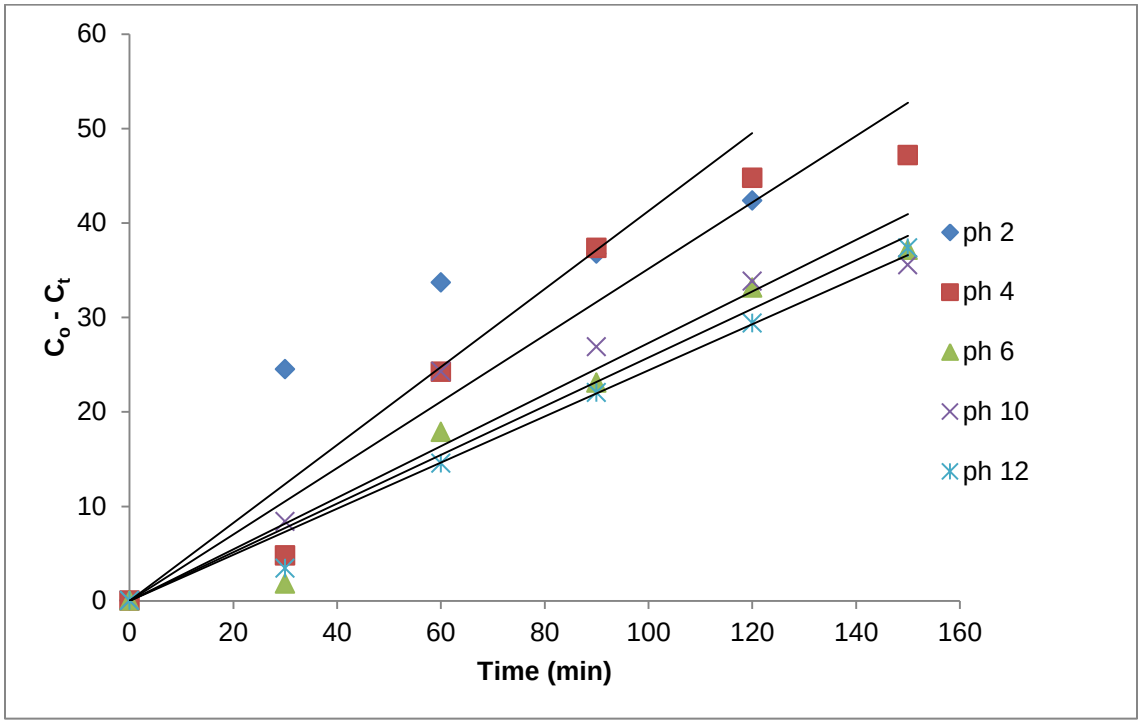

(a)

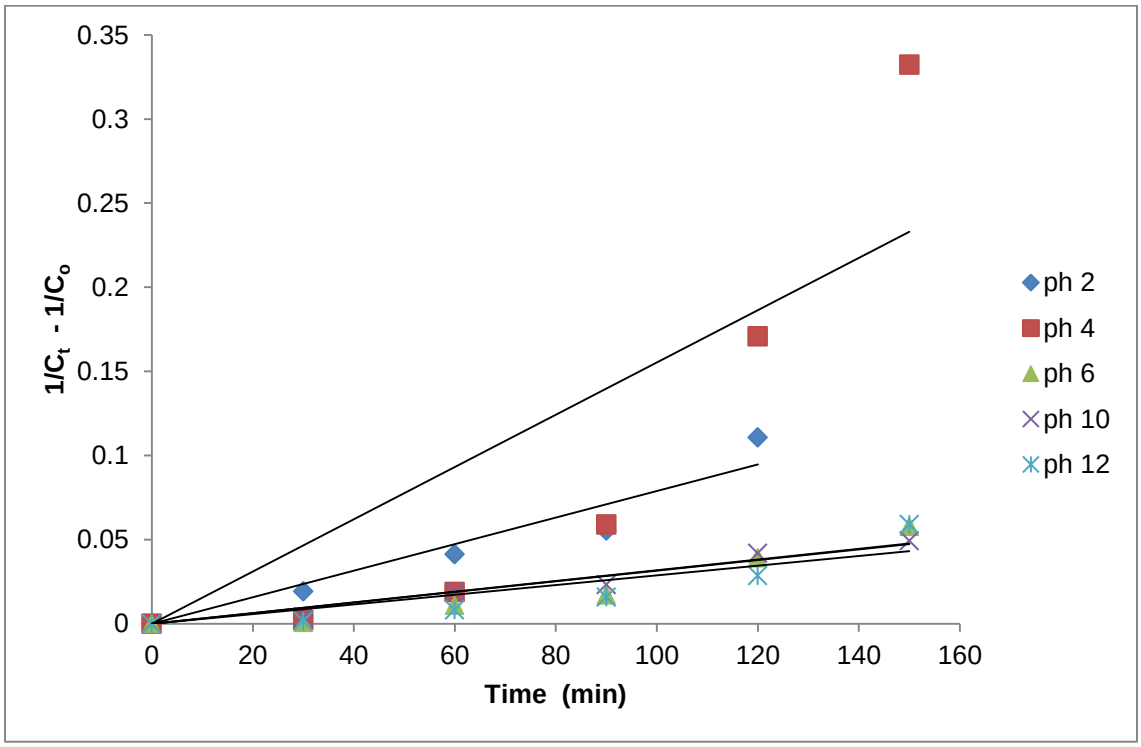

(b)

Appendix 10 Zeroth and second order kinetics at different calcination temperature

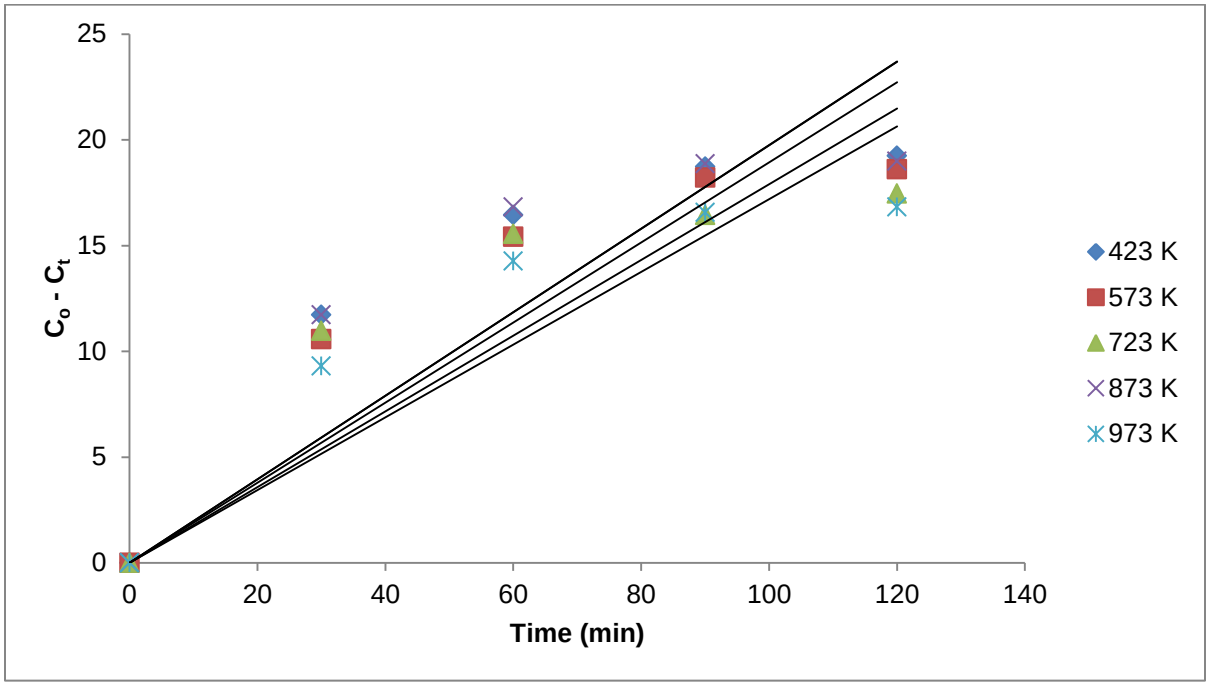

(a)

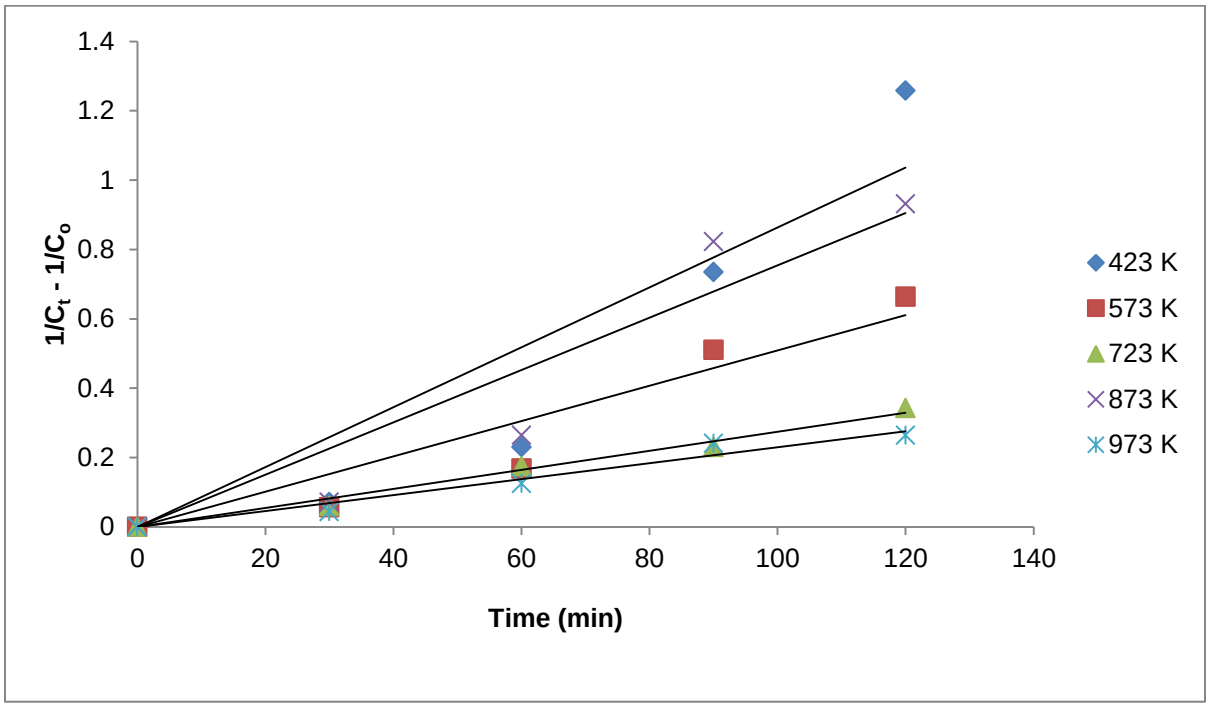

(b)

Appendix 11 Zeroth and second order kinetics in presence of different anions

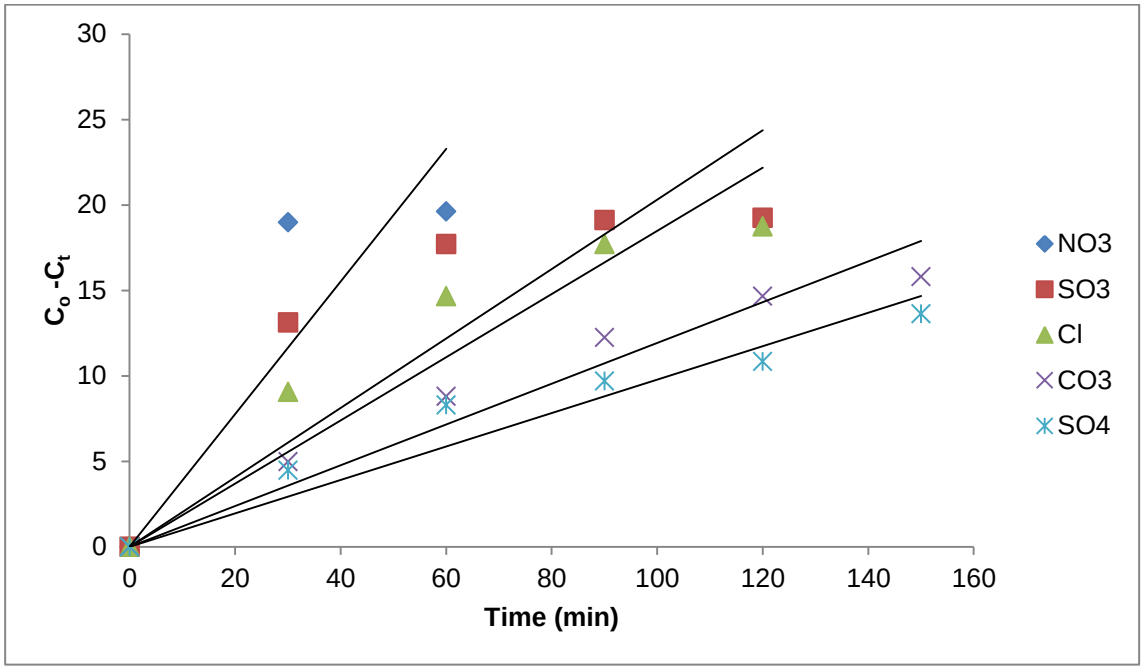

(a)

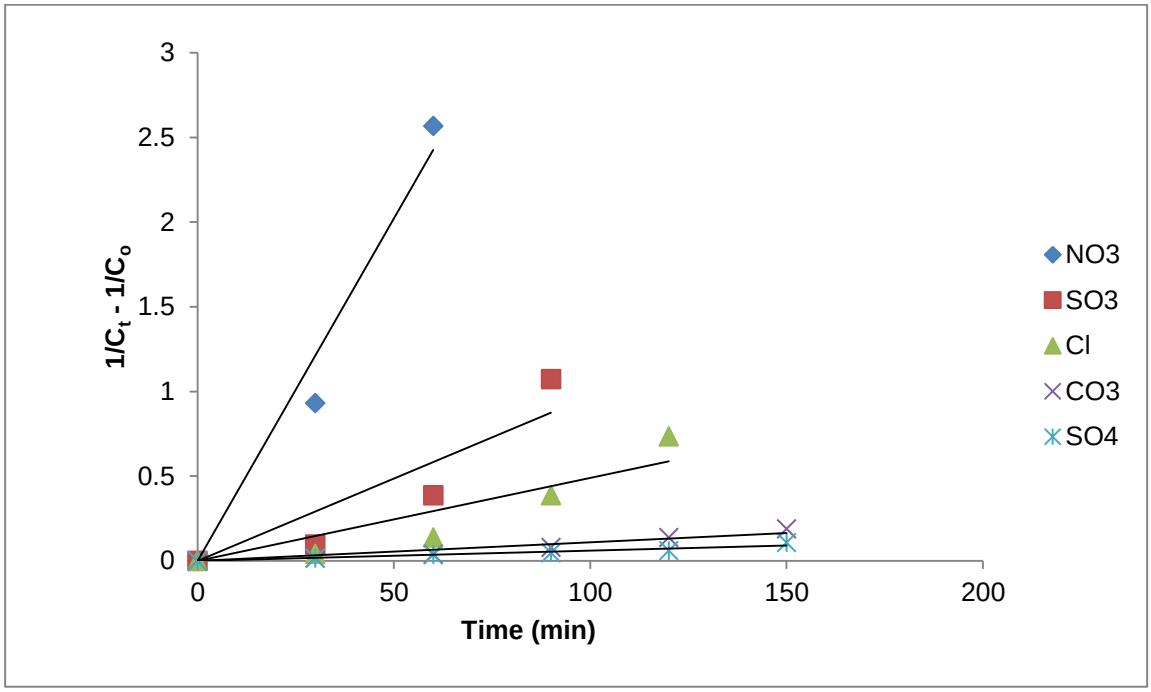

(b)

Appendix 12 Zeroth and second order kinetics at different recycling rate

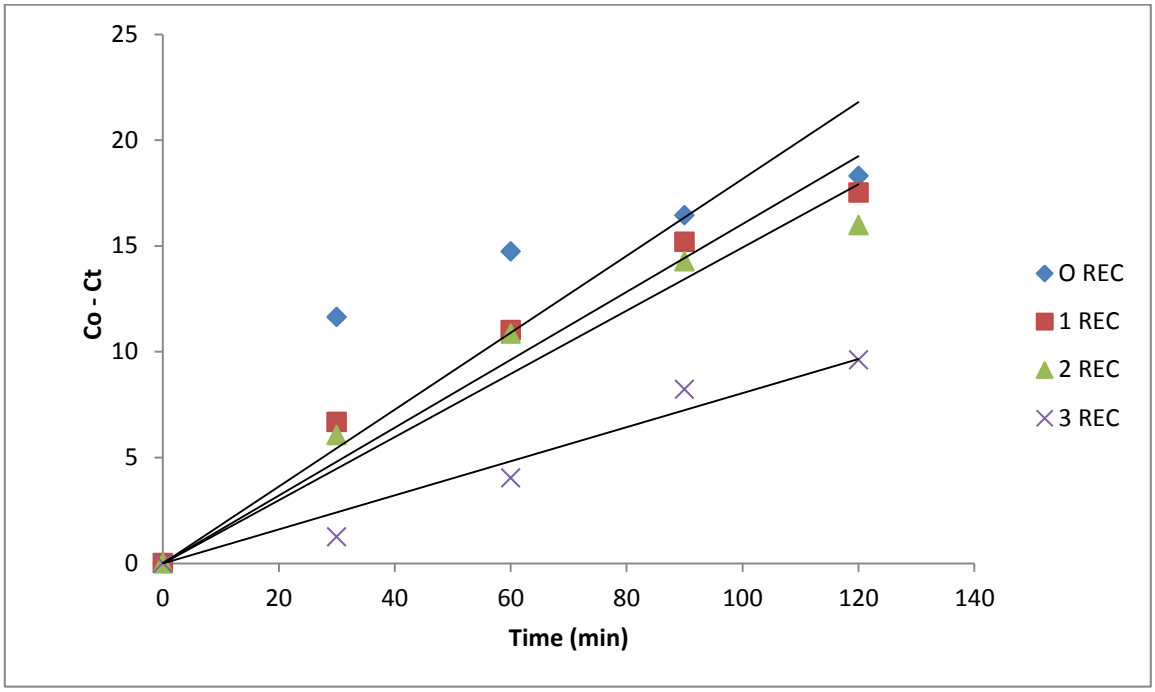

. (a)

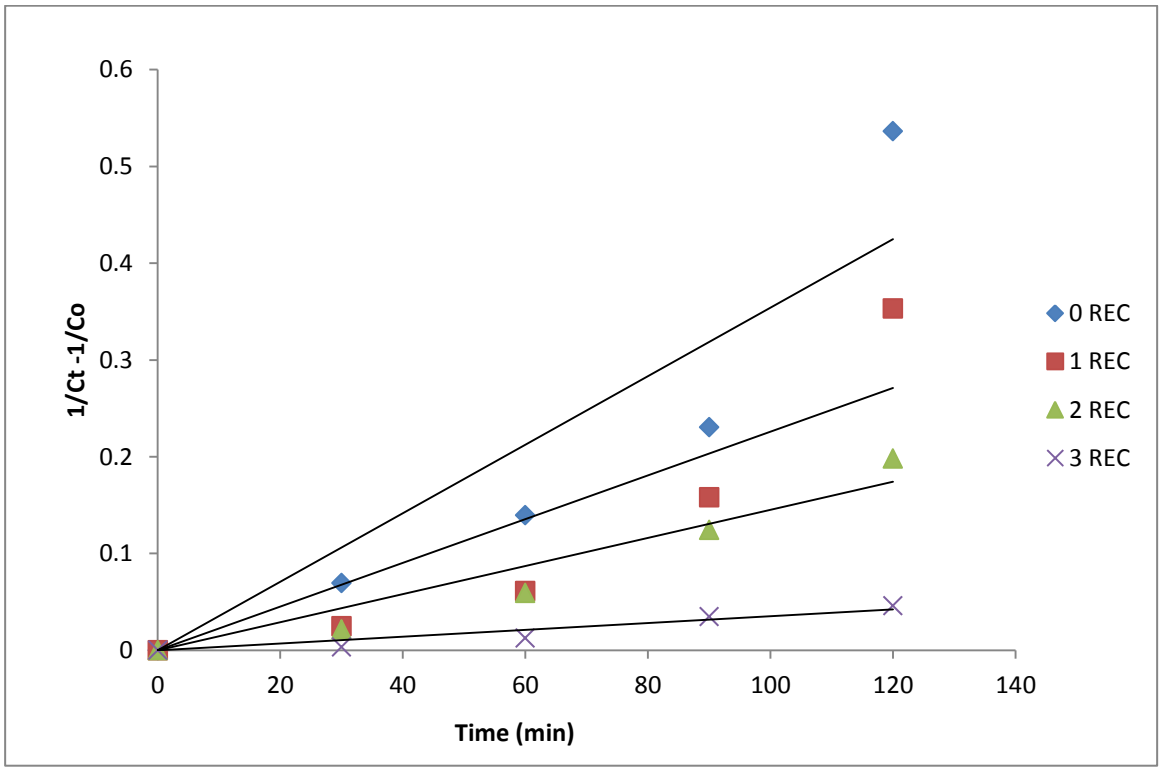

(b)

Appendix 13 Zeroth and pseudo first order kinetics in presence of oxidant

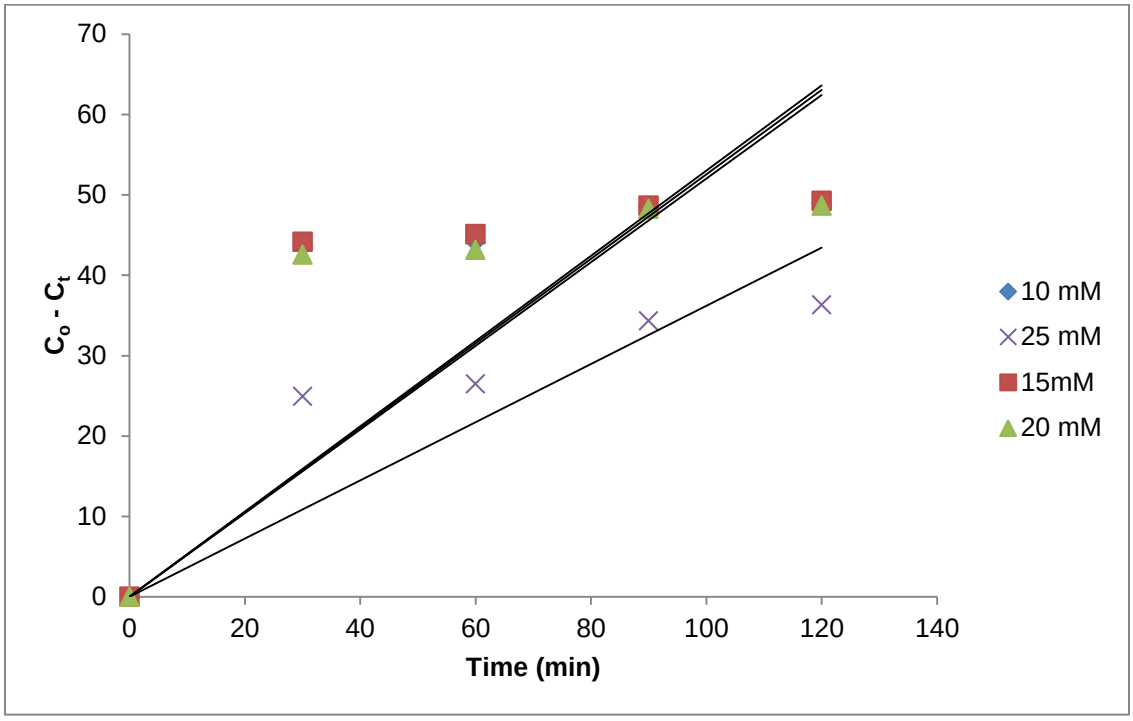

(a)

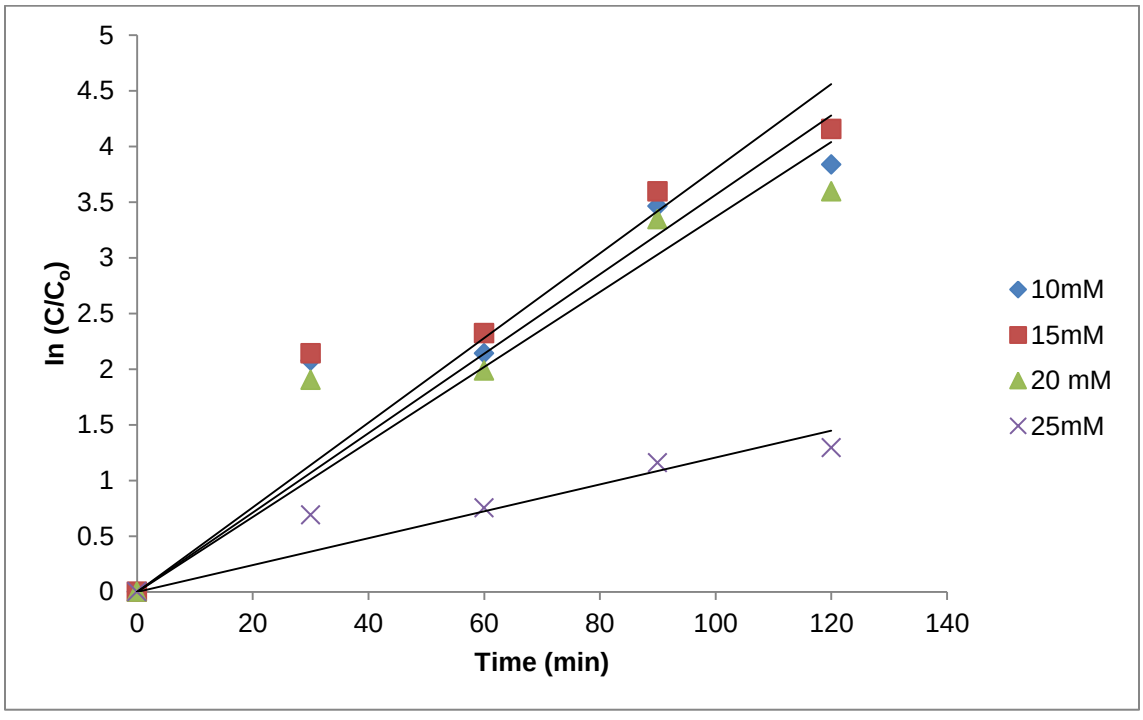

(b)

Appendix 14 Zeroth and pseudo first order kinetics for degradation of dye mixture

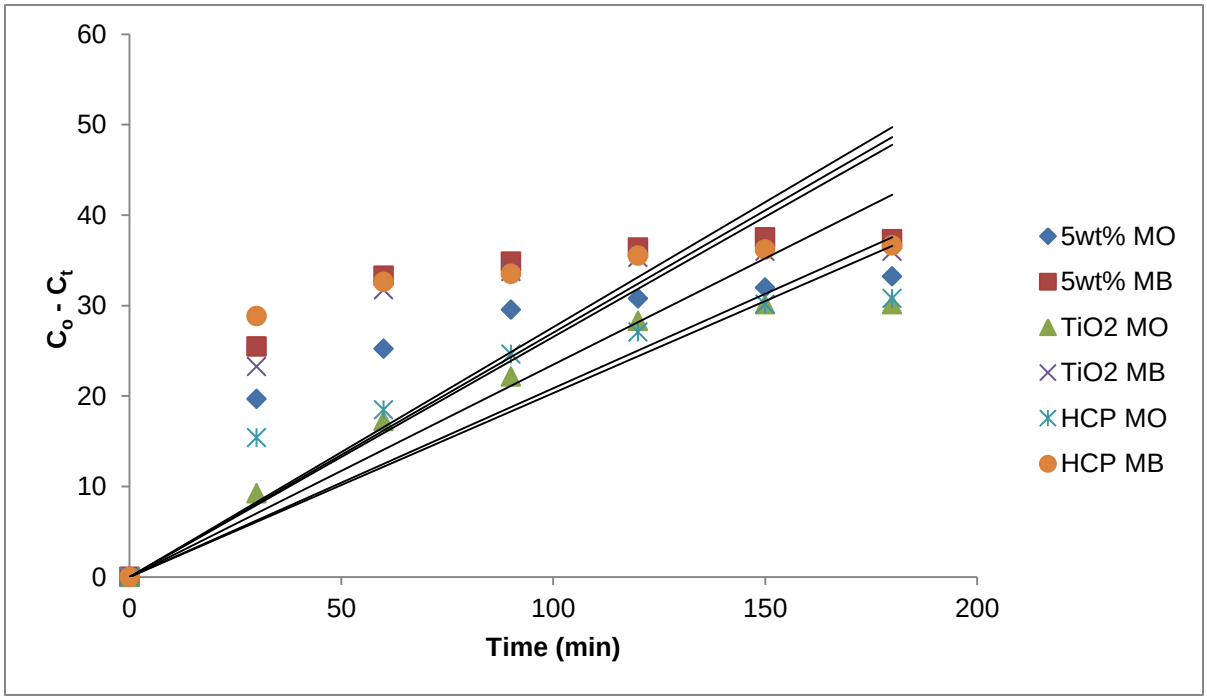

(a)

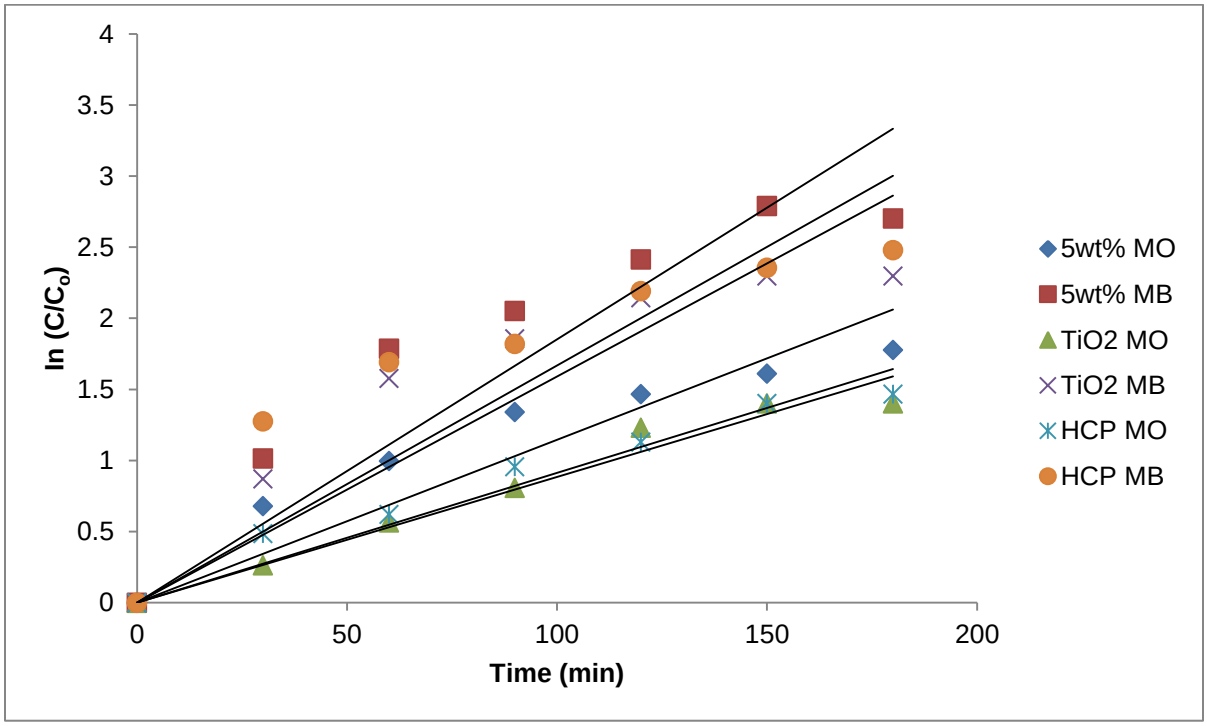

(b)

PUBLISHED JOURNAL

Advanced Materials Research Vols. 781-784 (2013) pp 2249-2252
© (2013) Trans Tech Publications, Switzerland
doi:10.4028/www.scientific.net/AMR.781-784.2249

TiO_2 Supported Clinoptilotile: Characterization and Optimization of Operational Parameters for Methyl Orange Removal.

Sanni O. Saheed[a], Sekomeng J. Modise[b,*], Allworth M.Sipamla[c]

Institute of Chemical and Biotechnology, Vaal University of Technology, Private Bag x021, Vanderbijlpark,1900 South Africa

[a]mosqit.saheed@gmail.com, [b]joe@vut.ac.za, [c]allworth@vut.ac.za

Keywords: Methyl Orange, Photocatalytic degradation, TiO_2/HCP, UV-irradiation, Optimization.

Abstract
Titania dispersed on dealuminatedClinoptilotile (TiO_2/HCP) was synthesized and characterized by Scanning Electron Microscope (SEM). Supporting characterization techniques reveals partly dispersion of TiO_2 within the cavities of dealuminated Clinoptilotile (HCP) and TiO_2 exist as nanoparticles or clusters on the HCP surface ascribed to lower loading of TiO_2. The photocatalytic degradation of methyl orange solution was conducted under UV-irradiation in the presence of TiO_2/HCP. The photocatalytic degradation of methyl orange in the presence of the photocatalyst was optimized at lower loading of TiO_2, at a lower initial dye concentration (30 ppm), calcination temperature of 873K and nitrate ion accelerates degradation activities of methyl orange. Kinetic studies depict the photocatalytic degradation of methyl orange follows the pseudo-first order reaction.

Introduction

Metal semiconductor found application as low cost, environmental and sustainable material in heterogeneous photocatalytic degradation of organic contaminants in wastewater to mineralized products [1]. TiO_2 possesses good photocatalytic properties as compared to other semiconductors and found wide application in heterogeneous photocatalysis. Challenges such as poor recycling of TiO_2 particles after degradation activities and rapid recombination of electron hole pair upon activation limits the efficiency of TiO_2. Immobilization of TiO_2 on support material layer assist in increasing active surface area and recycling of photocatalyst after degradation activities [2].
Zeolite serves as interesting host to disperse TiO_2 on its layers, which is ascribed to its uniform pores, high adsorption capacity and its photochemical stability. Clinoptilotile (CP), the most abundant zeolite in nature andiso-structural with heulandite, is employed as our natural zeolite in this study. In this currentstudy, investigation of influence of operational parameters on the photocatalytic degradation of Methyl orange (MO) in the presence of TiO_2 immobilized on dealuminated Clinoptilotile irradiated by the UV light is reported.

Experimental

A. Preparation of dealuminated Clinoptilotile

Natural Clinoptilotile was crushed in an agate mortar and sieved to less than 100μm particle size fractions. For dealumination experiment, 20g of sieved CP was added to 1M NH_4Cl solution, which was continuously stirred at 60-90^oC for 24hr to achieve the desired ion-exchange process [3]. The resultant mixture was filtered, washed well with distilled water until the supernatant was neutral and freed of chloride ions using silver nitrate. The obtained sample was dried in air at 120-150^oC for 8hr, which was ground to fine powder and further calcined in the muffle oven at 550^oC for 8hr required for activation of the dealuminatedclinoptilotile (HCP).

B. Sol-Gel Synthesis

TiO_2/HCP was synthesized via a sol-gel method, by adding titanium-n-butoxide slowly to HCP suspended in ethanol solution, with vigorous stirring at room temperature for 3hrs. A mixture of ethanol and water solution (1:1) was further added to hydrolyze titanium (IV)-n-butoxide adsorbed

on HCP under continuous stirring for 3hrs. The resultant mixture was filtered, air dried in the oven at 110-120^{o}C overnight. The obtained solid was crushed to fine material and further calcined in a muffle oven at 550^{o}C for 4hrs to achieve TiO_2/HCP.

C. *Photocatalytic Studies*

Photocatalytic degradation of methyl orange under UV light irradiation was conducted in the cylindrical Pyrex glass cell with 1.0L capacity, 10cm diameter and 15cm height conducted in batch mode. The radiation source Ace glass UV lamp (450W), placed in a 5cm diameter quartz tube with a magnetic stirrer applied for good mixing of the dye solution (500 ml of 50 ppm MO). Samples were withdrawn from the reactor after 30 min of irradiation time, and the absorbance of the Methyl orange was determined using an UV−Vis spectrophotometer (Perkin Elmer Lambda 25) at 465 nm.

Results and Discussion

The micrographs were taken at 1000 times magnification as depicted (Fig.1) and average particle size found to be less than 10μm. However, there was uniformly distribution of TiO_2 particles on HCP exists as clusters on the surface of HCP and not really in the pore or cavities of HCP. There exist no agglomerations of TiO_2 particles in the center during immobilization of TiO_2 on HCP surface.

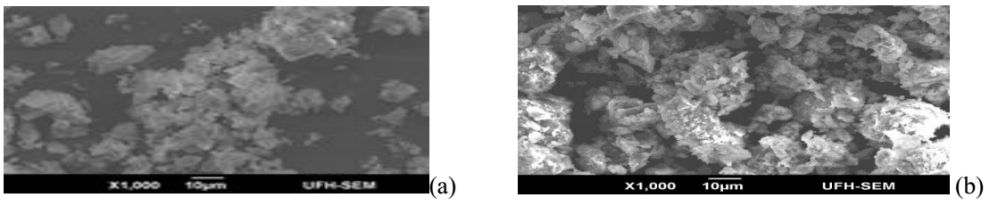

(a) (b)

Figure 1 SEM micrographs of (a) HCP and (b) TiO_2/HCP

In general, pseudo-first order has been used to describe dependencies of photocatalytic degradation of organic pollutants as shown in Eq.1,

$$-Ln(C/C_o) = K\,t \qquad \text{Equation 1}$$

Here $C_o$is initial concentration of dye (ppm), C is the concentration of the reactant at the degraded time (ppm), t is the degradation time (min), and K is the reaction rate constant (min^{-1}).

Fig.2 depicts 5wt%TiO_2/HCP possess optimum photodegradation efficiency (88%) at the relative interval as compared to 7.5wt% (69%) and 10wt% (73%), respectively. The high efficiency of 5wt% TiO_2/HCP can be ascribed to fine dispersion of TiO_2 on HCP surface and increased active sites for degradation of the dye [4]. However, as the TiO_2 loading increases on HCP surface, degradation efficiency drops which are ascribed to the agglomeration of TiO_2 particles on the HCP surface and decrease of the active site in the HCP. The pores in the HCP are also blocked, which leads to lower light penetration by ultraviolet light and reduces photoactivity as the TiO_2 loading increases further. The reaction follows pseudo-first order kinetics and reaction rate constants depicted in Fig.2.

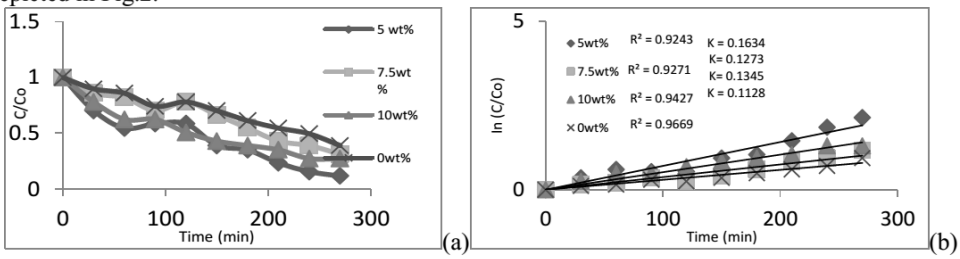

(a) (b)

Figure 2 Photocatalytic degradation of MO using (a) different TiO_2/HCP and (b) first order reaction degradation of MO

Fig.3 depicts the degradation efficiency of MO in relation with time and initial MO concentration, in contact with TiO_2/HCP under UV irradiation. Significant increase in efficiency (92-96%) from 20 ppm to 30 ppm, drastic decrease in photodegradation efficiency as initial MO concentration increases from 40-70 ppm, ascribed to the larger amount of methyl orange adsorbed on the surface of TiO_2. They have inhibiting effect on the reaction of methyl orange molecules with ·OH radicals created on the photocatalyst surface. Reactive sites are reduced as a result of the occupation by the increased methyl orange concentration (cloudy and opaque) and in turn limit light penetration (photons) to reach the photocatalyst surface [5]. Subsequently, the degradation activity is reduced, when fewer available ·OH radicals are required to oxidize more dye molecules. Formation of intermediate products during degradation of MO at high concentration will also result in lower photodegradation efficiency.

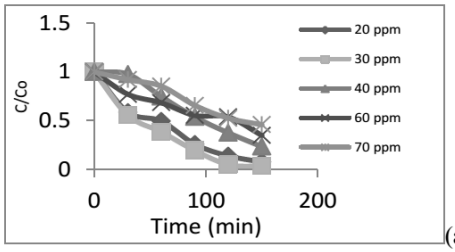

(a)

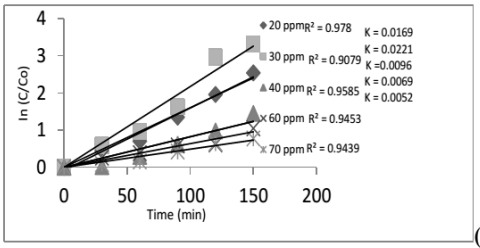

(b)

Figure 3 Photocatalytic degradation of MO at different initial dye concentration and first order reaction degradation of MO.

Fig.4 depicts $NO_3^-$and SO_3^{2-} anions accelerate the degradation of MO, while the Cl^- deactivates the photocatalyst slightly with degradation efficiency decreasing. · OH radical generation increases in the solution upon absorption of UV by NO_3^-, which accelerates the degradation rate of methyl orange [6]. This inhibitory effect of SO_4^{2-} and CO_3^{2-} ions can be ascribed to the reactions of anions with positive holes and hydroxyl radicals which in turns acting as h^+ and ·OH scavengers. These anions compete with MO for oxidizing species and in turn prolong catalytic activities.

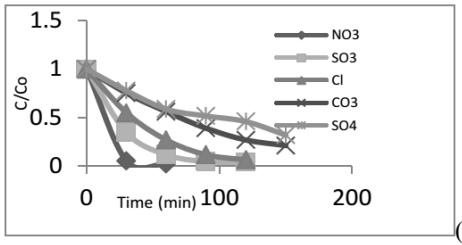

(a)

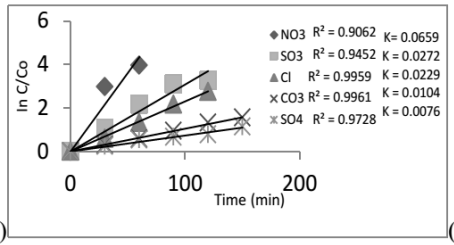

(b)

Figure 4 Photocatalytic degradation of MO using (a) different anions and (b) first order reaction degradation of MO.

Photocatalyst structure affects photodegradation activities of organic contaminants;the samples were being calcined at different temperatures to depict different crystal structures. The effect of calcination temperature was performed in presence of TiO_2/HCP with Methyl orange within a temperature range of 423-973K. From Fig.5, photodegradation efficiency increases with calcination temperature and maximal photocatalytic activity was obtained at 873K with close activity at 423K from 95-96%. This optimum calcination temperature is ascribed to the formation of anatase phase on the photocatalyst surface, which enhances degradation activities. Though as calcination temperature increases above 873K, the photodegradation activities decreases to 84% as a result of formation of rutile phase and also accelerated formation of TiO_2 particles on the surface of HCP. It also results in aggregation of TiO_2 and decrease in specific surface area of the particles.

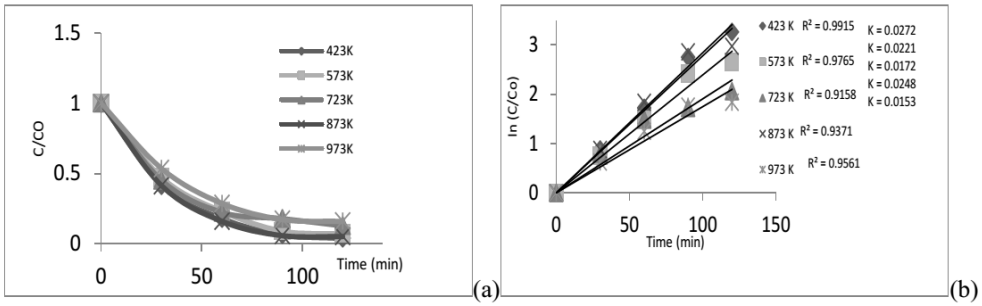

Figure 5 Photocatalytic degradation of MO (a) at different calcination temperature and (b) first order reaction degradation of MO.

Conclusions

In this present work, TiO_2 was successfully dispersed on HCP via sol-gel process and it exists as either nanoparticles or clusters on the Clinoptilotile surface. 5wt% exhibited highest photodegradation efficiency among the catalyst prepared in this study. The optimum photodegradation conducted at room temperature is favorable at an initial MO concentration of 30 ppm and calcination temperature of 873 K. Removal efficiency in the presence of anions was greatly influenced by NO_3^-, SO_3^-, Cl^- but retarded by the concentrations of CO_3^{2-} and SO_4^{2-}. Kinetic studies depict the photocatalytic degradation of Methyl orange follows the pseudo-first order reaction at different operational parameters.

Acknowledgement

This work was supported by the Institute of Chemical and Biotechnology, Vaal University of Technology. The Vaal University of Technology is acknowledged for funding.

References

[1] N.B. Parilti: Ekoloji 19 (2010), p.9–15.
[2] J. Li, C. Chen, J. Zhao, H. Zhu and J. Orthman, Appl. Catal. B. Environ. 37 (2002), p. 331-8.
[3] J.R. Kim, Y.A. Kim, J.H. Yoon, D.W. Park and H.C. Woo, Polymer Degradation and Stability 75 (2002) p. 287–294.
[4] C.C. Wang, C.K. Lee, M.D. Lyu and L.C. Juang, J. Dyes and Pigments. (2007), p. 1-8.
[5] M.V. Shankar, K.K. Cheralathan, B. Arabindoo, M. Palanichamy and V. Murugesan, J. Mol. Catal. 223 (2004), p. 195–200.
[6] W. Zhang, T. An, M. Cui, G. Sheng and J. Fu, J. Chem. Technol. Biotechnol. 80, (2005) p. 223−229.